(12)

AD

MEMORANDUM REPORT ARBRL-MR-03194

(Supersedes IMR No. 742)

ANGULAR MOTION OF A SPINNING PROJECTILE WITH A VISCOUS LIQUID PAYLOAD

Charles H. Murphy

August 1982

US ARMY ARMAMENT RESEARCH AND DEVELOPMENT COMMAND
BALLISTIC RESEARCH LABORATORY
ABERDEEN PROVING GROUND, MARYLAND

Destroy this report when it is no longer needed.
Do not return it to the originator.

Secondary distribution of this report is prohibited.

Additional copies of this report may be obtained from the National Technical Information Service, U. S. Department of Commerce, Springfield, Virginia 22161.

The findings in this report are not to be construed as an official Department of the Army position, unless so designated by other authorized documents.

The use of trade names or manufacturers' names in this report does not constitute indorsement of any commercial product.

UNCLASSIFIED

SECURITY CLASSIFICATION OF THIS PAGE (When Data Entered)

REPORT DOCUMENTATION PAGE	READ INSTRUCTIONS BEFORE COMPLETING FORM
1. REPORT NUMBER: Memorandum Report ARBRL-MR-03194	2. GOVT ACCESSION NO.: AD-A118 676
	3. RECIPIENT'S CATALOG NUMBER:
4. TITLE (and Subtitle): Angular Motion of a Spinning Projectile with a Viscous Liquid Payload	5. TYPE OF REPORT & PERIOD COVERED: Final
	6. PERFORMING ORG. REPORT NUMBER:
7. AUTHOR(s): Charles H. Murphy	8. CONTRACT OR GRANT NUMBER(s):
9. PERFORMING ORGANIZATION NAME AND ADDRESS: US Army Ballistic Research Laboratory, ATTN: DRDAR-BLL, Aberdeen Proving Ground, MD 21005	10. PROGRAM ELEMENT, PROJECT, TASK AREA & WORK UNIT NUMBERS: RDT&E 1L162618AH80
11. CONTROLLING OFFICE NAME AND ADDRESS: US Army Armament Research and Development Command, US Army Ballistic Research Laboratory (DRDAR-BL), Aberdeen Proving Ground, MD 21005	12. REPORT DATE: August 1982
	13. NUMBER OF PAGES: 117
14. MONITORING AGENCY NAME & ADDRESS (if different from Controlling Office):	15. SECURITY CLASS. (of this report): UNCLASSIFIED
	15a. DECLASSIFICATION/DOWNGRADING SCHEDULE:

16. DISTRIBUTION STATEMENT (of this Report)

Approved for public release; distribution unlimited.

17. DISTRIBUTION STATEMENT (of the abstract entered in Block 20, if different from Report)

18. SUPPLEMENTARY NOTES

Supersedes BRL IMR 742 dated April 1982.

19. KEY WORDS (Continue on reverse side if necessary and identify by block number)

Liquid-filled gyroscope
Liquid payload
Spinning projectile
Stability analysis
Stewartson-Wedemeyer theory
Eigenfrequency

20. ABSTRACT (Continue on reverse side if necessary and identify by block number) (eis)

Liquid payload motion can have a significant effect on the stability of a spinning projectile. A general definition of the liquid moment is developed and expressions are obtained for the frequencies and damping rates of the projectile's angular motion. An expression for the liquid pressure moment is derived without the unnecessary mathematical approximations of the Stewartson-Wedemeyer theory, and wall shear effects are added to this improved SW pressure moment to obtain the total liquid moment. This moment expression applies to cavities that are fully filled, partially filled or fully filled with a central rod. The improved

DD FORM 1 JAN 73 1473 EDITION OF 1 NOV 65 IS OBSOLETE

UNCLASSIFIED

SECURITY CLASSIFICATION OF THIS PAGE (When Data Entered)

20. ABSTRACT (Cont'd)

theory shows that as the Reynolds number decreases, (a) the eigenfrequency-related side moment peaks decrease steadily in size but that (b) the average side moment level first increases and then decreases. This latter predicted behavior is in good qualitative agreement with the D'Amico-Miller conjecture that relates the liquid spin-down moment to the liquid side moment. Good agreement is also obtained between the theory and all available published data from liquid-filled gyroscope experiments.

TABLE OF CONTENTS

TABLE OF CONTENTS (Continued)

LIST OF FIGURES

LIST OF FIGURES (Continued)

LIST OF FIGURES (Continued)

1. INTRODUCTION

The US Army has had a continuing interest in the design of spinning projectiles with liquid payloads. Many of these developmental shell have shown dramatic instabilities in their pitching and yawing motion. Initially, these instabilities have been identified by large range losses incurred during firing trials. In 1962 Karpov made direct angular motion measurements of liquid-payload-induced instabilities in a 20mm projectile fired in BRL's Aerodynamics Range[1]. In 1973 Mark and Mermagen[2] used instrumented solar sensors and telemetry units to observe liquid-payload-induced instabilities in 155mm shell. Since that time all developmental shell with liquid payloads have been tested with sunsonde instrumentation and a variety of strange behaviors has been observed. A complete listing of all yawsonde data reports is given in the Bibliography at the end of this report.

In 1959 Stewartson published a theoretical paper on the stability of a spinning liquid-filled top[3]. This paper assumed a right circular container partially or fully filled with an inviscid fluid. The liquid was assumed to be fully spun up and in steady state motion. This motion was assumed to be a circular or spiral motion at a frequency set by the top's static moment and spin rate. The Stewartson theory predicted liquid eigenfrequencies that were to be avoided in order to have stable angular motion of the top. According to the theory, liquid moments would become infinite for coning motion at any of the eigenfrequencies.

In 1965 Karpov[4] made additional 20mm firings. All shell in this series had the same fast frequencies but the payload eigenfrequencies were varied by use of different cavity fineness ratios. A resonance undamping rate was observed but was of a much smaller amplitude and at a slightly lesser frequency than that predicted by Stewartson.

At about that time Wedemeyer[5] introduced a boundary layer modification to the Stewartson theory and computed complex liquid eigenvalues. Since the Aerodynamics Range flights were too short to allow the liquid to be fully spun up and in steady state coning motion, Karpov developed the use of a free liquid-filled gyroscope to measure yaw growth rates near resonance. He

---

1. *B. G. Karpov, "Experimental Observations of the Dynamic Behavior of Liquid Filled Shell," BRL Report 1171, August 1961. AD 263142.*

2. *A. Mark and K. H. Mermagen, "Measurement of Spin Decay and Instability of Liquid-Filled Projectiles via Telemetry," BRL Memorandum Report 2353, October 1973. AD 771312.*

3. *K. Stewartson, "On the Stability of a Spinning Top Containing Liquid," Journal of Fluid Mechanics, Vol. 5, Part 4, September 1959, pp. 577-592.*

4. *B. G. Karpov, "Dynamics of Liquid-Filled Shells: Resonance and Effect of Viscosity," BRL Report 1279, May 1965. AD 466364.*

5. *E. P. Wedemeyer, "Viscous Corrections to Stewartson's Stability Criterion," BRL Report 1353, June 1966. AD 489681.*

found an exceptionally good agreement with Wedemeyer values at a Reynolds number of 520,000 and fair agreement at a Reynolds number of 5200[6].

The success of Karpov's gyroscope experiments led to an extensive use of this technique. A complete listing of gyroscope data reports is also included in the Bibliography. This excellent experimental work had the unfortunate effect of biasing most of the later theoretical and experimental work toward understanding liquid-filled gyroscopes and the application to projectiles was treated as a side effect.

A second difficulty with the later gyroscope-oriented work was a tunnel vision concentration on liquid eigenfrequencies. This was caused by the great success of Wedemeyer's modification of Stewartson's inviscid eigenfrequencies. The basic aim of any liquid payload theory should be the calculation of the complete moment the liquid payload exerts on the pitching and yawing projectile in flight. Wedemeyer's complex eigenfrequencies identify frequency and damping rate pairs for which the liquid pressure is infinite. For coning motion near any of these pairs the liquid moment is primarily due to the pressure at the edge of the boundary layer and is dominated by a simple pole function. This pole is an excellent approximation at high Reynolds number, but at lower Reynolds number it becomes quite poor even though the boundary layer assumptions are still valid. The pressure at the edge of the boundary layer has to be computed without the pole approximation. In addition an increment in pressure through the rotating boundary layer on the lateral wall must be computed, as well as the shear on both the lateral and end walls.

It is the aim, then, of this report to give the general formulation of the effect of liquid payload motion on projectile stability and to compute the liquid moments, pressures and wall shears for small-amplitude liquid motion with boundary layers but without the unnecessary mathematical approximations of the Stewartson-Wedemeyer theory. The results of this improved Stewartson-Wedemeyer theory will be compared with all available published gyroscope data for Reynolds numbers down to as low as 2400. Moreover, the theory will be extended to the special case of a fully-filled cylinder with a central rod[7-9]. Finally, a survey of extensions of the theory to partially spun-up liquids and other special cases will be given.

---

6. R. P. Whiting and N. Gerber, "Dynamics of a Liquid-Filled Gyroscope: Update of Theory and Experiment," BRL Technical Report ARBRL-TR-[illegible], March 1980. AD A083866.

7. J. T. Frasier and W. E. Scott, "Dynamics of a Liquid-Filled Shell: Cylindrical Cavity with a Central Rod," BRL Report 1691, February 1968. AD 667365.

8. J. T. Frasier, "Dynamics of a Liquid Filled Shell: Viscous Effects in a Cylindrical Cavity with a Central Rod," BRL Memorandum Report 1958, January 1969. AD 684344.

9. J. T. Frasier and F. F. D'Amico, "Stabilization of a Liquid-Filled Shell by Inserting a Cylindrical Partition in the Liquid Cavity," BRL Report 1432, August 1970. AD 874732.

2. PROJECTILE DYNAMICS

Two coordinate systems, both of which have X-axes along the projectile's axis of symmetry, are commonly used: the missile-fixed XYZ system and the aeroballistic $X\tilde{Y}\tilde{Z}$ non-rolling system with the $\tilde{Z}$-axis initially downward. If we introduce earth-fixed axes $X_e Y_e Z_e$ with the X_e-axis initially along the velocity vector and Z_e downward, a unit vector along the positive X-axis has earth-fixed components (n_{XE}, n_{YE}, n_{ZE}). The angle of attack $\tilde{\alpha}$ in the non-rotating system is the angle in the $X\tilde{Z}$ plane from the X-axis to the velocity vector, and the angle of sideslip $\tilde{\beta}$ is the angle in the $X\tilde{Y}$ plane from the X-axis to the velocity vector. Thus for a straight trajectory and small angles, these angles are the negatives of the direction cosines n_{ZE} and n_{YE}, respectively.

The primary lateral force on the projectile is the normal force, which can be easily expressed in terms of complex variables[10]:

$$\tilde{F_Y} + i\,\tilde{F_Z} = -\,(1/2)\,\rho V^2 S\,C_{N_\alpha}\,\tilde{\xi} \tag{2.1}$$

where

$$\tilde{\xi} = \tilde{\beta} + i\,\tilde{\alpha} \tag{2.2}$$

and where the other symbols are defined in the List of Symbols.

For an approximately straight trajectory, the usual linear aerodynamic moment can be expressed as the sum of three terms:

$$\tilde{M_Y} + i\,\tilde{M_Z} = (1/2)\,\rho V^2 S\ell\,\left\{\left[(\dot{\phi}\ell/V)\,C_{M_{p_\alpha}} - iC_{N_\alpha}\right]\tilde{\xi}\right.$$
$$\left. - i\,(C_{M_q} + C_{M_{\dot{\alpha}}})\,(\dot{\tilde{\xi}}\ell/V)\right\} \tag{2.3}$$

The first term is the very important Magnus moment, which is a viscous side moment caused by the spin and the angle of attack. The second term is the static moment which for most projectiles causes an increased angle in the plane of the total angle of attack. The last term is the damping moment, which usually resists the angular velocity. For simplicity we will neglect the effect of drag on the angular motion and assume V to be constant in Equations (2.1) and (2.3).

---

10. C. H. Murphy, "Free Flight Motion of Symmetric Missiles," BRL Report 1216, July 1963. AD 442757.

For small angles the usual dynamics[10] yield the following differential equation for $\tilde{\xi}$ in terms of an arbitrary force and moment:

$$I_y \ddot{\tilde{\xi}} - i\dot{\phi} I_x \dot{\tilde{\xi}} = i(M_y^{\sim} + iM_z^{\sim}) + \frac{(I_y d/dt - iI_x\dot{\phi})(F_y^{\sim} + iF_z^{\sim})}{mV} \tag{2.4}$$

For the force and moment of Eqs. (2.1) and (2.3) this reduces to

$$\ddot{\tilde{\xi}} + (\hat{H} - i\sigma\dot{\phi})\dot{\tilde{\xi}} - (\hat{M} + i\sigma\dot{\phi}\hat{T})\tilde{\xi} = 0 \tag{2.5}$$

where

$$\hat{H} = (\rho S\ell/2m)\left[C_{N_\alpha} - k_y^{-2}(C_{M_q} + C_{M_{\dot{\alpha}}})\right](V/\ell)$$

$$\hat{M} = (\rho S\ell^3/2I_y)\, C_{M_\alpha}(V/\ell)^2$$

$$\hat{T} = (\rho S\ell/2m)\left[C_{N_\alpha} + k_x^{-2} C_{M_{p\alpha}}\right](V/\ell)$$

$$\sigma = I_x/I_y$$

The solution to Equation (2.5) is an epicycle which generates the angular motion as the sum of two rotating and damping or undamping two-dimensional vectors:

$$\tilde{\xi} = K_1 e^{i\phi_1} + K_2 e^{i\phi_2} \tag{2.6}$$

where

$$\ln(K_j/K_{j_0}) = \varepsilon_j \tau_j |\dot{\phi}|\, t$$

$$\phi_j = \phi_{j0} + \tau_j \dot{\phi} t$$

$$\tau_j = (\sigma/2)\left[1 \pm \sqrt{1-(1/s_g)}\right],\quad s_g = \sigma^2 \dot{\phi}^2/4\hat{M}$$

$$\varepsilon_j = -\frac{\tau_j \hat{H} - \sigma\hat{T}}{(2\tau_j - \sigma)\tau_j|\dot{\phi}|}$$

Note that for coning motion in the direction of spin, $\tau_j > 0$ while $\varepsilon_j > 0$ for increasing K_j and $\varepsilon_j < 0$ for decreasing K_j. For coning motion in the direction opposite to the spin, the inequalities are reversed.

In analyzing the effect of a moving internal component on the angular motion of a spinning projectile[11], we found it convenient to consider only that part of the moment exerted by the internal component at one of the two frequencies of the projectile's angular motion. For steady-state linear liquid motion, this part will be the total liquid moment. For nonsteady or nonlinear liquid motion, this part will consist of two average components of the actual liquid moment. If we now non-dimensionalize this liquid moment by the liquid mass m_L, the spin rate $\dot{\phi}$ and the maximum liquid container diameter 2a, the following expression for the liquid moment can be obtained:

$$M_{LY}\tilde{} + iM_{LZ}\tilde{} = m_L a^2 \dot{\phi}^2 \left[\tau_1 C_{LM_1} K_1 e^{i\phi_1} + \tau_2 C_{LM_2} K_2 e^{i\phi_2}\right] \qquad (2.7)$$

For linear fluid motion, C_{LM_1} should depend on τ_1, ε_1, time, Reynolds number, fill ratio, the shape of the cavity, and the direction of the spin. A similar remark applies to C_{LM_2}. The τ_j's appear explicitly in definition (2.7) since the moment should vanish for $\tau_j = 0$.

It should be noted that the C_{LM_j} are complex quantities whose imaginary parts represent in-plane moments causing rotation in the plane of $\exp(i\phi_j)$ and whose real parts represent side moments causing rotations out of the plane of exp($i\phi_j$). We, therefore, introduce the following definition for the real and imaginary parts of C_{LM_j} and explicitly express the effect of the direction of spin[10]:

$$C_{LM_j} = \gamma C_{LSM_j} + i\, C_{LIM_j} \qquad (2.8)$$

where C_{LSM_j} and C_{LIM_j} are real and represent the liquid side moment and liquid in-plane moment contributions, respectively, and where $\gamma = \dot{\phi}/|\dot{\phi}|$.

The special values of these coefficients for infinitely viscous or frozen liquid can be obtained from Equation (2.4) with the external moments neglected.

$$(I_y + I_{Ly})\ddot{\tilde{\xi}} - i\dot{\phi}(I_x + I_{Lx})\dot{\tilde{\xi}} = 0 \qquad (2.9)$$

11. *C. H. Murphy, "Influence of Moving Internal Parts on Angular Motion of Spinning Projectiles," Journal of Guidance and Control, Vol. 1, March-April 1978, pp. 117-122. (See also BRL Memorandum Report 2731 dated February 1977. AD 037338.)*

where I_{Ly} and I_{Lx} are transverse and axial moments of inertia for the frozen liquid. Comparing Equations (2.4) and (2.9) we see that if the terms involving the frozen liquid moments of inertia are taken to the right side, they can be identified as i times the liquid moment.

$$M_{L\tilde{Y}} + iM_{L\tilde{Z}} = -i(I_{Ly}\ddot{\tilde{\xi}} - i\dot{\phi}I_{Lx}\dot{\tilde{\xi}}) \tag{2.10}$$

The epicylic solution of Equation (2.6) with $|\varepsilon_j|<<1$ can now be used to provide frozen liquid values of the liquid side moment and liquid in-plane moment coefficients.

$$C_{LIM_j} = \frac{I_{Lx} - \tau_j I_{Ly}}{m_L a^2} \tag{2.11}$$

$$C_{LSM_j} = \frac{\varepsilon_j(I_{Lx} - 2\tau_j I_{Ly})}{m_L a^2} \tag{2.12}$$

For a circular cylinder of length 2c and center located a distance h forward of the projectile's center of mass

$$C_{LIM_j} = \frac{1}{2} - \tau_j\left[\frac{1}{4} + \frac{c^2 + 3h^2}{3a^2}\right] \tag{2.13}$$

$$C_{LSM_j} = (\varepsilon_j/2)\left[1 - \tau_j\left(1 + \frac{4(c^2 + 3h^2)}{3a^2}\right)\right] \tag{2.14}$$

A simple interpretation for ε follows from the observation that for moderate damping $2\pi\varepsilon$ is approximately the fractional change in K_j in one cycle. If we restrict this change to be less than 20%, ε should be less than .03, and the frozen C_{LSM} would be less than .015.

In general, however, the liquid moment of Eq. (2.7) should be combined with the aerodynamic force and moment of Eqs. (2.1) and (2.3) to give a somewhat more complicated differential equation for $\tilde{\xi}$:

$$\ddot{\tilde{\xi}} + (\hat{H} - i\sigma\dot{\phi})\dot{\tilde{\xi}} - (\hat{M} + i\sigma\dot{\phi}\hat{T})\tilde{\xi}$$

$$= i\dot{\phi}^2(m_L a^2/I_y)\left[\tau_1 C_{LM_1} K_1 e^{i\phi_1} + \tau_2 C_{LM_2} K_2 e^{i\varphi_2}\right] \tag{2.15}$$

If the epicycle solution of Eq. (2.6) is substituted in Eq. (2.15), new relations for frequency and damping can be obtained.

$$\tau_j = (\sigma/2)\left[f_j - (-1)^j \sqrt{f_j^2 - (1/s_g)}\right] \tag{2.16}$$

where

$$f_j = 1 + (m_L a^2/I_x)C_{LIM_j}$$

and

$$\varepsilon_j = -\frac{\tau_j (\hat{H} + \hat{H}_{L_j}) - \sigma\hat{T}}{(2\tau_j - \sigma)\tau_j |\dot{\phi}|} \tag{2.17}$$

where

$$\hat{H}_{L_j} = -(\rho S\ell^3/2I_y)\, C_{LMq_j}(V/\ell)$$

$$C_{LMq_j} = \sigma_L\, C_{LSM_j}$$

$$\sigma_L = \frac{2m_L a^2 |\dot{\phi}|}{\rho S\ell^2 V}$$

As can be seen from Eq. (2.17), the liquid side moment has the same effect on the damping of the angular motion as the aerodynamic damping moment. The coefficient C_{LMq} is introduced so that the relative size of the aerodynamic damping moment and the liquid side moment can be directly evaluated. The direct impact of the liquid side moment on the damping per cycle can be seen from Eq. (2.17) for $\hat{H} = \hat{T} = 0$.

$$\varepsilon_j = (m_L a^2/I_x)(2\tau_j/\sigma - 1)^{-1}\, C_{LSM_j} \tag{2.18}$$

For the fast mode the coefficient of C_{LSM_1} is positive and a positive side moment causes an undamping of this motion. Similarly a negative C_{LSM_2} will undamp the slow mode. As we shall see, the linear liquid motion theory

usually yields a positive side moment, and thus only the fast mode motion is adversely affected by the liquid side moment.

Table 1. Parameter Values for Five Army Projectiles

Payload	Projectile	Diameter (mm)	c/a	σ	$\frac{m_L a^2}{I_x}$	σ_L
White Phosphorus Re = 4-40 x 10^6	M416	105	2.67	.17	.36	350
	M328	107	2.82	.11	.41	230
	XM825	155	4.60	.08	.12	150
Binary Chemical Re = 1-7 x 10^6	M687	155	4.52	.08	.07	80
	XM736	203	3.98	.12	.09	90

In Table 1 the parameters c/a, σ, $m_L a^2/I_x$ and σ_L are given for five Army projectiles. The first three are smoke projectiles containing white phosphorus, which is liquid for temperatures above 110°F, and the remaining two have special liquid payloads. Since τ_1 lies between $\sigma/2$ and σ, we see that the τ_1 range of interest is .04 to .17. $m_L a^2/I_x$ and σ_L are much larger for the smoke shell due to WP's greater density.

Equation (2.18) can be used to determine a lower bound on the side moment coefficient corresponding to a significant yaw growth rate of 13% per cycle, i.e., $\epsilon = .02$. For $\tau/\sigma = 3/4$ and $m_L a^2/I_x = .08$, this lower bound on C_{LSM} is .125. For $m_L a^2/I_x = .40$, which is appropriate to the older WP shell, this lower bound is .025. Thus our theoretical prediction of this liquid side moment coefficient should at least attempt to achieve an accuracy better than half the lower value, i.e., errors less than .01.

3. EQUATIONS OF LIQUID MOTION

We will consider a projectile with a cylindrical payload cavity with radius, a, and height, 2c. The axis of the cylinder is collinear with the projectile's axis, and its center is located a distance, h, from the projectile's center of mass. If the cavity is partially filled, the liquid is fully spun up, and the centrifugal force is large compared to the aerodynamic forces, the liquid will fill the space between the outer cylindrical wall and

an inner cylindrical free surface with radius, b. The ratio of the volume of this inner cylinder to the volume of the complete payload cavity is b^2/a^2. The fill ratio for the payload cavity is, therefore, $1-b^2/a^2$ and will be denoted by f. However, m_L will always be the liquid mass in a fully-filled cavity.

The objective of the linear theory is to predict the liquid moment response to coning or spiral motion of the form

$$\tilde{\xi} = K_j e^{i\phi_j} \qquad j = 1 \text{ or } 2 \qquad (3.1)$$

$$= \hat{K}\, e^{s\phi}$$

where

$$s = (\gamma\varepsilon_j + i)\,\tau_j$$

$$\phi = \dot{\phi}t$$

$$\hat{K} = K_{j0}\, e^{i\phi_{j0}}$$

The vector between the center of mass of the projectile and any other points on the projectile can be described in the aeroballistic cylindrical coordinates of this vector by $(\tilde{x}, \tilde{r}, \tilde{\theta})$. Cartesian coordinates of this vector in the earth-fixed coordinates would then be (x_e, y_e, z_e). For simplicity we will omit the subscript "e" for these earth-fixed coordinates throughout this report. Relations between the earth-fixed Cartesian coordinates and the aeroballistic cylindrical coordinates take on quite simple forms for small K_j.

$$x = \tilde{x} + \tilde{r}K_j \cos(\phi_j - \tilde{\theta}) \qquad (3.2)$$

$$y = \tilde{r}\cos\tilde{\theta} - K_j\tilde{x}\cos\phi_j \qquad (3.3)$$

$$z = \tilde{r}\sin\tilde{\theta} - K_j\tilde{x}\sin\phi_j \qquad (3.4)$$

If cylindrical coordinates with respect to the earth-fixed axes are denoted by (x, r, θ), the following simple relations between the two sets of polar coordinates follow from Eqs. (3.3 - 3.4) for small K_j.

$$r = \tilde{r} - K_j \tilde{x} \cos(\phi_j - \tilde{\theta}) \tag{3.5}$$

$$\sin(\tilde{\theta} - \theta) = (\tilde{x} K_j / \tilde{r}) \sin(\phi_j - \tilde{\theta}) \tag{3.6}$$

The cylindrical components of the velocity of any point on the projectile in aeroballistic coordinates are $\dot{\tilde{x}} = \dot{\tilde{r}} = 0$, $\tilde{r}\dot{\tilde{\theta}} = \tilde{r}\dot{\phi}$. In earth-fixed coordinates they can be obtained by differentiating* Eqs. (3.2, 3.5 - 3.6).

$$V_x = R\left\{\dot{\phi}(s - i) r \hat{K} e^{s\phi - i\theta}\right\} \tag{3.7}$$

$$V_r = -R\left\{\dot{\phi}(s - i) x \hat{K} e^{s\phi - i\theta}\right\} \tag{3.8}$$

$$V_\theta = \dot{r} + R\left\{i\dot{\phi}(s - i) x \hat{K} e^{s\phi - i\theta}\right\} \tag{3.9}$$

where

$$R\{\ \} = \left[\{\ \} + \overline{\{\ \}}\right]/2$$

is the real part of a complex quantity.

We will now make the very restrictive assumption that the liquid is in steady-state response to the coning and spinning motion of the projectile. Theoretical studies [12, 13] have been made and are in progress to determine the effect of partially spun-up liquid, and an experimental study of the transient response to coning motion has been made[14]. These studies show that spin-up and cone-up effects are large and important to a complete understanding of the liquid payload stability problem.

Nevertheless, we will assume that the liquid velocity components and liquid pressure have the same dependency on time and θ as the velocity components of points on the projectile and introduce four small dimensionless functions of r and x: u_s, v_s, w_s and p_s.

*See Appendix A for details.

12. Y. M. Lynn, "Free Oscillations of a Liquid During Spin-Up," BRL Report 1663, August 1973. AD 769710.

13. C. W. Kitchens, Jr., N. Gerber, and R. Sedney, "Oscillations of a Liquid in a Rotating Cylinder: Part I. Solid-Body Rotation," BRL Technical Report ARBRL-TR-02081, June 1978. AD A057752.

14. W. P. D'Amico, W. G. Beims, and T. H. Rogers, "Pressure Measurements of a Rotating Liquid for Impulsive Coning Motion," BRL Memorandum Report in publication. (See also AIAA Paper 82-0249, Jan 1982.)

$$V_x = R\left\{u_s e^{s\phi - i\theta}\right\}(a\dot{\phi}) \tag{3.10}$$

$$V_r = R\left\{v_s e^{s\phi - i\theta}\right\}(a\dot{\phi}) \tag{3.11}$$

$$V_\theta = r\dot{\phi} + R\left\{w_s e^{s\phi - i\theta}\right\}(a\dot{\phi}) \tag{3.12}$$

$$p = \rho_L \frac{r^2\dot{\phi}^2}{2} + R\left\{p_s e^{s\phi - i\theta}\right\}(\rho_L a^2\dot{\phi}^2) \tag{3.13}$$

Eqs. (3.10 - 3.13) can now be placed in the linearized unsteady Navier-Stokes equations and the continuity equation to yield

$$(s - i)v_s - 2w_s + a\frac{\partial p_s}{\partial r} = \gamma Re^{-1}\left[\nabla_\theta^2 v_s - \frac{a^2 v_s}{r^2} + \frac{2a^2 i w_s}{r^2}\right] \tag{3.14}$$

$$(s - i)w_s + 2v_s - \frac{iap_s}{r} = \gamma Re^{-1}\left[\nabla_\theta^2 w_s - \frac{a^2 w_s}{r^2} - \frac{2a^2 i v_s}{r^2}\right] \tag{3.15}$$

$$(s - i)u_s + a\frac{\partial p_s}{\partial x} = \gamma Re^{-1}\ \nabla_\theta^2 u_s \tag{3.16}$$

$$\frac{\partial(rv_s)}{\partial r} - iw_s + r\frac{\partial u_s}{\partial x} = 0 \tag{3.17}$$

where

$$\nabla_\theta^2 = a^2\left[\frac{\partial^2}{\partial r^2} + \frac{\partial}{r\partial r} + \frac{\partial^2}{\partial x^2} - \frac{1}{r^2}\right]$$

4. BOUNDARY LAYER SOLUTION

Wedemeyer[5] made the assumption that the velocity components and pressure could each be expressed as the sum of inviscid and viscous terms. The inviscid terms satisfy Eqs. (3.14 - 3.17) for $Re^{-1} = 0$ over the entire cylinder except for a small boundary layer region near the cylinder walls, while the viscous terms satisfy the boundary layer versions of Eqs. (3.14 - 3.17).

Although Wedemeyer considers the effect of these boundary layer terms only on the liquid eigenvalues, this report will consider all their contributions to the liquid moment. Since the effect of negative spin can easily be found from Eq. (2.8), we will only consider positive spin ($\gamma = 1$) for the remainder of this report.

$$u_s = u_{si} + u_{sv} \tag{4.1}$$

$$v_s = v_{si} + v_{sv} \tag{4.2}$$

$$w_s = w_{si} + w_{sv} \tag{4.3}$$

$$p_s = p_{si} + p_{sv} \tag{4.4}$$

On the lateral wall $r = a$, then, the usual boundary layer approximations* reduce Eqs. (3.14 - 3.17) to:

$$a \frac{\partial p_{sv}}{\partial r} = 2w_{sv} \tag{4.5}$$

$$(s - i)w_{sv} = a^2 Re^{-1} \frac{\partial^2 w_{sv}}{\partial r^2} \tag{4.6}$$

$$(s - i)u_{sv} = a^2 Re^{-1} \frac{\partial^2 u_{sv}}{\partial r^2} \tag{4.7}$$

$$\frac{\partial (r v_{sv})}{\partial r} = i w_{sv} - r \frac{\partial u_{sv}}{\partial x} \tag{4.8}$$

Far from the lateral wall, u_s, v_s, w_s, p_s must vanish. At the wall the velocities must be those required by Eqs. (3.7 - 3.9). The viscous tangential velocities can be determined and a condition for the inviscid normal velocity obtained.*

$$w_{sv} = \left[(1 + is)(x/a)\hat{K} - w_{si}\right] e^{(r-a)/a\delta_a} \tag{4.9}$$

$$u_{sv} = -\left[(i - s)\hat{K} + u_{si}\right] e^{(r-a)/a\delta_a} \tag{4.10}$$

* *See Appendix B for details.*

For r = a,

$$v_{si} - a\delta_a \frac{\partial v_{si}}{\partial r} = (i - s)(x/a)\hat{K} \tag{4.11}$$

where

$$\delta_a = \frac{1 + i}{\sqrt{2(1 + is)}} Re^{-1/2}$$

At the end walls, $\hat{x} = \frac{x - h}{c} = \pm 1$,

$$(s - i)v_{sv} - 2w_{sv} = a^2 Re^{-1} \frac{\partial^2 v_{sv}}{\partial x^2} \tag{4.12}$$

$$(s - i)w_{sv} + 2v_{sv} = a^2 Re^{-1} \frac{\partial^2 w_{sv}}{\partial x^2} \tag{4.13}$$

$$a \frac{\partial p_{sv}}{\partial x} = 0 \tag{4.14}$$

$$r \frac{\partial u_{sv}}{\partial x} = iw_{sv} - \frac{\partial (rv_{sv})}{\partial r} \tag{4.15}$$

Once again the solution for the tangential viscous velocities and a relation for the normal inviscid velocity can be obtained.

$$w_{sv} + iv_{sv} = - (w_{si} + iv_{si})e^{-\alpha(1 \mp \hat{x})} \tag{4.16}$$

$$w_{sv} - iv_{sv} = - \left[w_{si} - iv_{si} - 2(1 + is)\left(\frac{h \pm c}{a}\right) \hat{K} \right] e^{-\beta(1 \pm \hat{x})} \tag{4.17}$$

For $\hat{x} = \pm 1$,

$$u_{si} \mp \delta_c \frac{\partial u_{si}}{\partial \hat{x}} = - (i - s)(r/a)\hat{K} \tag{4.18}$$

where

$$\alpha = (c/a)\ \delta_a^{-1}\sqrt{(3 + is)/(1 + is)}$$

$$\beta = i(c/a)\ \delta_a^{-1}\sqrt{(1 - is)/(1 + is)}$$

$$\delta_c = \frac{-(a/c)\delta_a}{2\sqrt{1 + is}}\left[\frac{1 - is}{\sqrt{3 + is}} + \left(\sqrt{\frac{3 + is}{1 - is}}\right) i\right]$$

It is interesting to note that according to Eq. (4.14) the usual boundary condition of no pressure change through the boundary layer is present. Eq. (4.5) shows that this is not the case on the lateral wall. The pressure at the wall differs from that at the edge of the boundary layer by $p_{sv}(a)$. This pressure difference can be computed by inserting w_{sv} as given by Eq. (4.9) in Eq. (4.5) and integrating.

$$p_{sv}(a,\hat{x}) = 2\delta_a\left[(1 + is)(c/a)(\hat{x} + h/c)\ \hat{K} - w_{si}\ (a,\hat{x})\right] \tag{4.19}$$

5. INVISCID SOLUTION

The inviscid terms are solutions of Equations (3.14 - 3.17) for $Re^{-1} = 0$. These four equations can be easily manipulated to yield a partial differential equation for p_{si} and three equations for the three velocity components in terms of p_{si}.

$$(s - i)^2\left[\frac{\partial^2 p_{si}}{\partial r^2} + \frac{\partial p_{si}}{r\partial r} - \frac{p_{si}}{r^2}\right] = -(s^2 - 2\,is + 3)\frac{\partial^2 p_{si}}{\partial x^2} \tag{5.1}$$

$$(s - i)u_{si} = -a\frac{\partial p_{si}}{\partial x} \tag{5.2}$$

$$(s^2 - 2is + 3)v_{si} = -(s - i)\, a \frac{\partial p_{si}}{\partial r} + \frac{2iap_{si}}{r} \tag{5.3}$$

$$(s^2 - 2is + 3)w_{si} = 2a \frac{\partial p_{si}}{\partial r} + \frac{ai(s - i)p_{si}}{r} \tag{5.4}$$

On the outer walls of the container the boundary conditions are given by Equations (4.18) and (4.11). These equations can be rewritten by use of Equations (5.2) and (5.3).

For $\hat{x} = \pm 1$

$$\frac{\partial p_{si}}{\partial \hat{x}} \mp \delta_c \frac{\partial^2 p_{si}}{\partial \hat{x}^2} = -(s - i)^2 (c/a) (r/a) \hat{K} \tag{5.5}$$

For $r = a$

$$2i (1 + \delta_a)p_{si} - \left[s - i(1 - 2\delta_a)\right] a \frac{\partial p_{si}}{\partial r} +$$

$$a^2\delta_a(s - i) \frac{\partial^2 p_{si}}{\partial r^2} = -(s^2 + 1)(s - 3i)(x/a) \hat{K} \tag{5.6}$$

On the inner free boundary, $r = b$, the pressure must be a constant.

$$\frac{dp}{dt} = \frac{\partial p}{\partial t} + V_x \frac{\partial p}{\partial x} + V_r \frac{\partial p}{\partial r} + V_\theta \frac{\partial p}{r\partial \theta} = 0 \tag{5.7}$$

or

$$(s - i)\, p_{si} + (r/a)\, v_{si} = 0 \tag{5.8}$$

Note that for a fully filled projectile, Equation (5.8) requires p_{si} to be zero for $r = b = 0$. Equation (5.8) can now be simplified by use of Equation (5.3).

For $r = b$

$$\left[(s^2 + 1)(s-3i) + 2i\right]p_{si} - (s - i)\, r \frac{\partial p_{si}}{\partial r} = 0 \tag{5.9}$$

An obvious solution to Eq. (5.1) which satisfies Eq. (5.5) is

$$p_{si} = -(s - i)^2(xr/a^2)\,\hat{K} \tag{5.10}$$

We, therefore, assume the general solution to be

$$p_{si} = -(c/a)\left[(s - i)^2(x/c)(r/a) + \sum R_k(r)X_k(\hat{x})\right]\,\hat{K} \tag{5.11}$$

Substitution of Eq. (5.11) in Eq. (5.1) shows that X_k is a linear combination of a sine and a cosine. Eq. (5.5) can be used to completely specify this combination* for small δ_c.

$$X_k = \cos(k\lambda\hat{x}), \quad k \text{ even} \tag{5.12}$$

$$= \sin(k\lambda\hat{x}), \quad k \text{ odd} \tag{5.13}$$

$$= 1, \quad k = 0 \tag{5.14}$$

where

$$\lambda \doteq (\pi/2)[1 + \delta_c]$$

Corresponding to these X_k's, Eq. (5.1) gives the general form of the R_k's. Eqs. (5.6) and (5.9) can then be used to completely specify the R_k's. In order to do this, x in Eqs. (5.6) and (5.11) must be replaced by a series in the X_k's. This is easy when the X_k's are orthogonal. Unfortunately, for δ_c not equal to zero the X_k's of Eqs. (5.12 - 5.13) are not orthogonal. We can, however, approximate x by a least squares fit to a truncated series in X_k.

$$\frac{x}{c} \simeq \sum_{k=0}^{N} a_k X_k(\hat{x}) \tag{5.15}$$

*See Appendix C for details. As can be seen there, our "obvious" solution is a special form of $X_0 R_0$ that satisfies the inhomogeneous form of Eq. (5.5). In general, inhomogeneous boundary conditions are not so friendly, and much more algebraic labor is required.

where

$$a_0 = h/c$$

$$a_k = 0 \text{ for } k \text{ even},$$

and a_k is computed in Appendix D for k odd. A first approximation for small δ_c is the usual orthogonal relation

$$a_k = b_k/b_{kk} \tag{5.16}$$

where

$$b_k = \int_{-1}^{1} \hat{x}\, \overline{X}_k(\hat{x})\, d\hat{x}$$

$$b_{kk} = \int_{-1}^{1} X_k\, \overline{X}_k\, d\hat{x}$$

p_{si} now assumes the slightly simpler form

$$p_{si} = -(c/a)\, \hat{K} \sum_{k=0}^{N} X_k(\hat{x}) \left[R_k(r) + (s-1)^2\, (r/a) a_k\right] \tag{5.17}$$

Equation (5.1) can now be used to get the general form* of the R_k's.

$$R_0 = (h/c) \left[E_0\, r/a + F_0\, a/r\right] \tag{5.18}$$

For k odd

$$R_k = a_k \left[E_k J_1(k\hat{r}/c) + F_k Y_1(k\hat{r}/c)\right] \tag{5.19}$$

* *See Appendix C for details.*

where

$$\hat{\lambda}^2 = - \left[\frac{s^2 - 2is + 3}{(s - i)^2} \right] \lambda^2$$

E_k, F_k are coefficients to be determined by boundary conditions,
J_n is a Bessel function of the first kind of order n,
Y_n is a Bessel function of the second kind of order n.

The radial functions $R_k(r)$ must satisfy boundary conditions (5.6) and (5.9). Direct substitution of Eq (5.17) in these equations yields the following conditions:

$$2i\ (1 + \delta_a)\ R_k(a) - \left[s - i\ (1 - 2\delta_a) \right]\ a\ R'_k(a) + (s - 1)\delta_a a^2\ R''_k(a) = 2a_k s\ (s - i)(s - 3i) \qquad (5.20)$$

$$\left[(s^2 + 1)(s - 3i) + 2i \right] R_k(b) - (s - i)\ b\ R'_k(b) = - a_k\ (b/a)\ s^2\ (s - i)^2\ (s - 3i) \qquad (5.21)$$

Equations (5.20 - 5.21) can be used to find E_0 and F_0 for specific values of (c/a), (b/a), and s. For non-zero k, $R_k(r)$ is a sum of Bessel functions with derivatives given by the following equations[15]:

$$rR'_k = (k\hat{\lambda}r/c)a_k \left[E_k J_0(k\hat{\lambda}r/c) + F_k Y_0\ (k\hat{\lambda}r/c) \right] - R_k \qquad (5.22)$$

$$r^2 R''_k = R_k \left[1 - (k\hat{\lambda}r/c)^2 \right] - rR'_k \qquad (5.23)$$

With these relations the boundary conditions (5.20 - 5.21) yield pairs of linear equations for E_k and F_k which can be quickly solved.

---

15. *N. W. McLachlan, Bessel Functions for Engineers, Oxford University Press, London, 1955.*

5. PRESSURE MOMENT

The major components of the liquid moment are due to the pressure on the lateral and end walls of the container. Lesser components are due to the viscous wall shear on the lateral and end walls. Thus the liquid moment coefficient can be given as a sum of four terms.

$$\tau C_{LM} = m_{p\ell} + m_{pe} + m_{v\ell} + m_{ve} \tag{6.1}$$

The sum of the first two terms is the pressure moment coefficient, m_p, and will be computed in this section. The wall shear moment coefficient will be computed in the next section.

By use of Eq. (3.5), we can express the fluctuating part of the inviscid pressure given by Eq. (3.13) as

$$\begin{aligned} \frac{\Delta p}{\rho_L a^2 \dot{\phi}^2} &= R\left\{\left[p_{si} - (rx/a^2)\hat{K}\right] e^{s\phi - i\theta}\right\} \\ &= R\left\{C_p e^{i\phi_p}\ \hat{K}\, e^{(s\phi - i\theta)}\right\} \end{aligned} \tag{6.2}$$

Equation (5.17) can now be used to give the following series for the pressure coefficient:

$$\begin{aligned} C_p e^{i\phi_p} &= -(c/a)\sum_{k=0}^{N} X_k(\hat{x})\left[R_k(r) + (s - 2i)s\,(r/a)a_k\right] \\ &= -(c/a)\sum X_k(\hat{x})\, C_{pk}(r) \end{aligned} \tag{6.3}$$

The pressure moment coefficient on the lateral wall can be computed by an integral of the real pressure over this wall, with the appropriate lever arm.

$$m_{p\ell} = i(c/a)(2\pi\hat{K})^{-1}\, e^{-s\phi} \int_{-1}^{1}\int_{0}^{2\pi} (\hat{x} + h/c)e^{i\theta}\, R\left\{C_p^* e^{s\phi - i\theta}\right\}_{r=a} d\theta\ d\hat{x}$$

$$= i(c/2a) \int_{-1}^{1} \hat{x}\, \left[C_p^*\right]_{r=a} d\hat{x} + (h/c)^2\, m_{p\ell h} \qquad (6.4)$$

where

$$m_{p\ell h} = i(c^2/2ah) \int_{-1}^{1} C_{p_0}(a)\, d\hat{x};\quad C_p^* = C_p \hat{K} e^{i\phi_p} + p_{sv}$$

Since the complex pressure dependence on $\hat{x}$ is a sum of sine functions, this integral can be easily evaluated.

The end wall pressure moment coefficient is the difference of two similar integrals on each end wall.

$$m_{pe} = -i\,(a/c)(2\pi\hat{K})^{-1}\, a^{-3}\, e^{-s\phi}\left[\int_{b}^{a}\int_{0}^{2\pi} e^{i\theta}\, R\left\{C_p \hat{K} e^{s\phi + i(\phi_p - \theta)}\right\} r^2 d\theta\, dr\right]_{\hat{x}=-1}^{\hat{x}=1}$$

$$= -i(a/2c)\, a^{-3} \int_{b}^{a} \left[e^{i\phi_p} C_p\right]_{x=-1}^{x=1} r^2\, dr \qquad (6.5)$$

This moment coefficient involves the integrals of Bessel functions but these particular integrals can be easily obtained in closed form.[15]

Stewartson[3] incorrectly used a complex Δp in his pressure integral and, therefore, his moment calculation lacks the ($\frac{1}{2}$) factors of Eqs. (6.4 - 6.5). Later he made a similar error of a factor of two in computing a complex direction cosine so that these cancelling errors give the correct yaw growth rates, ε_j. These yaw growth rates when modified by Wedemeyer[5] gave outstanding agreement with gyroscope measurements for large Reynolds numbers.

In order to compute the pressure moment coefficient, it is necessary to determine the parameters E_k and F_k from the boundary condition equations (5.20 - 5.21). For Stewartson's inviscid case ($\delta_a = 0$) and constant amplitude coning motion ($\epsilon = 0$) the conditions for the coefficients of the Bessel functions ($k \neq 0$) are*

$$c_{11} E_k + c_{12} F_k = 2\tau (\tau-1)(\tau-3) \tag{6.6}$$

$$c_{21} E_k + c_{22} F_k = (b/a) \tau^2 (\tau-1)^2 (\tau-3) \tag{6.7}$$

where the c_{ij} are given in Table 2 and are functions of the ratio of coning frequency to spin (τ), reduced fineness ratio ($f^* = c/ka$), and fill ratio f.

Table 2. Coefficients in the Equations (6.6, 6.7) That Determine E_k and F_k for $\delta_a = \epsilon = 0$

$$c_{11} = \left[(\tau - 1)\,\hat{\lambda}/f^*\right] J_1'(\hat{\lambda}/f^*) - 2J_1(\hat{\lambda}/f^*)$$

$$c_{12} = \left[(\tau - 1)\,\hat{\lambda}/f^*\right] Y_1'(\hat{\lambda}/f^*) - 2Y_1(\hat{\lambda}/f^*)$$

$$c_{21} = (\tau-1)(\hat{\lambda}/f^*)(b/a)\, J_1'(\hat{\lambda}b/f^*a) + \left[(\tau^2-1)(\tau-3)-2\right] J_1(\hat{\lambda}b/f^*a)$$

$$c_{22} = (\tau-1)(\hat{\lambda}b/f^*a)\, Y_1'(\hat{\lambda}b/f^*a) + \left[(\tau^2-1)(\tau-3)-2\right] Y_1(\hat{\lambda}b/f^*a)$$

$$\hat{\lambda}^2 = \left(\frac{\Pi}{2}\right)^2 \left[\frac{3 + 2\tau - \tau^2}{1 - 2\tau + \tau^2}\right]$$

The $k = 0$ mode is only present for liquid payload offset $h \neq 0$. This small moment term is included in the computer program. Since h is zero in all available experimental data, the zero mode will not be considered further in this report.

For fixed reduced fineness ratio and fill ratio, the determinant of Eqs. (6.6 - 6.7) is zero for certain values of τ which are the eigenvalues of the system, τ_{kn}. In the vicinity of these eigenvalues, the parameters E_k and F_k can be approximated as poles.

$$E_k = \frac{\hat{E}_k\ (\tau_{kn})}{\tau - \tau_{kn}} \tag{6.8}$$

$$F_k = \frac{\hat{F}_k\ (\tau_{kn})}{\tau - \tau_{kn}} \tag{6.9}$$

Spiral motions are represented by complex values of s while pure imaginary values of s correspond to constant amplitude coning motion. Eqs. (6.8 - 6.9) can now be extended to approximate the response to spiral motions in the vicinity of the eigenfrequencies since the parameters are analytic functions.

$$E_k = \frac{i\ \hat{E}_k\ (\tau_{kn})}{s - i\ \tau_{kn}} \tag{6.10}$$

$$F_k = \frac{i\ \hat{F}_k\ (\tau_{kn})}{s - i\ \tau_{kn}} \tag{6.11}$$

Stewartson assumed that near an eigenfrequency the pressure was dominated by that mode and computed the total pressure moment from that assumption.

$$m_p = \frac{[f^*\ R\ (f^*,\ f,\ \tau_{kn})]^2}{2\pi k^2\ (s - i\ \tau_{kn})} \tag{6.12}$$

Stewartson[3] and later authors[16, 17] have constructed tables of τ_{kn} and R as functions of f* and f.

A portion of one of these tables for a fully filled shell is given in Table 3. As can be seen from the table, R decreases rapidly with increasing n. Since the moment varies as R^2, eigenvalues for $n > 3$ are of little importance for estimating the liquid moment. Eq. (6.12) also shows the decay of the moment with increasing k values. For these reasons, our computer code only considers the first ten k modes (k = 1, 3, 5, ..., 19).

16. *B. G. Karpov, "Dynamics of Liquid-Filled Shell. Aids for Designers: (a) Milne's Graph; (b) Stewartson's Tables," BRL Memorandum Report 1477, May 1963. AD 410484.*

17. *J. T. Frasier, "Dynamics of Liquid-Filled Shell: Aids for Designers," BRL Memorandum Report 1892, December 1967. AD 665356.*

Table 3. f* and R for 100% Filled Cylinder (f = 1)

τ_{kn}	n = 1		n = 2		n = 3		n = 4	
	f*	R	f*	R	f*	R	f*	R
0	.9949	0	.4780	0	.3103	0	.2291	0
.01	1.0064	.0144	.4842	.00172	.3144	.00048	.2322	.00019
.02	1.0180	.0290	.4904	.00349	.3186	.00097	.2353	.00039
.03	1.0297	.0440	.4968	.00532	.3228	.00148	.2384	.00060
.04	1.0417	.0592	.5032	.00721	.3271	.00201	.2416	.00081
.05	1.0538	.0747	.5098	.00915	.3315	.00256	.2449	.00104
.06	1.0661	.0905	.5165	.01116	.3360	.00312	.2482	.00127
.07	1.0786	.1065	.5233	.01323	.3405	.00370	.2516	.00150
.08	1.0913	.1229	.5302	.01536	.3451	.00431	.2550	.00175
.09	1.1042	.1395	.5372	.01755	.3498	.00493	.2585	.00200
.10	1.1173	.1564	.5443	.01981	.3546	.00558	.2621	.00227
.11	1.1306	.1736	.5516	.02214	.3595	.00624	.2657	.00254
.12	1.1442	.1911	.5591	.02453	.3645	.00693	.2695	.00282
.13	1.1579	.2088	.5666	.02700	.3695	.00764	.2732	.00311
.14	1.1720	.2269	.5743	.02954	.3747	.00837	.2771	.00341
.15	1.1862	.2452	.5822	.03215	.3800	.00913	.2810	.00372
.16	1.2008	.2638	.5902	.03484	.3854	.00992	.2851	.00405
.17	1.2156	.2826	.5983	.03761	.3908	.01073	.2892	.00438
.18	1.2307	.3018	.6067	.04046	.3965	.01156	.2934	.00472
.19	1.2460	.3213	.6152	.04339	.4022	.01242	.2977	.00508
.20	1.2617	.3410	.6239	.04640	.4080	.01332	.3020	.00545
.21	1.2777	.3610	.6327	.04951	.4140	.01424	.3065	.00583
.22	1.2940	.3813	.6418	.05270	.4201	.01519	.3111	.00623
.23	1.3107	.4019	.6511	.05599	.4264	.01617	.3158	.00664
.24	1.3277	.4227	.6605	.05937	.4328	.01719	.3206	.00706
.25	1.3450	.4439	.6702	.06284	.4394	.01824	.3255	.00750
.26	1.3628	.4653	.6801	.06642	.4461	.01933	.3305	.00795
.27	1.3809	.4871	.6903	.07010	.4529	.02045	.3357	.00842
.28	1.3995	.5091	.7007	.07389	.4600	.02161	.3410	.00891
.29	1.4185	.5314	.7113	.07779	.4672	.02281	.3464	.00941
.30	1.4379	.5540	.7222	.08180	.4746	.02406	.3520	.00994

The major difficulty with the inviscid Stewartson eigenfrequency theory is that it predicts much too large liquid moments near the eigenfrequencies. Wedemeyer introduced a viscous boundary layer theory and sought to predict the resulting liquid moment by a simple manipulation of Stewartson's tables[5]. By a very clever approach, he showed that viscous eigenvalues, s_{kn}, could be computed from Stewartson's table of inviscid eigenfrequencies, τ_{kno}, by the relations

$$s_{kn} = (\epsilon_{kn} + i)\, \tau_{kn} \tag{6.13}$$

$$\tau_{kn} = \tau_{kno} + \Delta\tau_{kn} \tag{6.14}$$

where

$$\varepsilon_{kn}\,\tau_{kn} + i\Delta\tau_{kn} = i\left[\frac{\partial\tau_{kn}}{\partial f^*}\,(f^*\delta_a - k^{-1}\delta_c) + 2\,\frac{\partial\tau_{kn}}{\partial f}\,(f - 1)\,\delta_a\right]$$

He then replaced $i\tau_{kn}$ in the denominator of Eq. (6.12) with the s_{kn} of Eq. (6.13) to obtain an excellent approximation of the pressure moment for large Reynolds numbers.

The maximum value of the pressure side moment occurs for τ near the Stewartson eigenfrequency and is approximately

$$\left(C_{LSM}\right)_{max} = \frac{-(f^*R)^2}{2\pi k^2\,\tau_{kn}^{\,2}\left[\varepsilon_{kn} - \varepsilon\right]} \tag{6.15}$$

For $\varepsilon = 0$ and constant f* the maximum SW side moment coefficient varies inversely with $k^2\varepsilon_{kn}$ and, hence, it varies as $Re^{-\frac{1}{2}}$. Its dependence on k is somewhat more complicated since $k^{-1}\delta_c$ varies as k^{-2} for constant f*. The maximum side moment coefficient should vary with k by a factor between k^{-2} and unity.

Equations (6.3 - 6.5) have been coded for N = 19 by Bradley[18] and a number of computations made for a variety of values of c/a, f, and Re. To illustrate his results, a series of calculations have been made for τ_{k1} near .07, ε = 0, .02, and Re = 500,000 and 15,000. Table 3 shows that a suitable value of f* to obtain τ_{k1} near .07 is 1.08. For the first three k-modes, the corresponding fineness ratios, c/a, are 1.08, 3.24 and 5.40.

Figures 1 and 2 show the side moment for fineness ratio 1.08 at two Reynolds numbers. The ratio of the square roots of the two Reynolds numbers is 5.8 while the ratio of peak C_{LSM}'s for ε = 0 at the two Reynolds numbers is 5.6. Notice the strong sensitivity of the side moment to damping per cycle for the higher Reynolds number. This sensitivity is considerably reduced for R_e of 15,000.

Figures 3-4 show similar curves for a fineness ratio of 3.24. The maximum side moment for the higher Reynolds number is reduced by a factor of 5 from that of Figure 1. Since k is 3, the predicted range of this factor is 1 to 9. The sensitivity to damping per cycle is quite similar to that shown by Figures 1-2.

18. *J. W. Bradley, "Calculations of Liquid Payload Moment," BRL Memorandum Report in preparation.*

Finally, Figures 5-6 show the side moment for a fineness ratio of 5.40. Here the reduction of peak side moment in Figure 5 relative to Figure 1 is by a factor of 12, which also lies in the predicted range of 1 to 25. The dependence on damping per cycle and Reynolds number is quite similar to that of the preceding figures.

Since the in-plane moment only affects frequency, it is of much less interest than the side moment. It is, of course, available from Eqs. (6.3 - 6.5). Figure 7 is an example of the in-plane moment coefficient for a Reynolds number of 500,000 and fineness ratio of 3.24. For zero τ, it is quite near the frozen value of $\frac{1}{2}$, undergoes a disturbance near the eigenfrequency, and asymptotically approaches zero.

The side moment has contributions from the two flat endwalls as well as from the cylindrical lateral wall. The ratio of the two contributions is shown in Figures 8-9 for the two Reynolds numbers of 500,000 and 15,000. We see that these contributions are opposing and roughly equal. Indeed for a fineness ratio of 1.08 (k = 1) the lateral contribution is only 20% larger in magnitude than the endwall contribution! Thus the side moment is the difference of two nearly equal quantities, and a small change on one wall could have a large effect on the side moment.

7. WALL SHEAR MOMENT

In addition to the pitch and yaw moment due to pressure on the walls of the liquid container, moments due to viscous wall shear are present. These can be computed from the derivatives of the viscous velocity components of Section 4. The liquid moment coefficient due to shear on the cylindrical lateral wall is

$$m_{v\ell} = (2\pi\hat{K}\,Re)^{-1}\, e^{-s\phi} \int_{-1}^{1}\int_{0}^{2\pi} e^{i\theta}\, m^*_{v\ell}\, d\theta\, d\hat{x} \qquad (7.1)$$

where

$$m^*_{v\ell} = aR\left\{\frac{\partial u_{sv}}{\partial r}\, e^{s\phi} - i\theta\right\} - ix\,R\left\{\frac{\partial w_{sv}}{\partial r}\, e^{s\phi} - i\theta\right\}$$

Equation (7.1) simplifies to

$$m_{v\ell} = (2\hat{K}\,Re)^{-1}\int_{-1}^{1}\left[ia\,\frac{\partial u_{sv}}{\partial r} + c\hat{x}\,\frac{\partial w_{sv}}{\partial r}\right]_{r=a} d\hat{x} + (h/c)^2\, m_{v\ell h} \qquad (7.2)$$

where

$$m_{v\ell h} = (2\hat{K}\,Re)^{-1}(c^2/h)\int_{-1}^{1}\left[\frac{\partial w_{sv}}{\partial r}\right]_{r=a} d\hat{x}$$

The velocity derivatives in Eq. (7.2) can be computed from Eqs. (4.9 - 4.10) and the resulting equation has been coded by Bradley.[18]

The wall shear moment coefficient on the forward flat end wall is

$$m_{vel} = (2\pi\hat{K}\ Re)^{-1}\ e^{-s\phi}\ (ac)^{-1}\int_b^a\int_0^{2\pi} e^{i\theta} m^*_{vel}\, r\ d\theta\ dr \qquad (7.3)$$

where

$$m^*_{vel} = (h + c)\left[R\left\{\frac{\partial w_{sv}}{\partial x}\, e^{s\phi} - i\theta\right\} - iR\left\{\frac{\partial v_{sv}}{\partial x}\, e^{s\phi} - i\theta\right\}\right]_{\hat{x} = 1}$$

A similar expression applies for the rearward endwall. The sum of these moment coefficients has the simple form:

$$m_{ve} = (2a\hat{K}\ Re)^{-1}\int_b^a\left[\frac{\partial}{\partial x}\,(w_{sv} - iv_{sv})\right]_{\hat{x} = -1}^{\hat{x} = 1} rdr + (h/c)^2\, m_{veh} \qquad (7.4)$$

where

$$m_{veh} = (2\hat{K}\ Re)^{-1}\ (c/ah)\int_b^a\left[\frac{\partial}{\partial x}\,(w_{sv} - iv_{sv})_{\hat{x} = 1} + \frac{\partial}{\partial x}\,(w_{sv} - iv_{sv})_{\hat{x} = -1}\right] rdr$$

The velocity derivatives in Equation (7.4) can be found by use of Equation (4.17) and the results have also been coded by Bradley.[18]

Since all the velocity derivatives are proportional to δ_a^{-1} and δ_a is proportional to $Re^{-\frac{1}{2}}$, the viscous liquid moment coefficient itself varies as $Re^{-\frac{1}{2}}$ and is important for low Reynolds number. In Figure 10 the wall shear side moment coefficient is given for Re = 15,000 and our three sample fineness ratios. Comparing this component with the pressure-induced liquid side moment coefficients of Figures 2, 4, and 6, we see that the maximum wall shear component is from 10% to 35% of the wall pressure component.

In Figures 11-13, the total side moment coefficients for Re = 1,000 and ϵ = 0 are compared with their pressure components for c/a = 1.08, 3.24, and 5.40. The differences between these curves are the wall shear components and we see that these components are quite important and must be computed for low Reynolds flows.

D'Amico and Miller show a very interesting effect of very low Reynolds numbers[19]. In a special gyroscope experiment[20], Miller forced a spinning cylinder filled with liquid to precess at an angle of 20° and measured the despin moment. The fineness ratio was 4.29, τ varied between .12 and .25, and liquids with kinematic viscosities varying between 1 and 10^6 centistokes were tested. As can be seen from Figure 14, the despin moment varied from a small value for water (ν = 1 cs) to a value thirty times bigger for corn syrup ($\nu = 2 \times 10^5$ cs). The Reynolds number of this peak was about 10.

D'Amico and Miller conjectured that this large despin moment would be associated with a large side moment which would produce flight instabilities. Flight tests were made and this otherwise unexpected instability was observed. We now can use the theory of this report to estimate the liquid side moment for Miller's cylinder and Reynolds number as low as 100, which is probably the extreme lower bound of validity of a boundary layer theory.

In Figure 15a, C_{LSM} is plotted versus τ for Miller's cylinder with $Re = 10^6$. The four local maxima on these curves are caused by four eigenfrequencies, τ_{nk}. By use of Table 3 these eigenfrequencies can be identified. In order of increasing τ their (k, n) mode numbers are (15, 4), (11, 3), (7, 2) and (13, 4). As we would expect, the largest maximum has n = 2 while the two quite small maxima have n = 4.

In Figures 15b--15e, C_{LSM} is computed for $Re = 10^5, 10^4, 10^3, 10^2$. The first effect of decreasing Reynolds number is to decrease the size of the maxima associated with the eigenfrequencies. Next we see that the average level of the side moment coefficient curves increases with decreasing Reynolds number. In Figure 16, C_{LSM} is plotted versus Re for τ = .10, .15, .20, .25. To facilitate comparison of these curves, we normalized each side moment coefficient by its values at $Re = 10^6$. We see that the side moments increase to maximum values 18 - 33 times their values for water and these maxima occur around Re = 300. This striking qualitative agreement with the D'Amico-Miller conjecture is very exciting, and theoretical work on predicting the despin moment at low Reynolds number is being given a much greater emphasis as a result.

19. *W. P. D'Amico and M. C. Miller, "Flight Instability Produced by a Rapidly Spinning, Highly Viscous Liquid," Journal of Spacecraft and Rockets, Vol. 16, January-February 1979, pp. 62-64.*

20. *M. C. Miller, "Flight Instabilities of Spinning Projectiles Having Nonrigid Payloads," Journal of Guidance, Control, and Dynamics, Vol. 5, pp. 151-157, March-April 1982.*

8. EXPERIMENTAL RESULTS

In 1980 the first wall pressure measurements in a precessing and spinning liquid-filled cylinder were made by Whiting[21]. For the 100% filled cylinder, he compared his measurements with theoretical calculations by Gerber et al[22]. Gerber's theory was developed for fully-filled cylinders only and was used to compute the viscous influence of the lateral wall exactly without the use of a boundary layer approximation. Its results for fully-filled cylinders should, therefore, be better than that of this report when they differ. For the Reynolds numbers of the Whiting tests, they did not differ significantly; and thus, the good experimental agreement Whiting got for Gerber's calculations also applies to our theory. In two cases, however, Whiting measured the pressure on the flat end wall of a partially-filled cylinder (f = .92). Comparisons of these measurements with the theoretical prediction of Equation (6.3) is given in Figures 17a-17b. The agreement with theory is quite satisfactory.

In most gyroscope experiments[6,23] the yaw growth rates and coning rates are measured for a variety of test conditions. In all experiments the center of mass is located at the pivot point so that the gyroscopic stability factor is infinitely large and Equations (2.16, 2.18) for frequency and damping become:

$$\tau = \sigma \left[1 + \left(m_L a^2 / I_x \right) C_{LIM} \right] \doteq \sigma \qquad (8.1)$$

$$\varepsilon = \left(m_L a^2 / I_x \right) \left(2\tau/\sigma - 1 \right)^{-1} C_{LSM}(\tau, \varepsilon) \qquad (8.2)$$

We first consider D'Amico and Rogers'[23] measurements for a cylinder with fineness ratio of 1.042 for which $\tau_{11} = .040$. The frequency was changed by varying I_y and measurements were made for Reynolds numbers of 12,400 and 2,400. Comparisons of theory with these data are shown in Figures 18a-18b. Agreement is fair, but there appears to be a systematic bias. Theoretical curves for different fineness ratios in steps of .001 were computed and the best fits are shown as dashed curves for c/a = 1.047 and 1.048 in the respective figures. An effective fineness ratio .5% greater than the measured value is not unreasonable and gives excellent experimental agreement. Figure 19 compares the complete side moment coefficient with pressure side moment coefficient and its Stewartson-Wedemeyer approximation for c/a = 1.048 and Re = 2400, and we see

21. *R. D. Whiting, "An Experimental Study of Forced Asymmetric Oscillations in a Rotating Liquid-Filled Cylinder," BRL Technical Report ARBRL-TR-02379, October 1981. AD A107948.*

22. *N. Gerber, R. Sedney, and J. M. Bartos, "Pressure Moment on a Liquid-Filled Projectile: Solid Body Rotation," BRL Technical Report in press.*

23. *W. P. D'Amico and T. H. Rogers, "Yaw Instabilities Produced by Rapidly Rotating, Highly Viscous Liquids," AIAA Paper No. 81-0284, January 1981.*

that the complete moment coefficient which gave such excellent experimental agreement is quite different from the other more approximate curves.

The remaining three sets of experiments are summarized by Whiting and Gerber[6], and all involve very similar fineness ratios; i.e., c/a = 3.149, 3.013, 3.077. The Stewartson eigenfrequency for the first set, which was the only one that had 100% filled cylinders, is $\tau_{31} = .047$. The appropriate eigenfrequency for the other two is τ_{31}, but the proper values cannot be obtained from Table 3.

In the first two sets of experimental data presented by Whiting and Gerber, the frequency was changed by varying I_x and I_y. For this procedure, Equation (8.2) gives ε as a function of τ and I_x and thus a simple theoretical curve cannot be plotted. What was done was to compute theoretical values for each experimental pair of values (τ, I_x), plot these values as points in Figures 20a-b and 21a-d and connect the points with straight lines. An examination of these figures shows fair to good agreement between theory and experiment. It is interesting to note that agreement with experiment for Re = 520,000 (Fig. 20a) can be considerably improved by a 0.1% change in fineness ratio. The side moment coefficients for the lowest Reynolds number of each set (namely, 9000 and 5200) are given in Figures 22-23.

In the final experiment to be considered, the fill ratio, f, was varied and the frequencies and yaw damping rates were measured. Here, too, the theoretical yaw damping rate is a function of two variables - fill ratio and frequency - and must be represented by individually computed points connected by line segments. Although the agreement for Re = 520,000 given in Figure 24a is quite good, the situation for Re = 5,200 in Figure 24b is poor.

9. CENTRAL ROD

In 1969 Frasier[7,8] extended the SW theory to the fully-filled cylinder with a central rod. This had the effect of replacing the free surface boundary condition of Eq. (5.8) with an inner lateral surface condition of the same form as the outer lateral surface (Eqs. (4.9 - 11)). For a rod with radius d, these conditions are

$$w_{sv} = \left[(1 + is)(x/a)\,\hat{K} - w_{si}\right] e^{-(r - d)/a\delta_a} \tag{9.1}$$

$$u_{sv} = -\left[(i - s)(d/a)\,\hat{K} + u_{si}\right] e^{-(r - d)/a\delta_a} \tag{9.2}$$

For $r = d$,

$$v_{si} + a\delta_a \frac{\partial v_{si}}{\partial r} = (i - s)(x/a)\,\hat{K} \tag{9.3}$$

Equation (9.3) can be used to derive an inner boundary condition to substitute for Eq. (5.21).

$$2i\,(1 - a\delta_a/d)\,R_k(d) - \left[s - i\,(1 + 2a\delta_a/d)\right] d\,R'_k(d)$$

$$- (s - 1)\,\delta_a\, adR''(d) = 2(d/a)\,a_k s\,(s - i)(s - 3i) \quad (9.4)$$

Using boundary conditions (5.20) and (9.4) for $\delta_a = 0$, Frasier and Scott[7] calculated tables of inviscid eigenfrequencies, τ_{nk}.

These frequencies are functions of the reduced fineness ratio and rodded fill ratio f_d.

$$\tau_{kn} = \tau_{kn}\,(f^*, f_d) \quad (9.5)$$

where

$$f_d = 1 - d^2/a^2$$

The revised Wedemeyer relation for the viscous eigenvalue is simply

$$s_{kn} = (\epsilon_{kn} + i)\,\tau_{kn} \quad (9.6)$$

where

$$\epsilon_{kn}\,\tau_{kn} + i\Delta\tau_{kn} = i\left[\frac{\partial\tau_{kn}}{\partial f^*}\,(f^*\delta_a - k^{-1}\delta_c) - 2\frac{\partial\tau_{kn}}{\partial f_d}\,(d/a)(1 + d/a)\,\delta_a\right]$$

Table 4 is a sample table of τ_{kn}, f^*, and R for $f_d = .98$ $(d/a = .14)$. A similar table of τ_{kn}, f^*, and R for fill ratio (f) of .98 is given as Table 5 for comparison purposes.

Two more moment coefficient terms must be added to Eq. (6.1). These are due to the pressure on the rod, m_{pr}, and the wall shear on the rod, m_{vr}.

Table 4. f* and R for Cylinder With Rod (f_d = .98)

τ_{kn}	n = 1		n = 2		n = 3		n = 4	
	f*	R	f*	R	f*	R	f*	R
.00	.9028	.0000	.4102	.00000	.2615	.00000	.1921	.00000
.01	.9141	.0127	.4160	.00092	.2652	.00039	.1948	.00008
.02	.9256	.0257	.4219	.00189	.2690	.00080	.1975	.00017
.03	.9373	.0389	.4279	.00290	.2728	.00122	.2003	.00027
.04	.9491	.0525	.4339	.00395	.2766	.00165	.2031	.00036
.05	.9611	.0664	.4401	.00505	.2806	.00210	.2059	.00046
.06	.9733	.0806	.4464	.00620	.2846	.00257	.2089	.00057
.07	.9856	.0951	.4528	.00740	.2887	.00305	.2118	.00068
.08	.9981	.1100	.4593	.00865	.2929	.00355	.2149	.00079
.09	1.0109	.1251	.4659	.00995	.2971	.00407	.2180	.00091
.10	1.0238	.1405	.4726	.01130	.3015	.00461	.2211	.00103
.11	1.0369	.1562	.4795	.01271	.3059	.00516	.2244	.00116
.12	1.0503	.1723	.4865	.01418	.3104	.00574	.2276	.00130
.13	1.0638	.1886	.4936	.01571	.3150	.00633	.2310	.00144
.14	1.0776	.2053	.5009	.01729	.3197	.00694	.2344	.00159
.15	1.0916	.2223	.5083	.01894	.3245	.00758	.2379	.00174
.16	1.1059	.2395	.5159	.02066	.3294	.00824	.2415	.00190

Table 5. f* and R for 98% Filled Cylinder (f = .98)

τ_{kn}	n = 1		n = 2		n = 3		n = 4	
	f*	R	f*	R	f*	R	f*	R
.00	.9942	.0000	.4753	.00000	.3053	.00000	.2224	.00000
.01	1.0057	.0144	.4814	.00171	.3094	.00047	.2254	.00018
.02	1.0173	.0290	.4877	.00346	.3135	.00095	.2284	.00037
.03	1.0291	.0439	.4940	.00527	.3176	.00145	.2315	.00057
.04	1.0410	.0591	.5005	.00713	.3219	.00197	.2346	.00077
.05	1.0532	.0746	.5070	.00904	.3262	.00250	.2378	.00098
.06	1.0656	.0904	.5137	.01100	.3307	.00306	.2410	.00119
.07	1.0781	.1064	.5205	.01302	.3352	.00363	.2443	.00141
.08	1.0909	.1227	.5275	.01510	.3398	.00423	.2477	.00164
.09	1.1039	.1393	.5346	.01724	.3444	.00484	.2511	.00188
.10	1.1171	.1562	.5418	.01944	.3492	.00548	.2547	.00212
.11	1.1306	.1733	.5492	.02170	.3541	.00614	.2583	.00237
.12	1.1443	.1907	.5567	.02402	.3591	.00682	.2619	.00263
.13	1.1583	.2084	.5644	.02641	.3642	.00752	.2657	.00290
.14	1.1725	.2264	.5722	.02887	.3694	.00825	.2695	.00318
.15	1.1871	.2447	.5802	.03139	.3747	.00901	.2734	.00347
.16	1.2019	.2632	.5884	.03399	.3802	.00979	.2774	.00376

$$m_{pr} = -i(cd/2a^2)\int_{-1}^{1} \hat{x}\left[e^{i\phi_p} C_p\right]_{r=d} d\hat{x} + (h/c)^2\, m_{prh} \tag{9.7}$$

$$m_{vr} = -(2\hat{K}\,Re)^{-1}(d/a)\int_{-1}^{1}\left[id\frac{\partial u_{sv}}{\partial r} + c\hat{x}\frac{\partial w_{sv}}{\partial r}\right]_{r=d} d\hat{x}$$

$$+ (h/c)^2\, m_{v\ell h} \tag{9.8}$$

where

$$m_{prh} = -i(dc^2/2a^2h)\int_{-1}^{1} e^{i\phi_p} C_{po}(d)\, d\hat{x}$$

$$m_{v\ell h} = -(2\hat{K}\,Re)^{-1}(dc^2/ah)\int_{-1}^{1}\left[\frac{\partial w_{sv}}{\partial r}\right]_{r=d} d\hat{x}$$

Frasier ran gyroscopic experiments for a rodded cylinder with c/a = 2.864, f_d = .977 (d/a = .15) and three Reynolds numbers. Figures 25a - 25c show his data and the improved SW theoretical prediction. The agreement is rather good although the peak C_{LSM} is not predicted very well. In Figure 26 the side moment coefficient for f_d = .977 is compared with that for f = .977. The side moment for rodded cavity shows an eigenfrequency* at .059 while that for partially-filled cavity shows no eigenfrequencies and is a small negative value. Thus, we see that the presence of an inner cylindrical wall can have a very strong effect on the side moment. The insertion of a cylindrical partition to improve the stability of liquid-filled shell has been proposed by Frasier and D'Amico[5], and D'Amico[24] has experimentally studied the side moment during transition from a free surface to a fully-wetted central rod.

---

24. *W. P. D'Amico, "Dynamics of Liquid Filled Shell: Liquid-Central Burster Interference," BRL Memorandum Report 1985, June 1969. AD 855134.*

* *According to Table 4, τ_{31} is .045 for f_d = .980 and we would identify this peak at .059 in Fig. 26 to be caused by τ_{31}.*

10. OTHER THEORETICAL EXTENSIONS

The extended SW theory of this report has a number of restrictions. Some of these restrictions have been relaxed by the work of a number of researchers. These restrictions include those requiring: (1) a single liquid filler; (2) a centrally located circular cylinder container; (3) small amplitude motion; (4) steady-state motion; and (5) fully spun-up liquid. In this section we will survey the work in these five areas.

10.1 Single Liquid Filler

In 1972 Scott[25] considered the eigenfrequencies for an inviscid two-component liquid. He included the possibility of partial fill, computed eigenfrequencies, and got fair experimental agreement.

10.2 Centrally Located Circular Cylinder Container

Scott[26] also considered the inviscid eigenfrequencies and moments for eccentrically located fully filled circular cylinders and showed that these frequencies and moments are the same as those for a centrally located cylinder. In an earlier work Wedemeyer[27] derived an approximate relation for inviscid eigenfrequencies of a slightly noncylindrical cavity. He showed that the Stewartson eigenfrequency tables could be used through the use of an average fineness ratio.

$$(c/a)_{av} = c \int_{-1}^{1} \frac{d\hat{x}}{a(\hat{x})} \tag{10.1}$$

Karpov[28] made a number of gyroscope experiments that showed good results for this Wedemeyer concept.

25. *W. E. Scott, "The Inertial Wave Frequency Spectrum in a Cylindrically Confined, Inviscid, Incompressible, Two Component Liquid," BRL Report 1609, September 1972. AD 752439.*

26. *W. E. Scott, "The Dynamical Effect of Inertial Waves on the Free Flight Motion of a Body Containing Several Eccentrically Located, Liquid-Filled Cylinders," BRL Report 1551, September 1971. AD 733365.*

27. *E. H. Wedemeyer, "Dynamics of Liquid Filled Shell: Non-Cylindrical Cavity," BRL Report 1326, August 1966. AD 489899.*

28. *B. G. Karpov, "Dynamics of Liquid-Filled Shell: Resonance in Modified Cylindrical Cavities," BRL Report 1332, August 1966. AD 804825.*

10.3 Small Amplitude Motion

Gyroscope experiments by Scott and D'Amico[29] have shown that the yaw growth rate changes from the linear SW values at coning angles as low as 1°. Indeed, pressure coefficient measurements by Whiting[21] have shown nonlinearities for coning angles as low as .05°!! The Scott-D'Amico data also showed a shift in eigenfrequency for coning angles in excess of 1°. Scott[30] later derived a modified fineness ratio that was fairly good in predicting this frequency shift.

10.4 Steady-State Motion

D'Amico et al[14] made liquid pressure coefficient measurements on the endwall of a spinning cylinder whose coning motion was impulsively started and found that cone-up time for the pressure coefficient to reach the steady-state SW value could be as large as five seconds. He made an estimate of this time from the real part of the appropriate s_{kn} and found good agreement. Since these cone-up times are a significant part of a projectile's flight time, work in this important area is continuing.

10.5 Fully Spun-Up Liquid

This area has received much more attention than that given to the preceding four areas. Wedemeyer[31] developed a very simple model of the spin-up process which was extended by Kitchens et al[32,33]. Spin-up times greater than the cone-up times have been predicted and measured. Karpov[34] made use of Wedemeyer's suggestion to obtain an estimate of the effect of spin-up on the liquid side moment. This very approximate result is now being

29. *W. E. Scott and W. P. D'Amico, "Amplitude-Dependent Behavior of a Liquid-Filled Gyroscope," Journal of Fluid Mechanics, Vol. 60, Part 4, 1973, pp. 751-758.*

30. *W. E. Scott, "The Large Amplitude Motion of a Liquid-Filled Gyroscope and the Non-Interaction of Inertial and Rossby Waves," Journal of Fluid Mechanics, Vol. 72, Part 4, 1975, pp. 649-660.*

31. *E. H. Wedemeyer, "The Unsteady Flow Within a Spinning Cylinder," Journal of Fluid Mechanics, Vol. 20, Part 3, 1964, pp. 383-399. (See also BRL Report 1225, October 1963, AD 431946.)*

32. *C. W. Kitchens, Jr., "Ekman Compatibility Conditions in Wedemeyer Spin-Up Model," Physics of Fluids, Vol. 23, Part 5, May 1980, pp. 1062-1064.*

33. *C. W. Kitchens, Jr., N. Gerber, and R. Sedney, "Spin Decay of Liquid-Filled Projectiles," Journal of Spacecraft and Rockets, Vol. 15, November-December 1978, pp. 348-354. (See also BRL Report 1995, July 1977, AD A043875 and BRL Report 2026, October 1977, AD A050311.)*

34. *E. G. Karpov, "Dynamics of Liquid-Filled Shell: Instability During Spin-Up," BRL Memorandum Report 1629, January 1965. AD 463926.*

replaced by the current efforts of Sedney et al[13,22] to develop a very refined perturbation analysis for computing the liquid side moment during spin-up. The only direct pressure measurements during spin-up have been made by Aldridge[35,36], and these were for the simple case of axisymmetric oscillations and not the three-dimensional oscillation induced by coning motion.

11. SUMMARY

1. A general definition of the liquid moment has been developed, and the expression for frequencies and damping of projectile angular motion has been obtained.

2. An exact pressure moment has been computed for the Stewartson-Wedemeyer theory.

3. Wall shear effects have been added to the improved SW pressure moment.

4. The improved theory shows a decrease in the size of eigenfrequency-associated peaks in the side moment with decreasing Reynolds number.

5. The average level of the side moment, however, grows with decreasing Reynolds number to a peak, in good qualitative agreement with the D'Amico-Miller conjecture.

6. Good agreement with all available published experimental data has been shown.

ACKNOWLEDGEMENT

All of the figures of this report and their associated computer coding have been prepared by the very capable and mathematically sophisticated J. W Bradley. The author is very much indebted to Mr. Bradley for this unique effort as well as for the characteristic wit and intellectual insight he provided during many discussions of the material of this report.

35. *K. D. Aldridge, "Experimental Verification of the Inertial Oscillations of a Fluid in a Cylinder During Spin-Up," BRL Contract Report 273, November 1975, AD A018797.*

36. *K. D. Aldridge, "Axisymmetric Inertial Oscillations of a Fluid in a Cylindrical Cavity During Spin-Up from Rest," Geophys. Astrophys. Fluid Dynamics, Vol. 8, 1977, pp. 279-301.*

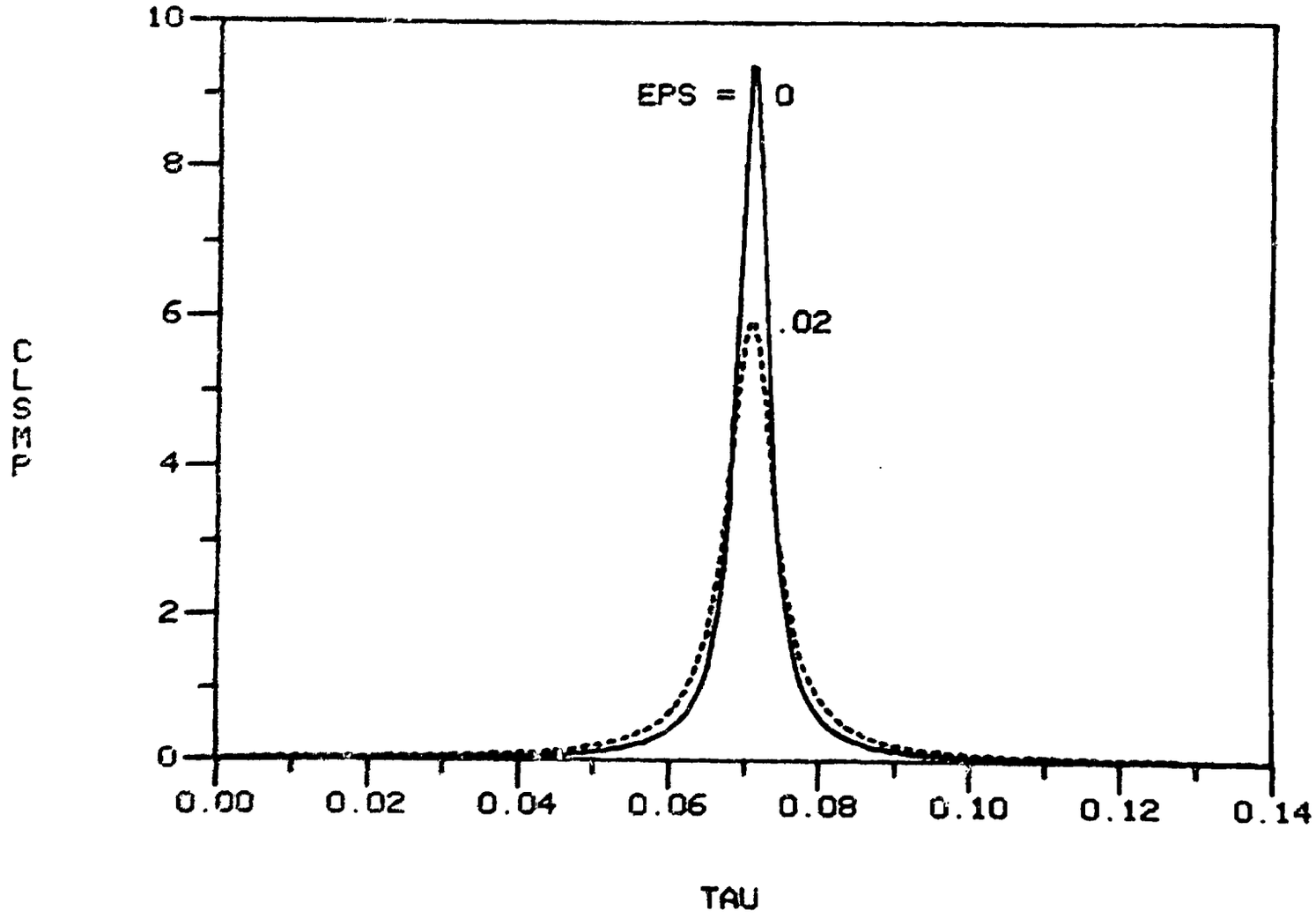

Figure 1. The Pressure Component of C_{LSM} vs τ for Re = 500,000, c/a = 1.08, f = 1, ϵ = 0 and .02

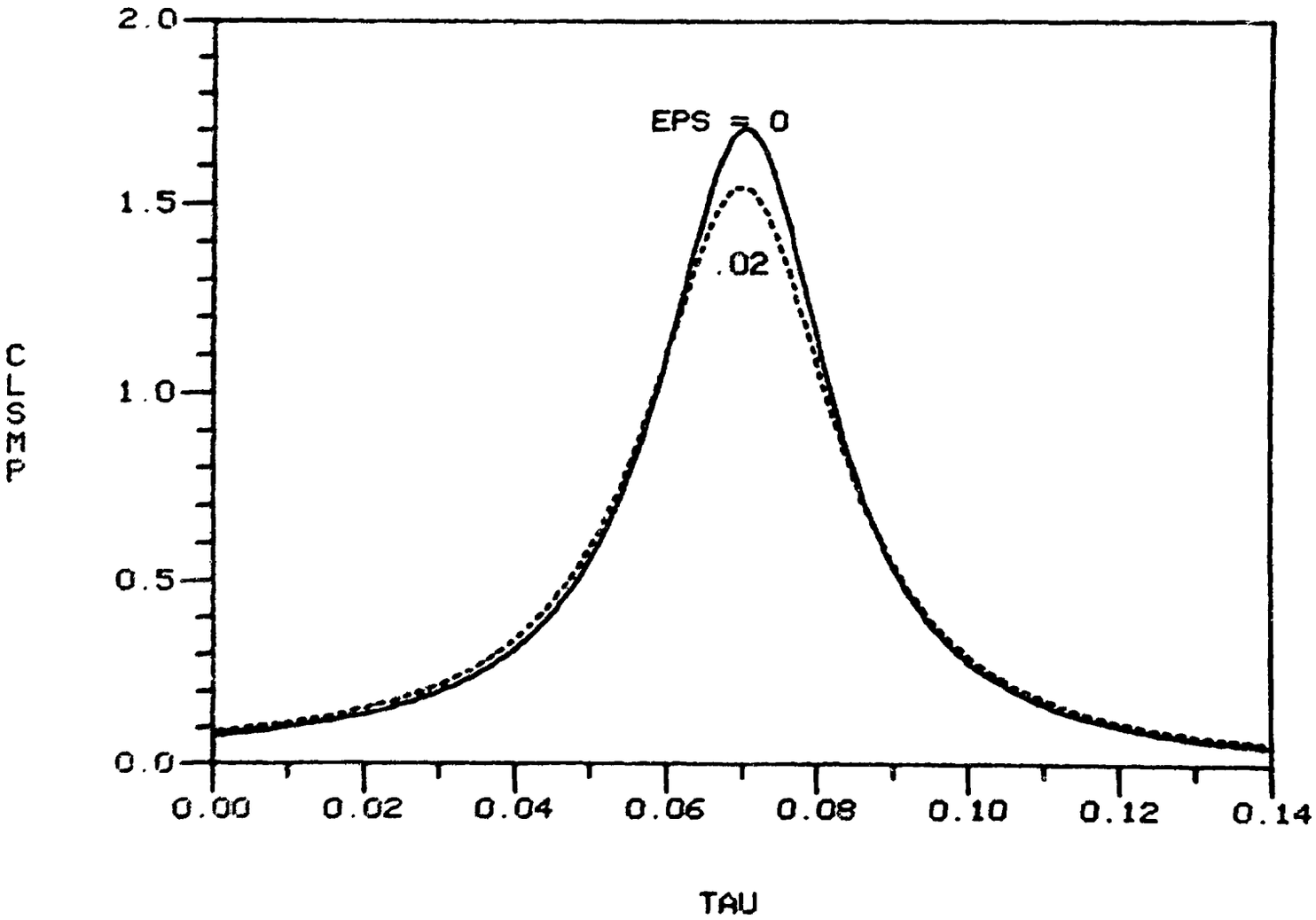

Figure 2. The Pressure Component of C_{LSM} vs τ for Re = 15,000, c/a = 1.08, f = 1, ϵ = 0 and .02

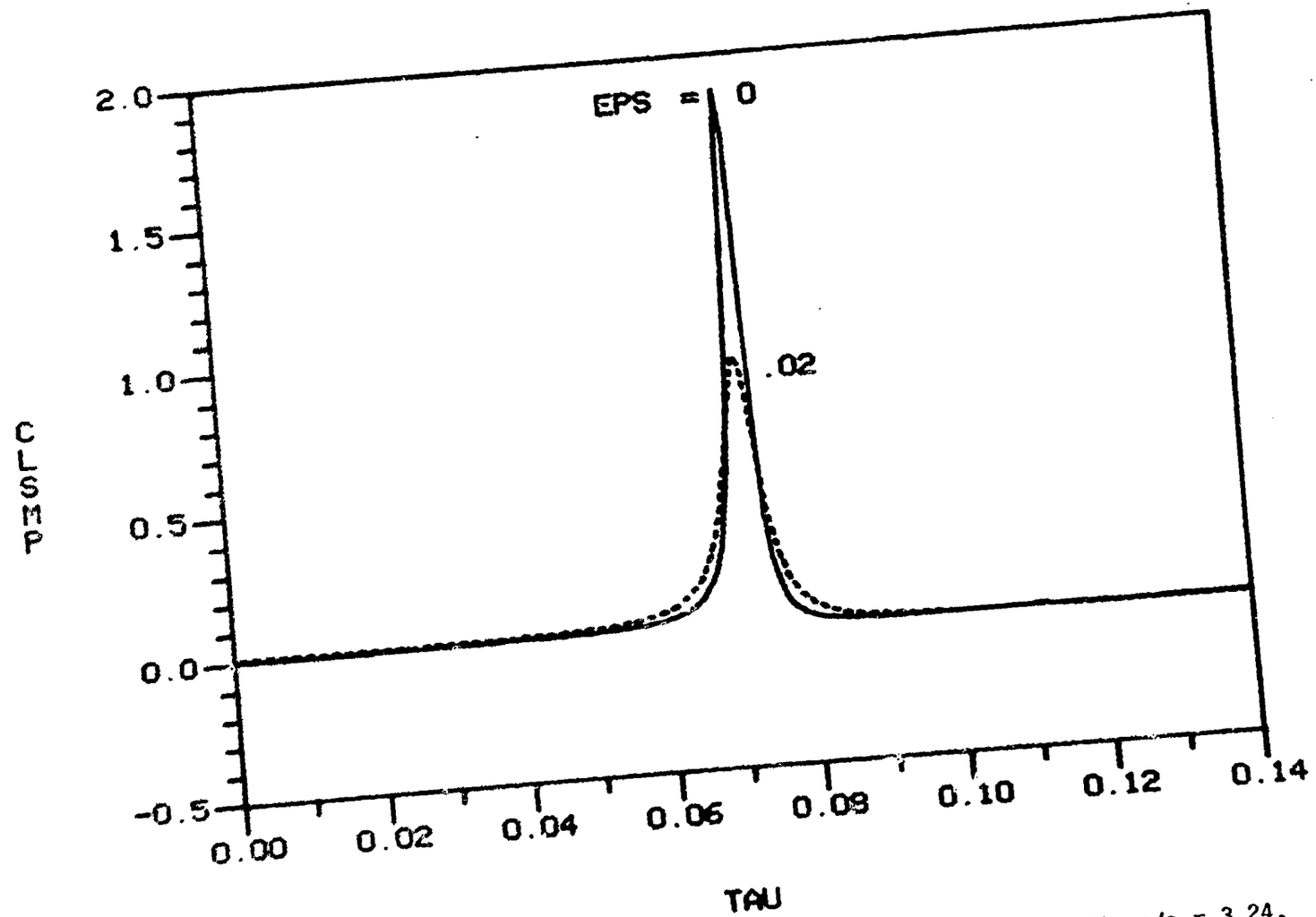

Figure 3. The Pressure Component of C_{LSM} vs τ for Re = 500,000, c/a = 3.24, f = 1, ϵ = 0 and .02

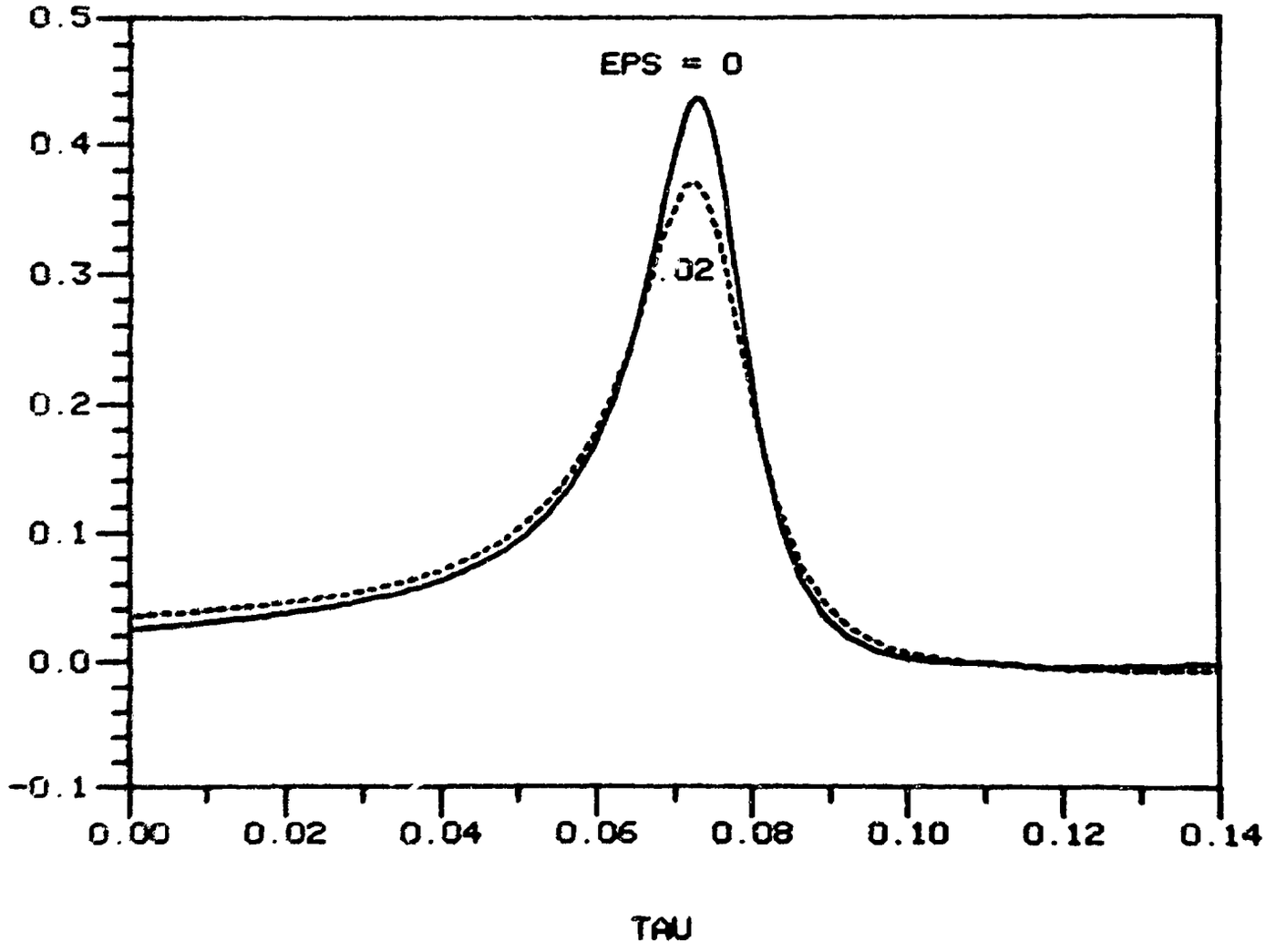

Figure 4. The Pressure Component of C_{LSM} vs τ for Re = 15,000, c/a = 3.24, f = 1, ε = 0 and .02

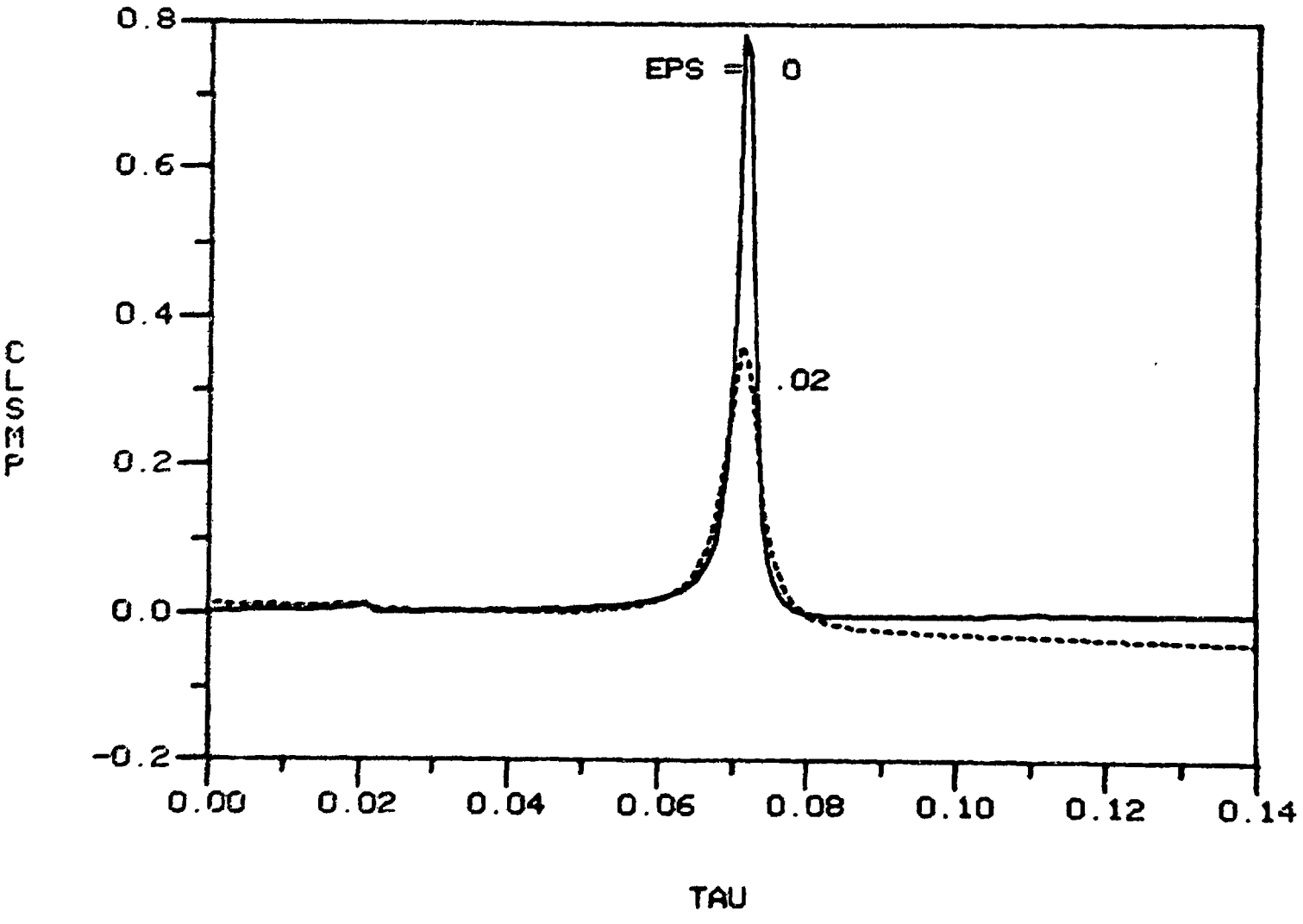

Figure 5. The Pressure Component of C_{LSM} vs τ for Re = 500,000, c/a = 5.40, f = 1, ϵ = 0 and .02

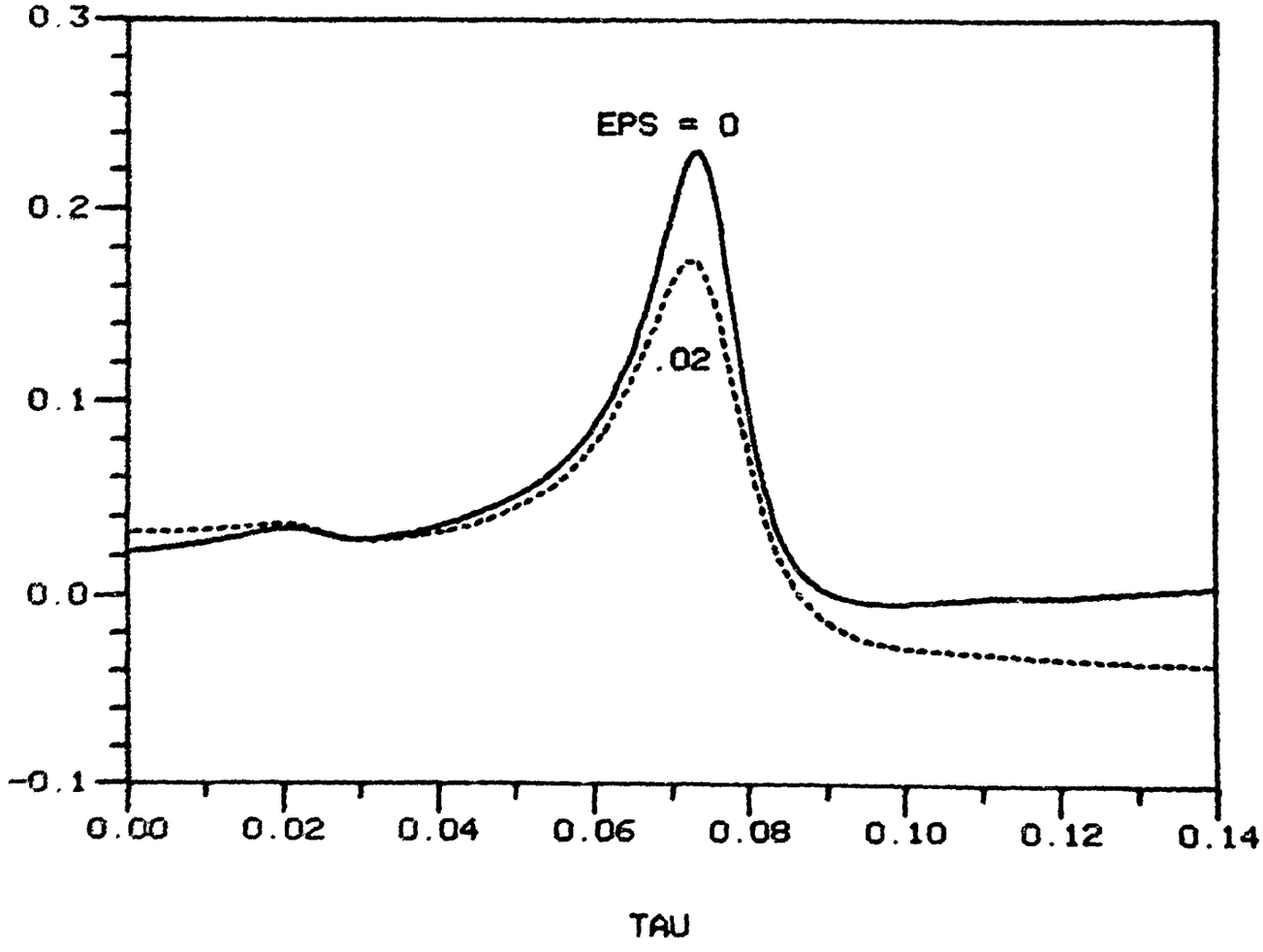

Figure 6. The Pressure Component of C_{LSM} vs τ for Re = 15,000, c/a = 5.40, f = 1, ϵ = 0 and .02

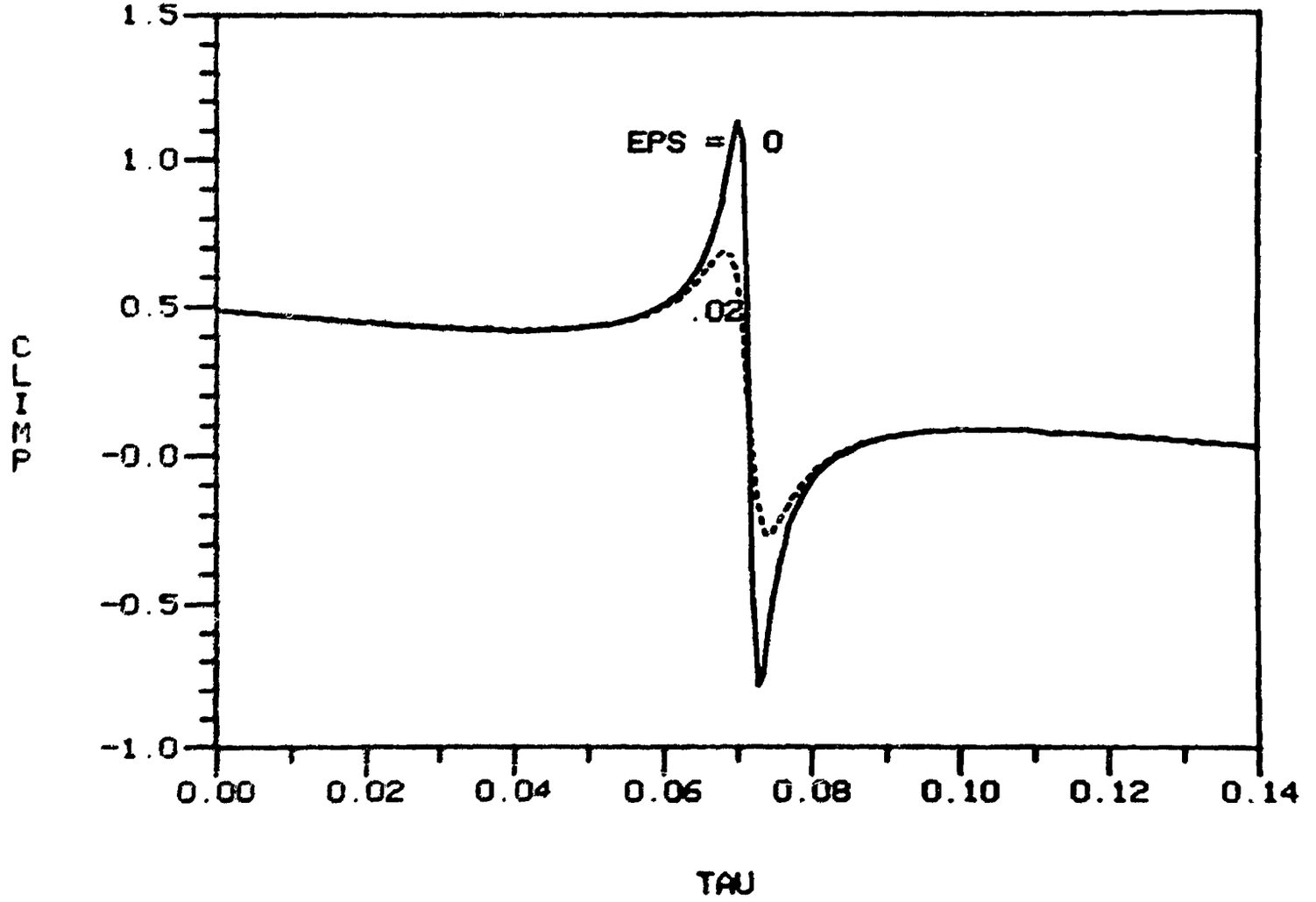

Figure 7. The Pressure Component of C_{LIM} vs τ for Re = 500,000, c/a = 3.24, f = 1, ε = 0 and .02

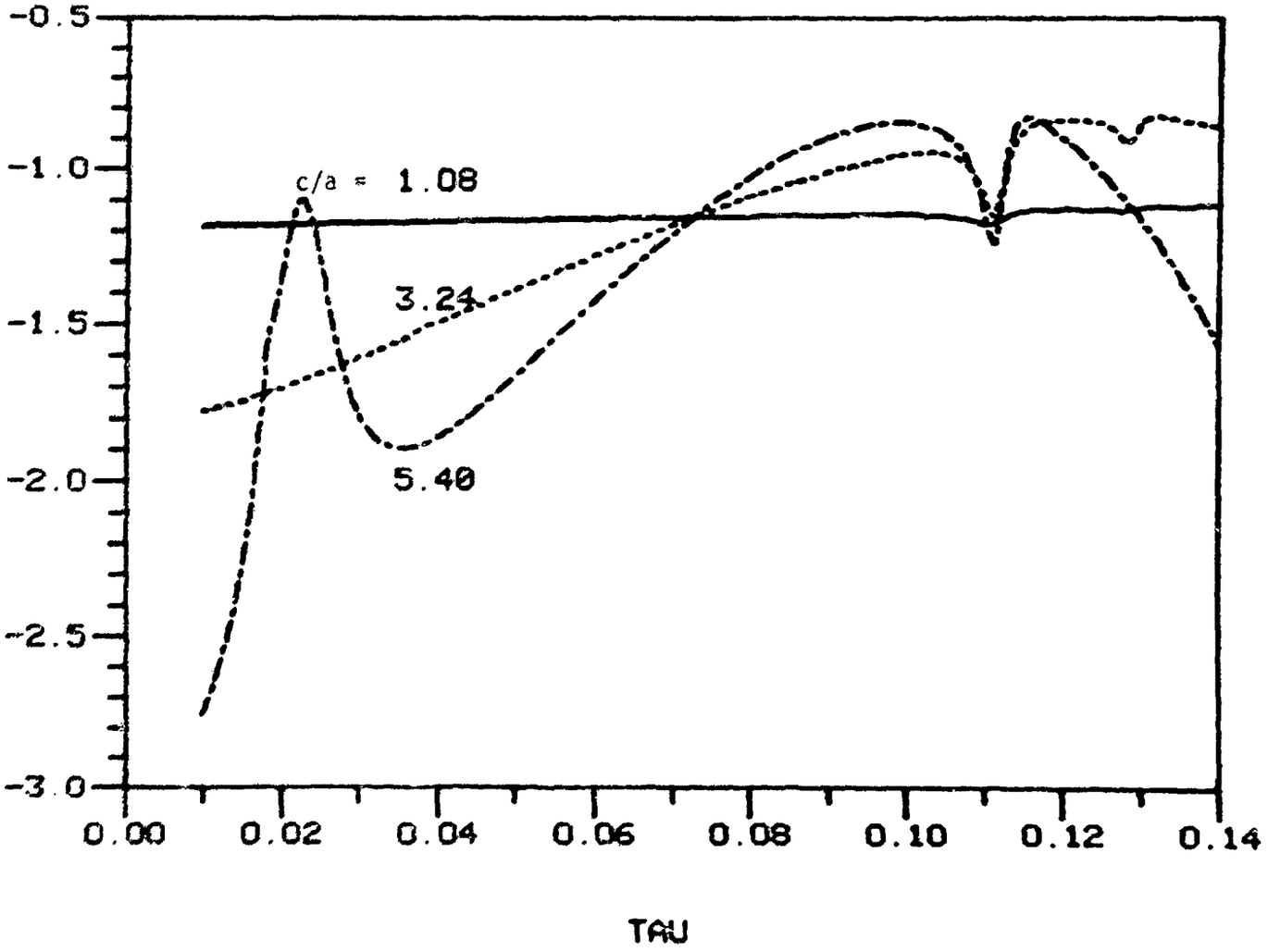

Figure 8. The Ratio of the Lateral Pressure Component of C_{LSM} to the Endwall Pressure Component vs τ for Re = 500,000, f = 1, $\bar{c}$ = 0, c/a = 1.08, 3.24, 5.40

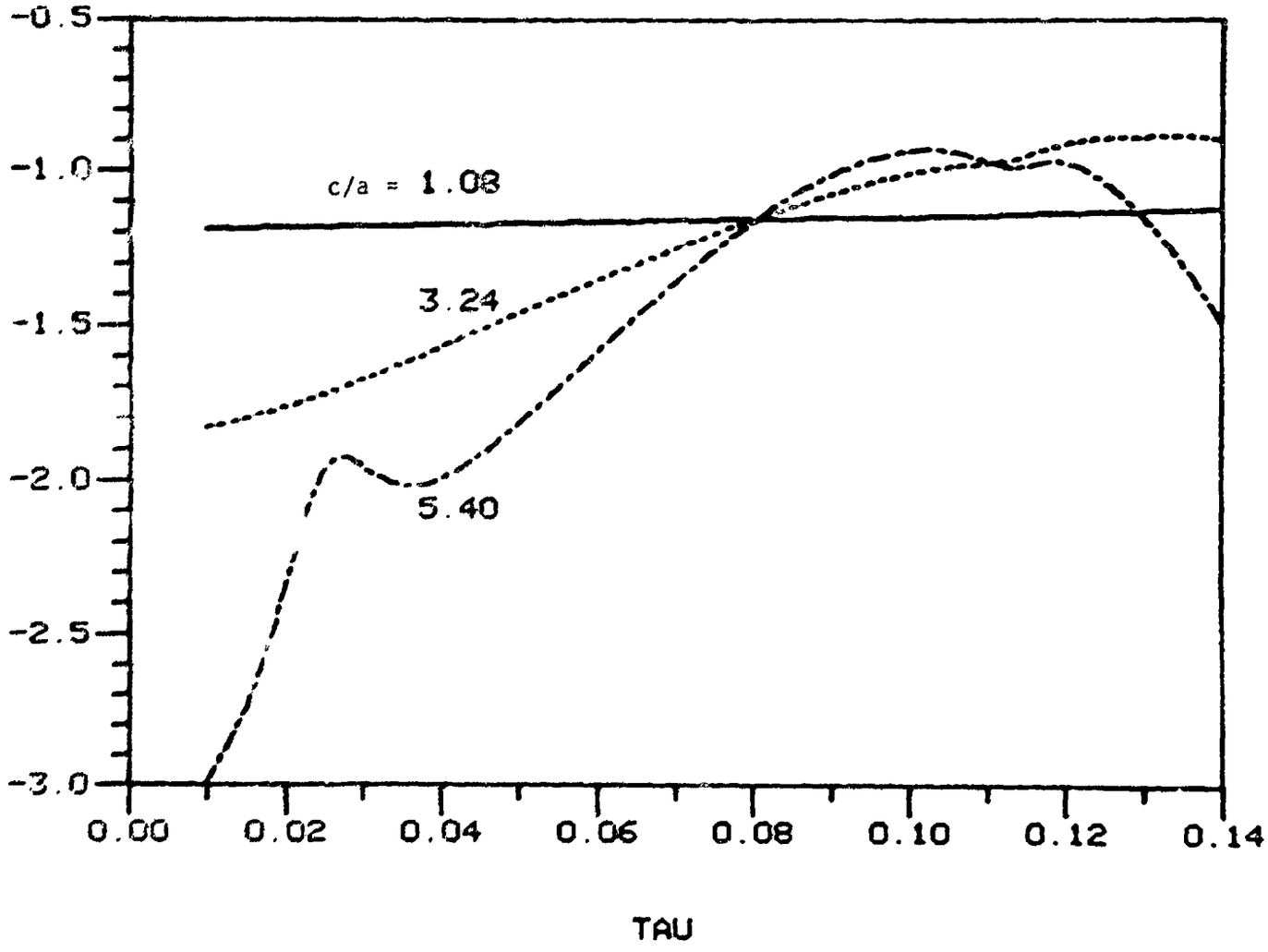

Figure 9. The Ratio of the Lateral Pressure Component of C_{LSM} to the Endwall Pressure Component vs τ for Re = 15,000, f = 1, $\varepsilon = 0$, c/a = 1.08, 3.24, 5.40

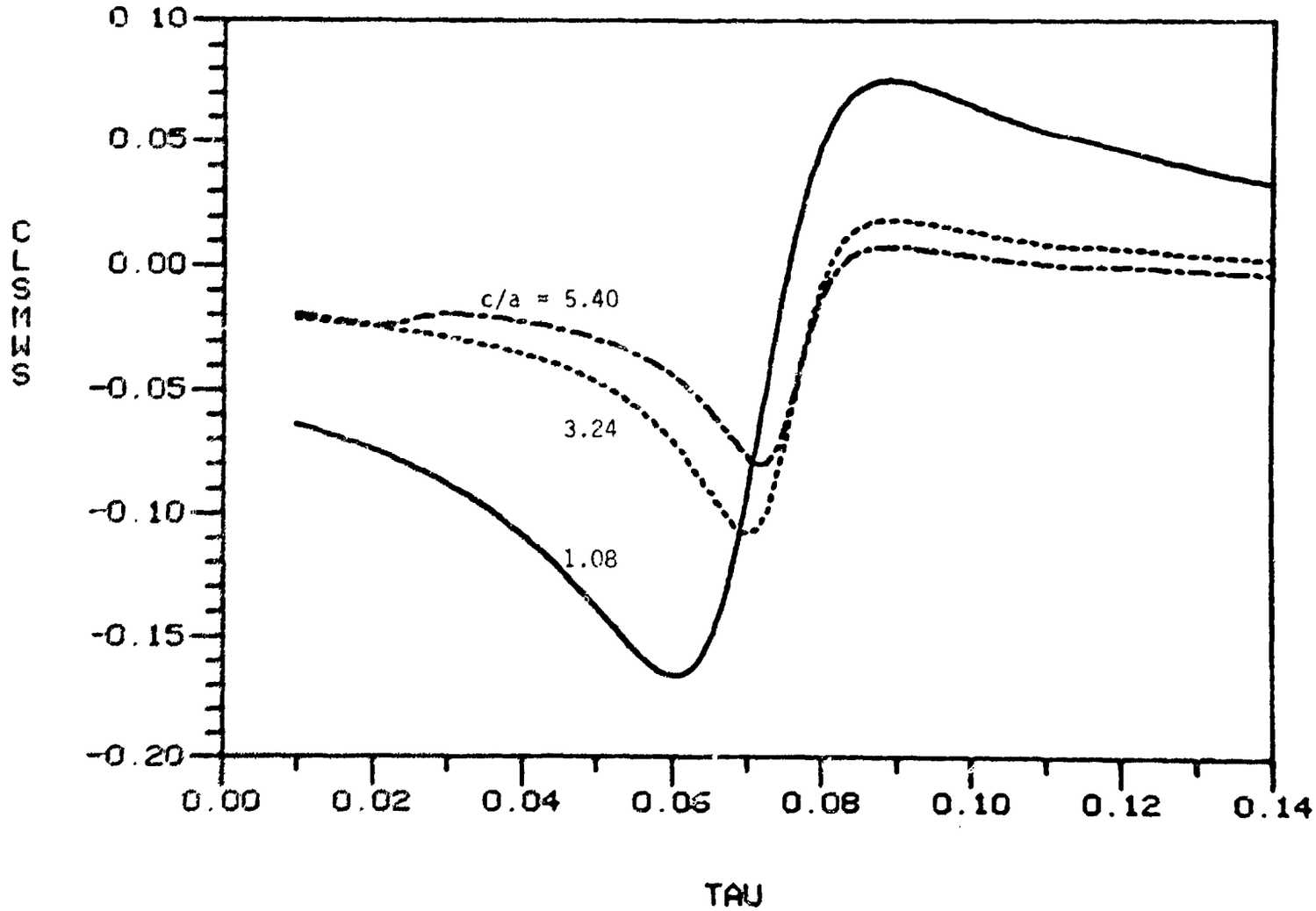

Figure 10. The Wall Shear Component of C_{LSM} vs τ for Re = 15,000, f = 1, ε = 0, c/a = 1.08, 3.24, 5.40

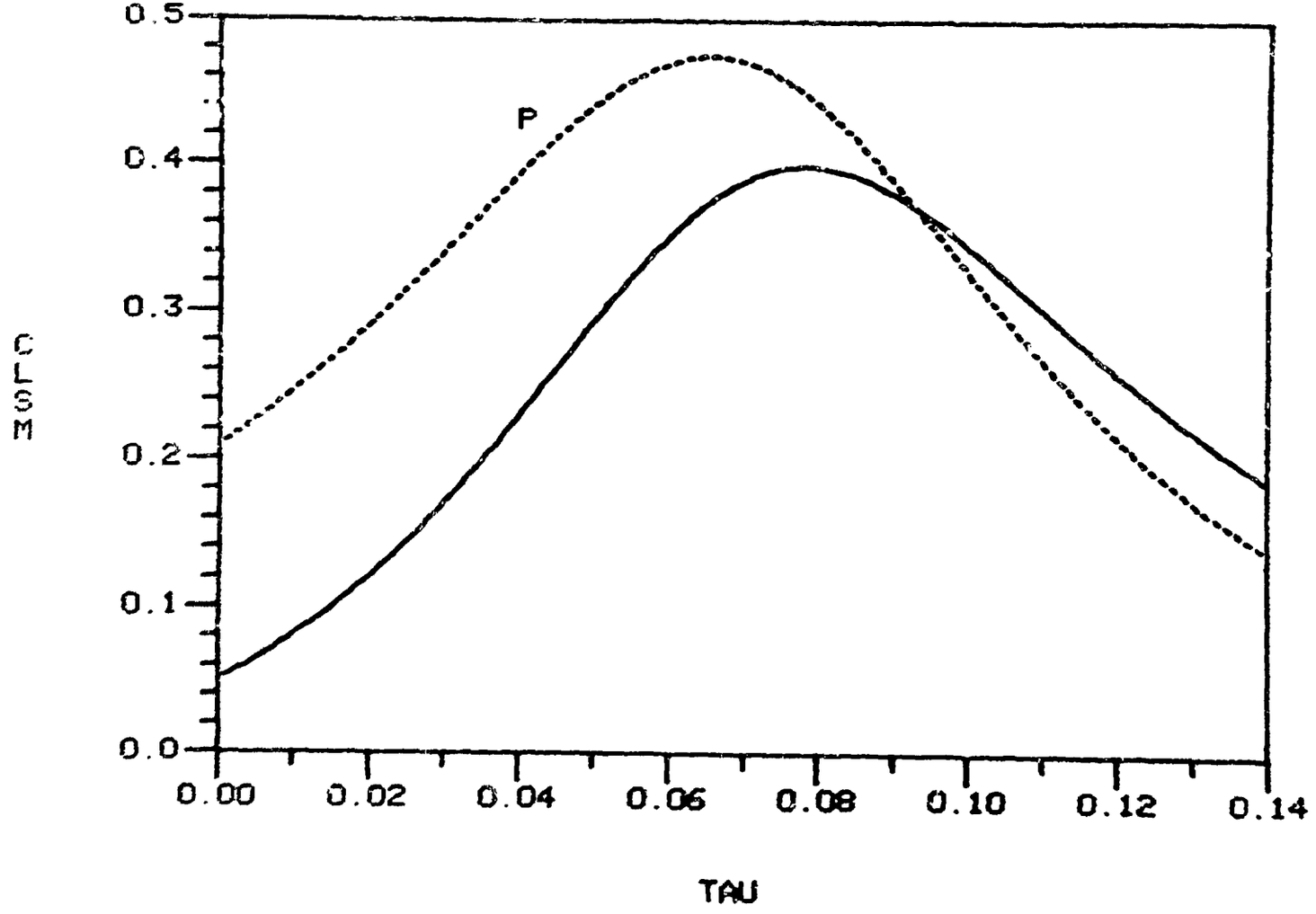

Figure 11. C_{LSM} and Its Pressure Component vs τ for Re = 1,000, f = 1, ε = 0, c/a = 1.08

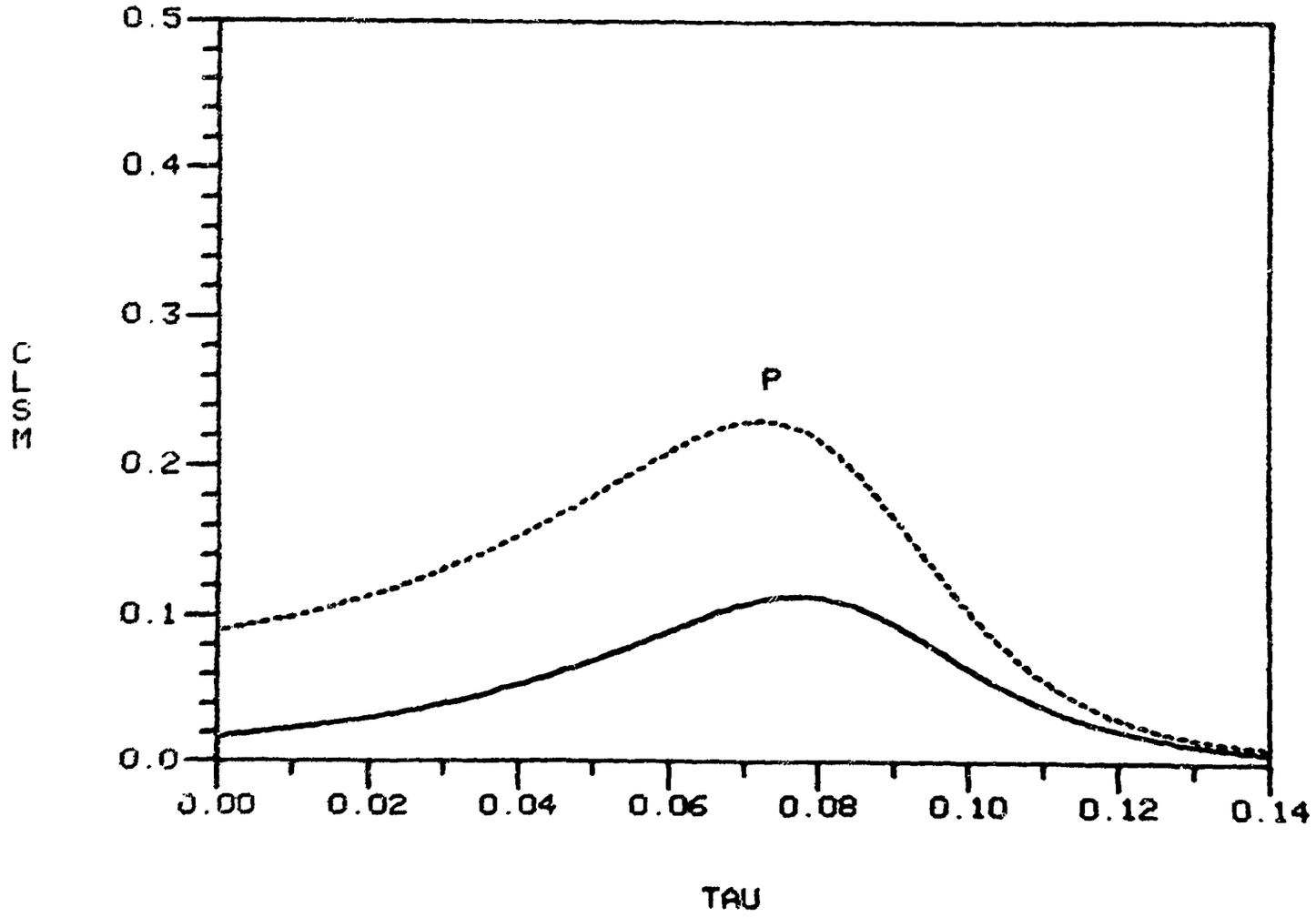

Figure 12. C_{LSM} and Its Pressure Component vs τ for Re = 1,000, f = 1, ϵ = 0, c/a = 3.24

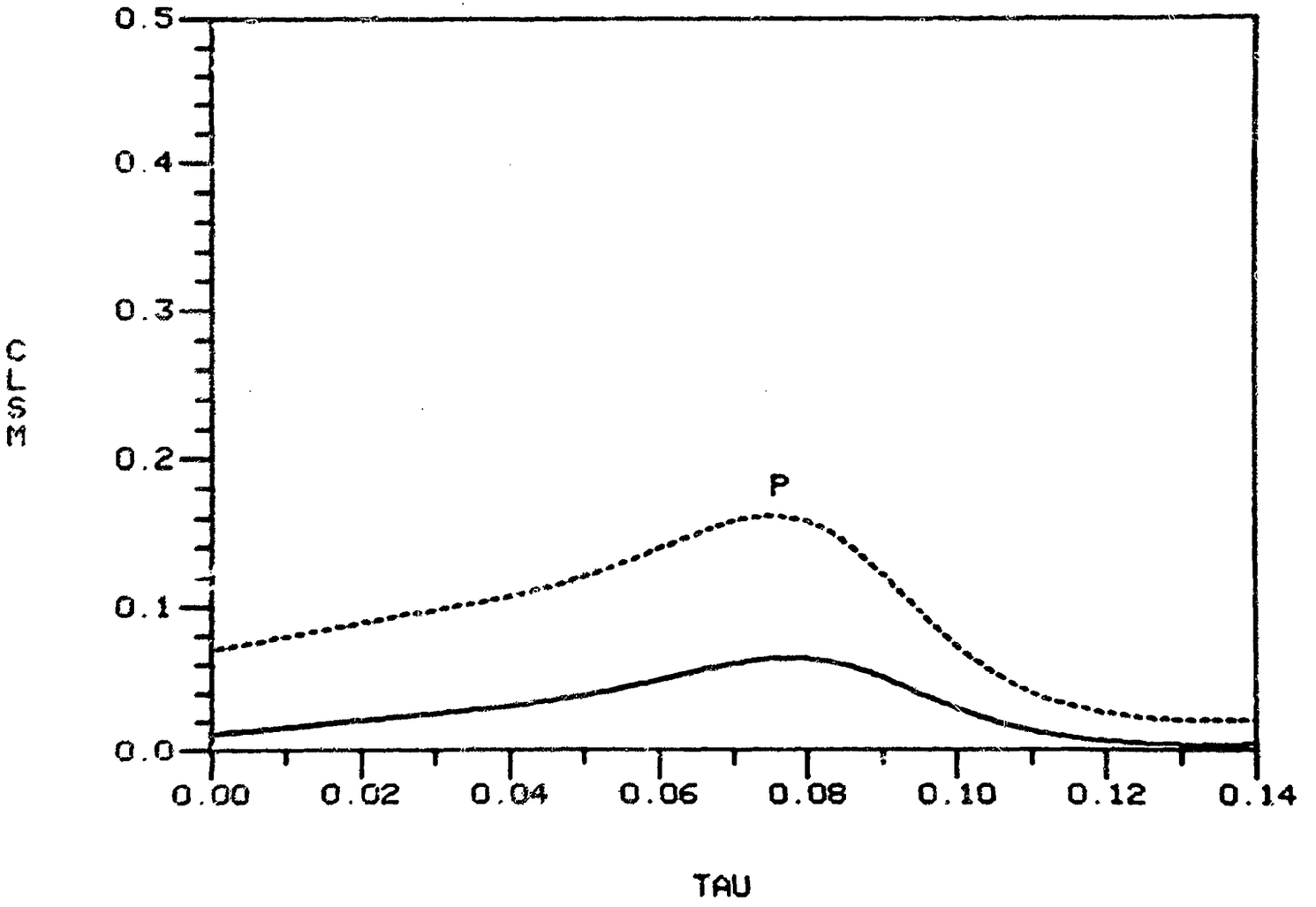

Figure 13. C_{LSM} and Its Pressure Component vs τ for Re = 1,000, f = 1, ε = 0, c/a = 5.40

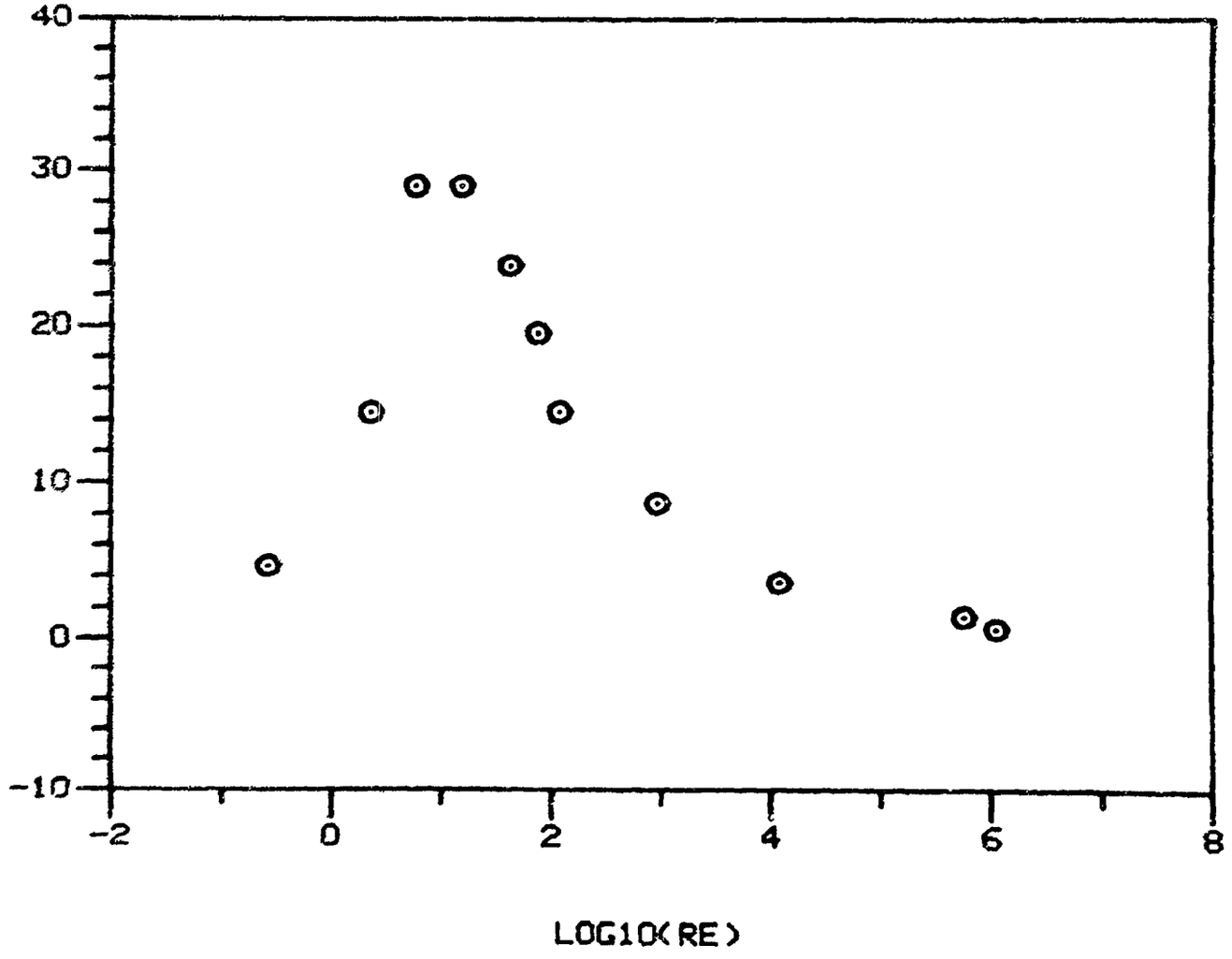

Figure 14. D'Amico-Miller Spin Fixture Data (see Ref 19, Fig 1): The Ratio of Despin Moment at a Given Re to the Despin Moment at Re = 10^6, for c/a = 4.291, f = 1

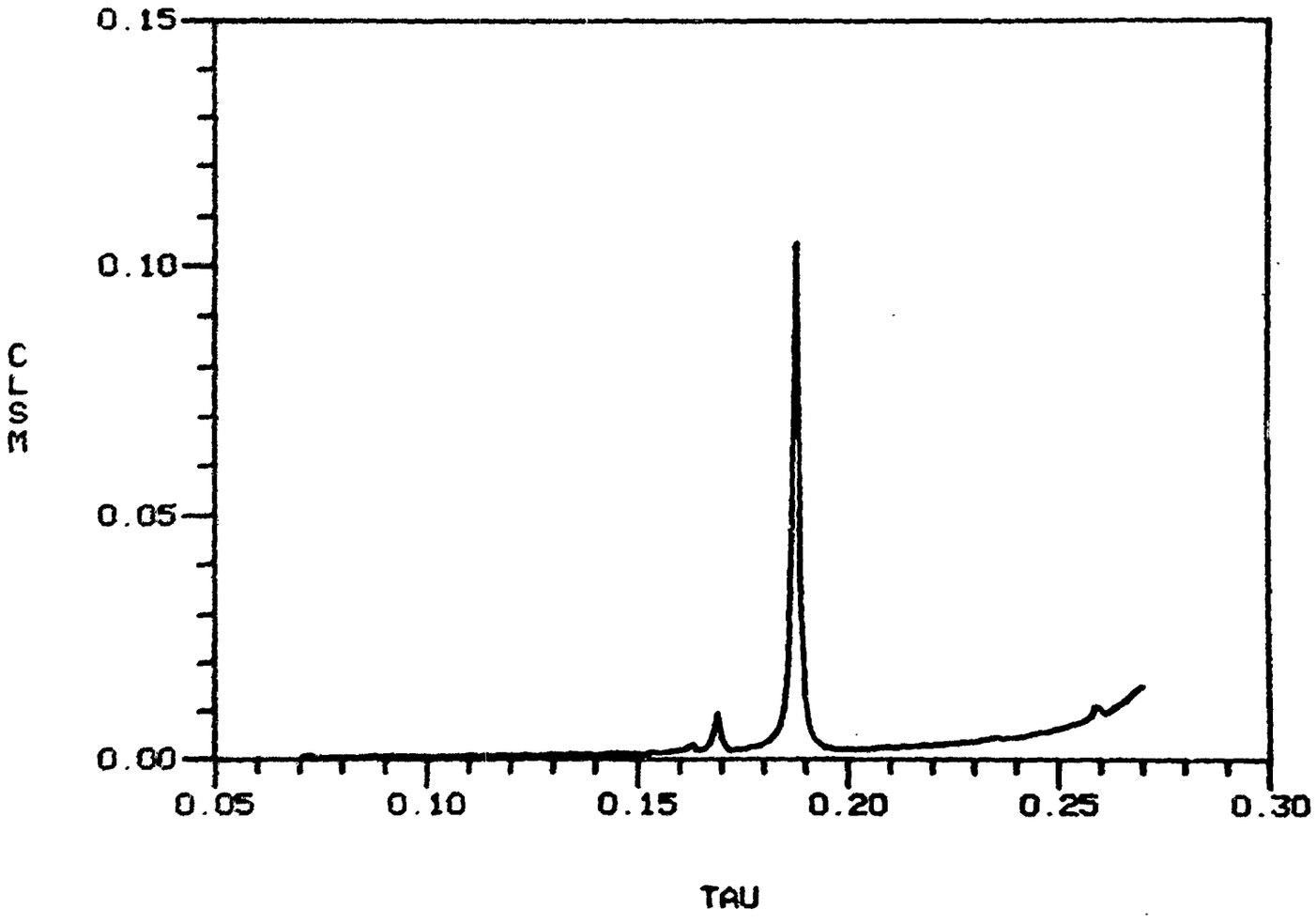

Figure 15a. C_{LSM} vs τ for Re = 10^6, ε = 0 and the D'Amico-Miller Parameters: c/a = 4.291, f = 1

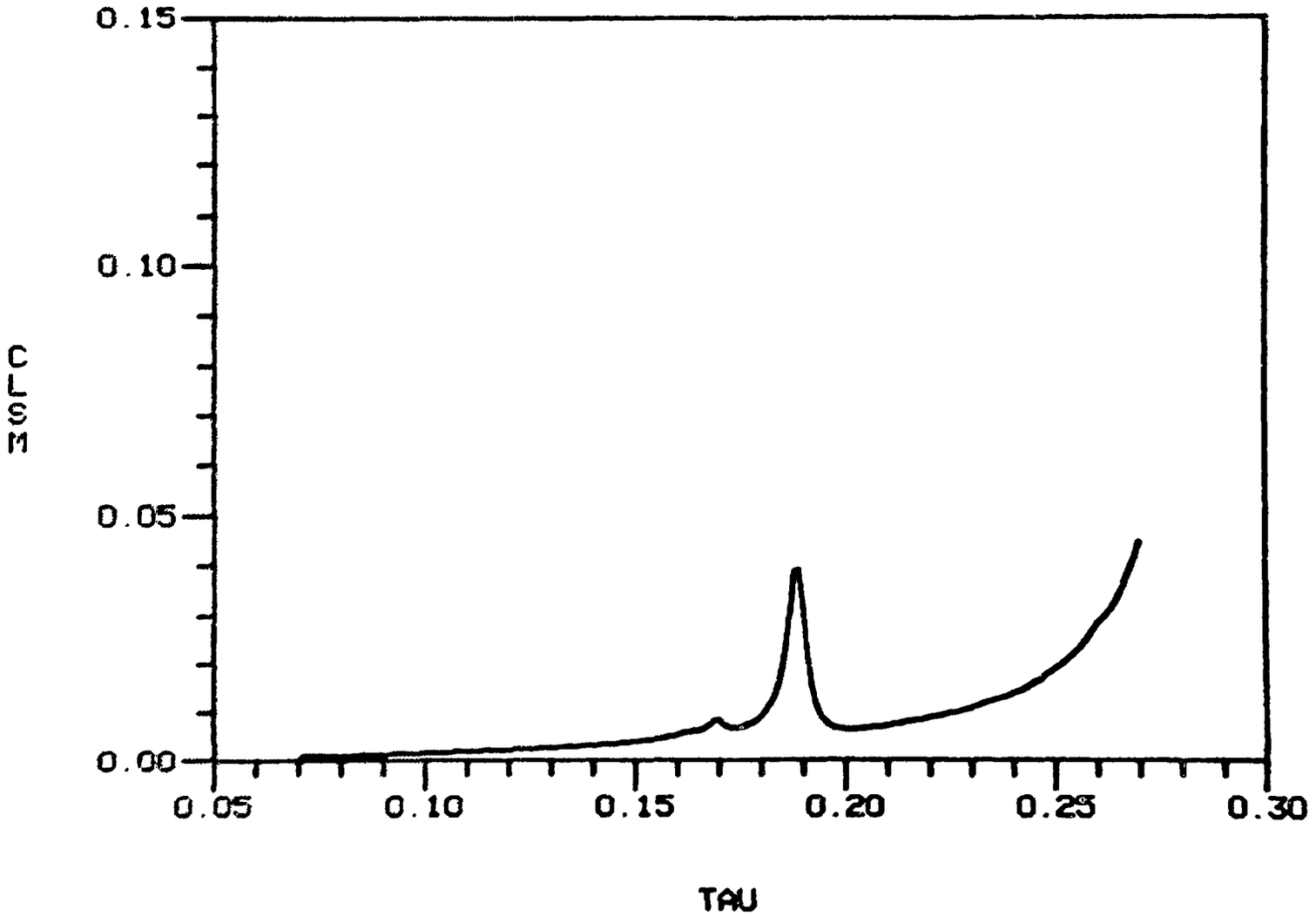

Figure 15b. C_{LSM} vs τ for Re = 10^5, ε = 0, and the D'Amico-Miller Parameters: c/a = 4.291, f = 1

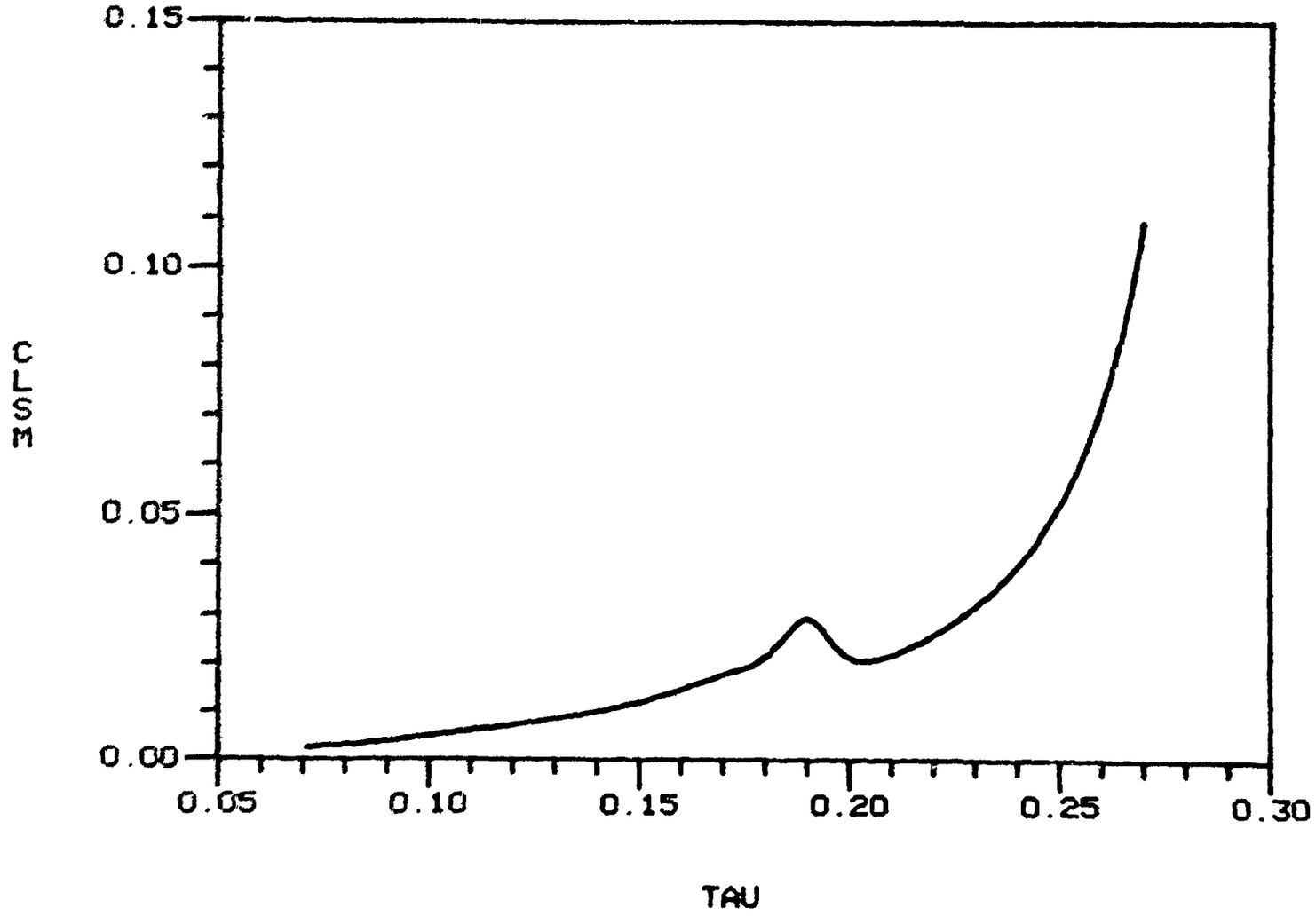

Figure 15c. C_{LSM} vs τ for Re = 10^4, ε = 0, and the D'Amico-Miller Parameters: c/a = 4.291, f = 1

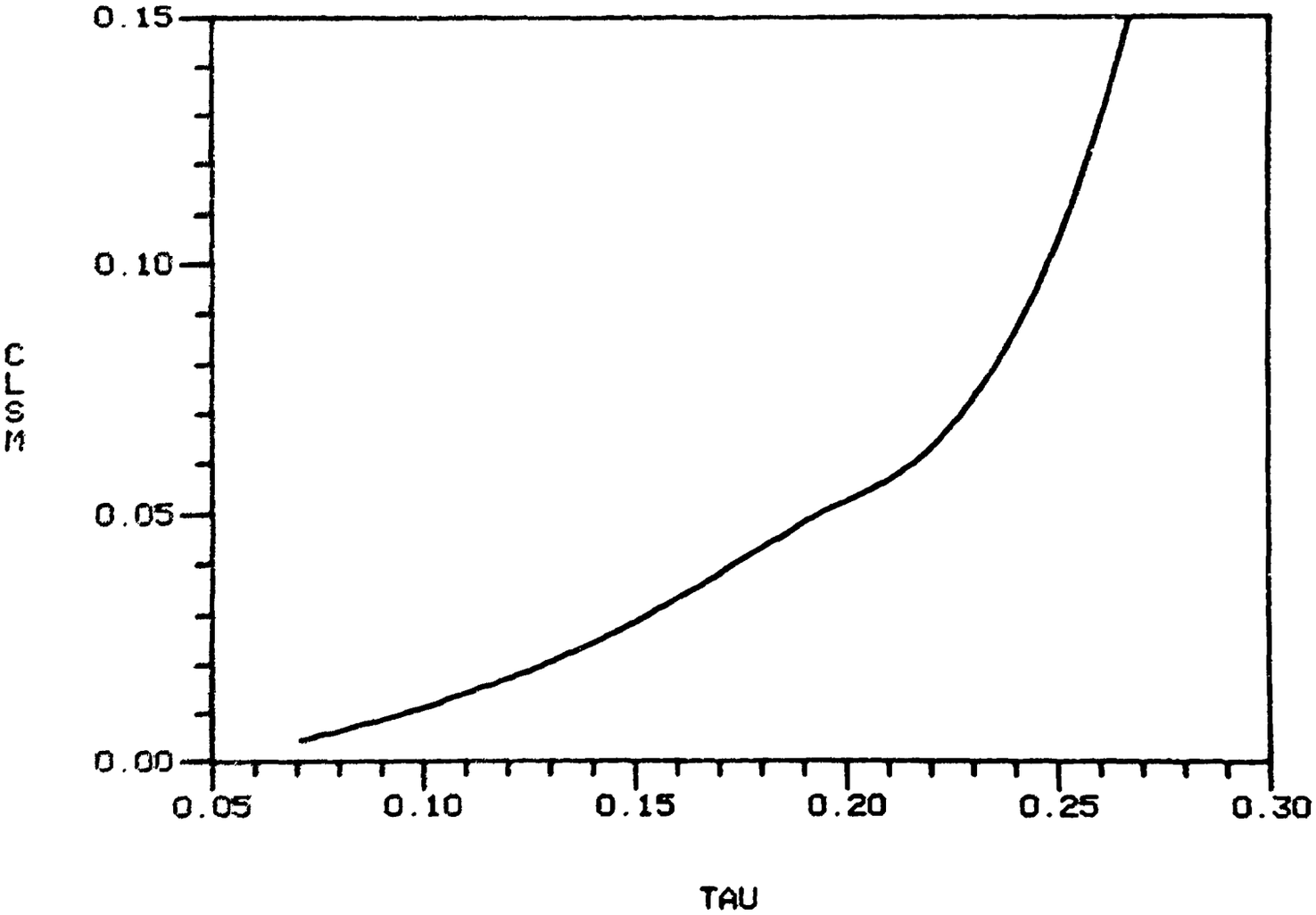

Figure 15d. C_{LSM} vs τ for Re = 10^3, ε = 0, and the D'Amico-Miller Parameters: c/a = 4.291, f = 1

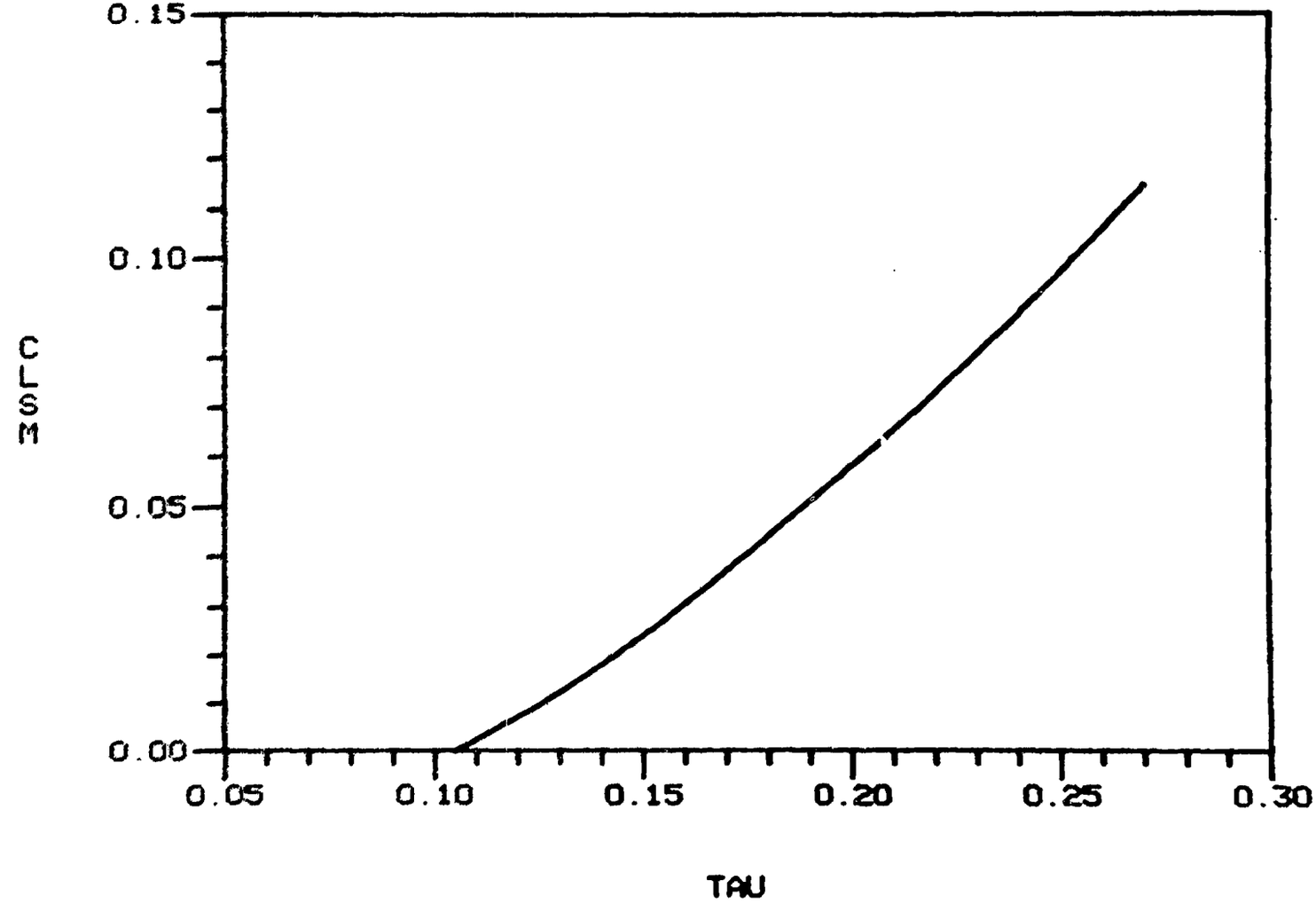

Figure 15e. C_{LSM} vs τ for Re = 10^2, ε = 0, and the D'Amico-Miller Parameters: c/a = 4.291, f = 1

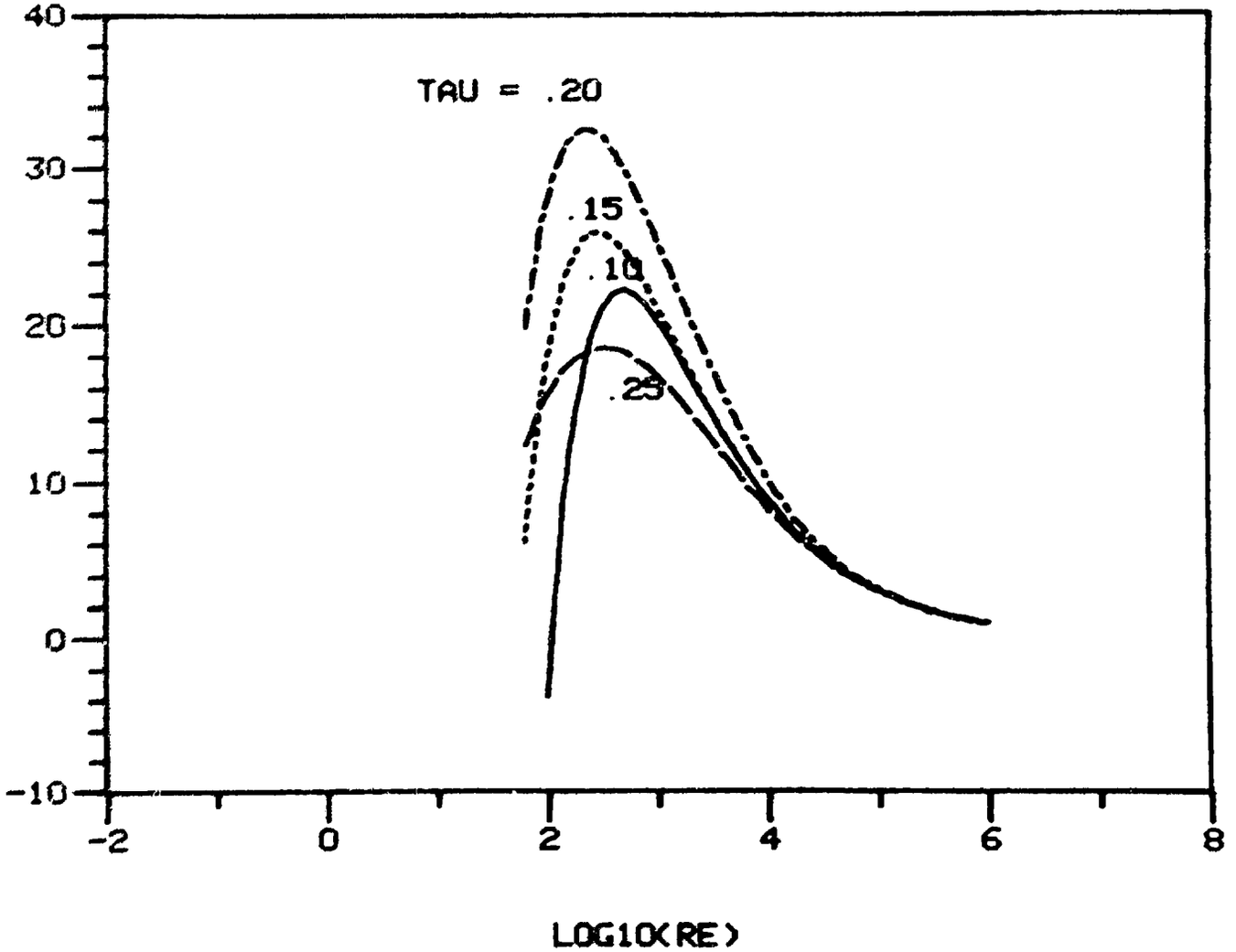

Figure 16. Ratio of $C_{LSM}(\tau, Re)$ to $C_{LSM}(\tau, 10^6)$ vs Re for $\varepsilon = 0$, $\tau = .10$, .15, .20, .25, and the D'Amico-Miller Parameters: c/a = 4.291, f = 1

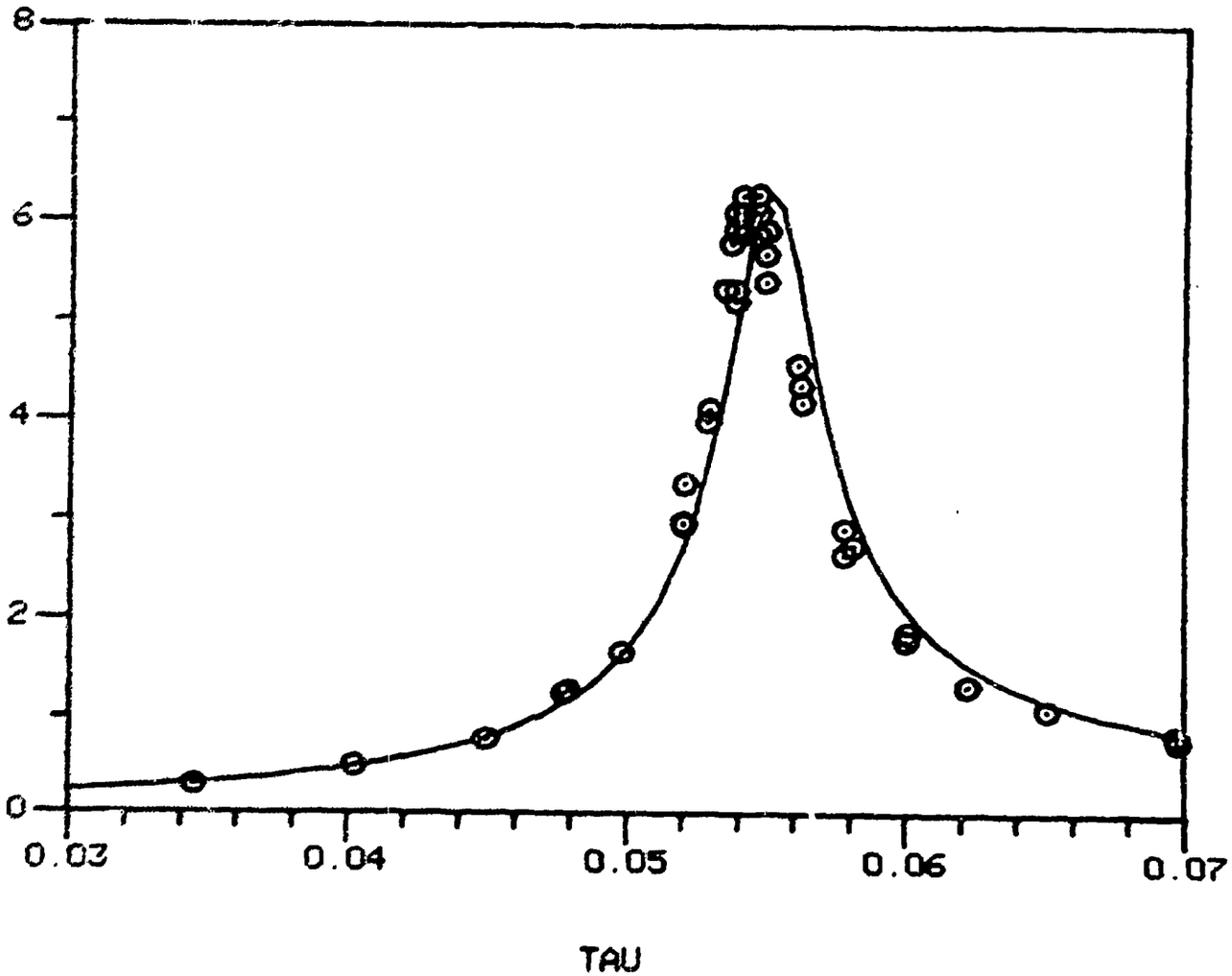

Figure 17a. C_p vs τ for a Partially-Filled Cavity (f = .920), Predicted Curve and Whiting Data (see Ref 21, Fig 10f), Re = 400,000, c/a = 3.148, Transducer at r/a = .668

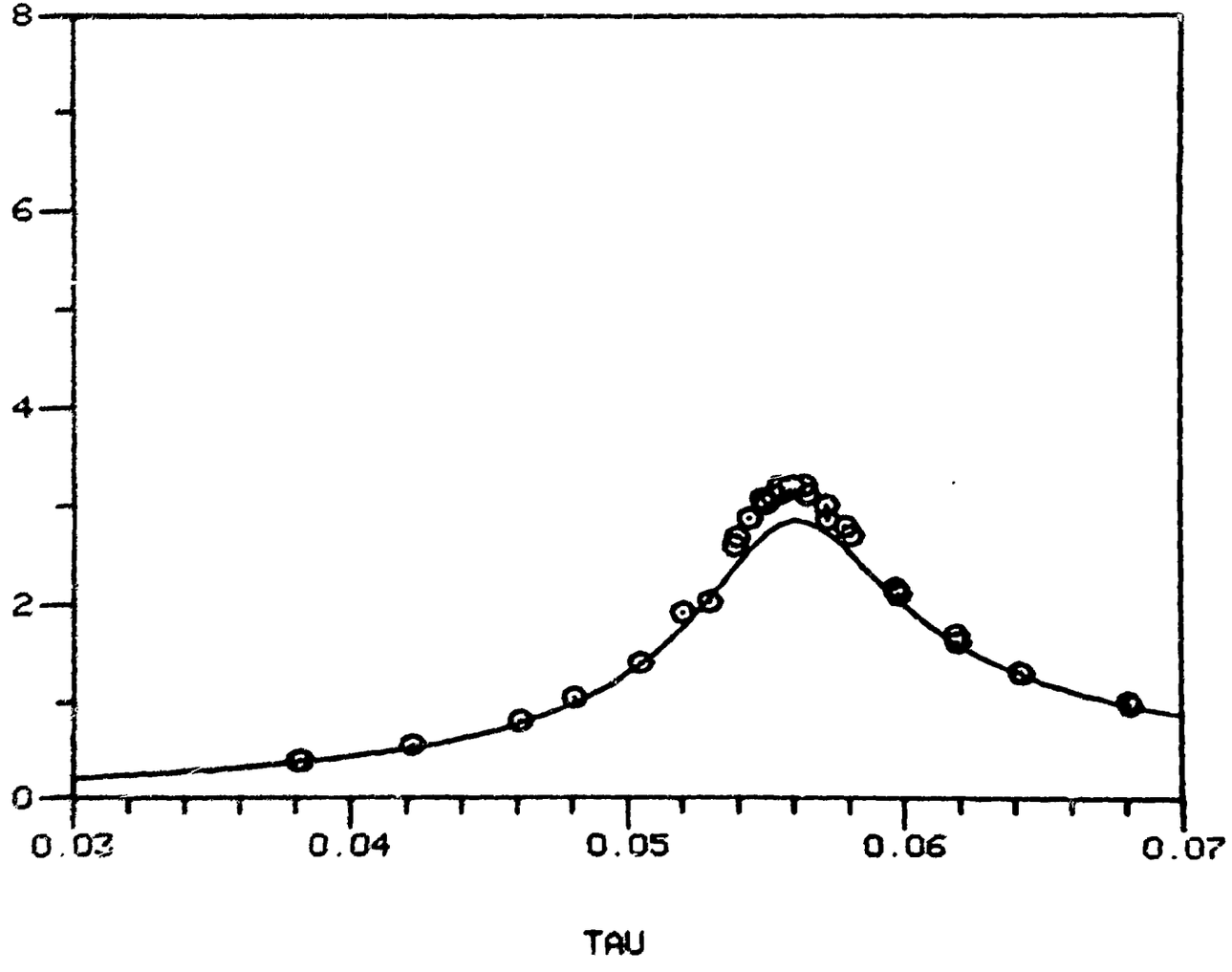

Figure 17b. C_p vs τ for a Partially-Filled Cavity (f = .920), Predicted Curve and Whiting Data (see Ref 21, Fig 10g), Re = 80,000, c/a = 3.148, Transducer at r/a = .668

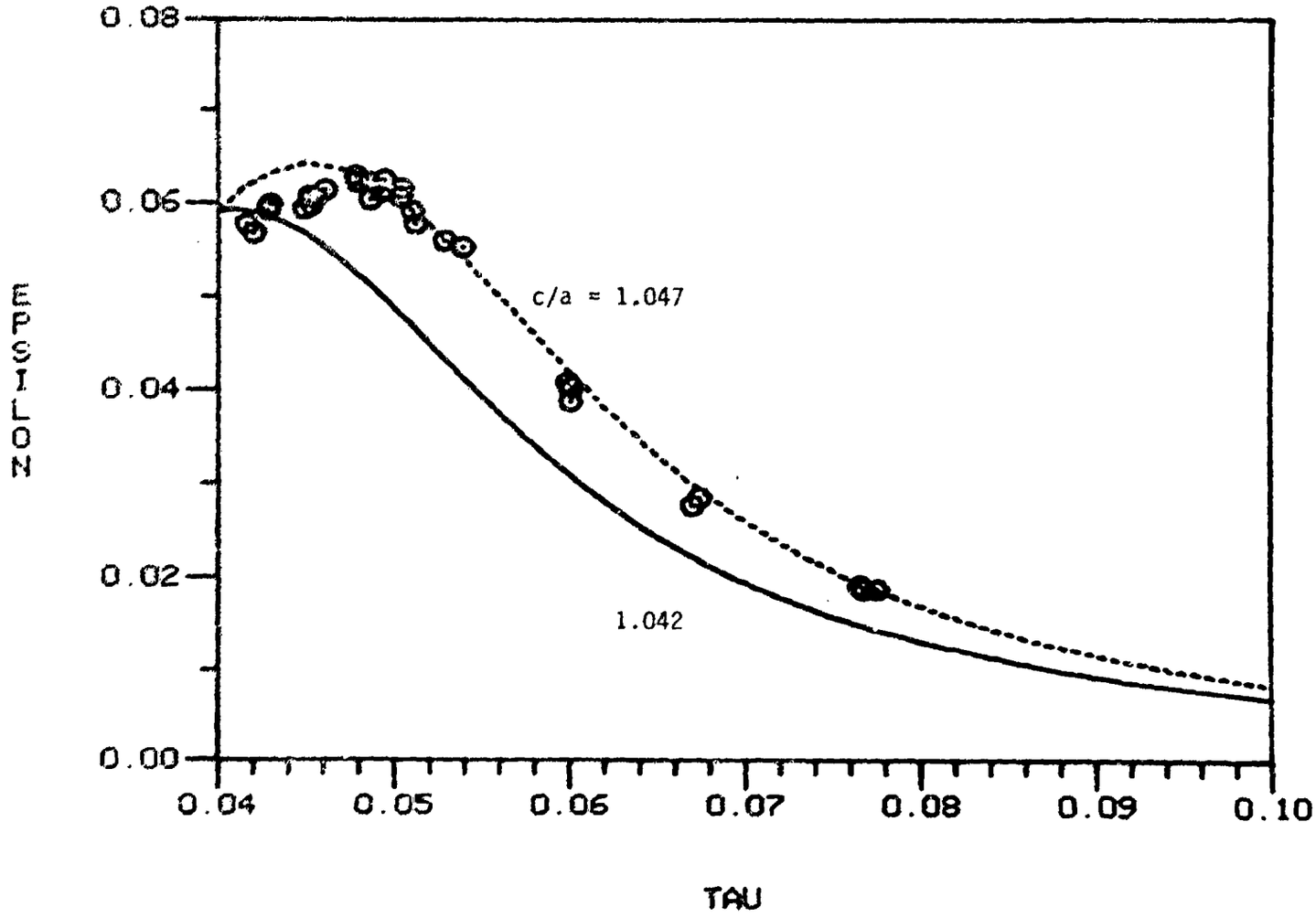

Figure 18a. ε vs τ for a Fully-Filled Cavity, Predicted Curve and D'Amico Data (see Ref 23, Fig 5), Re = 12,400, c/a = 1.042 (Nominal) and 1.047 (Fitted), $m_L a^2/I_x$ = .0833

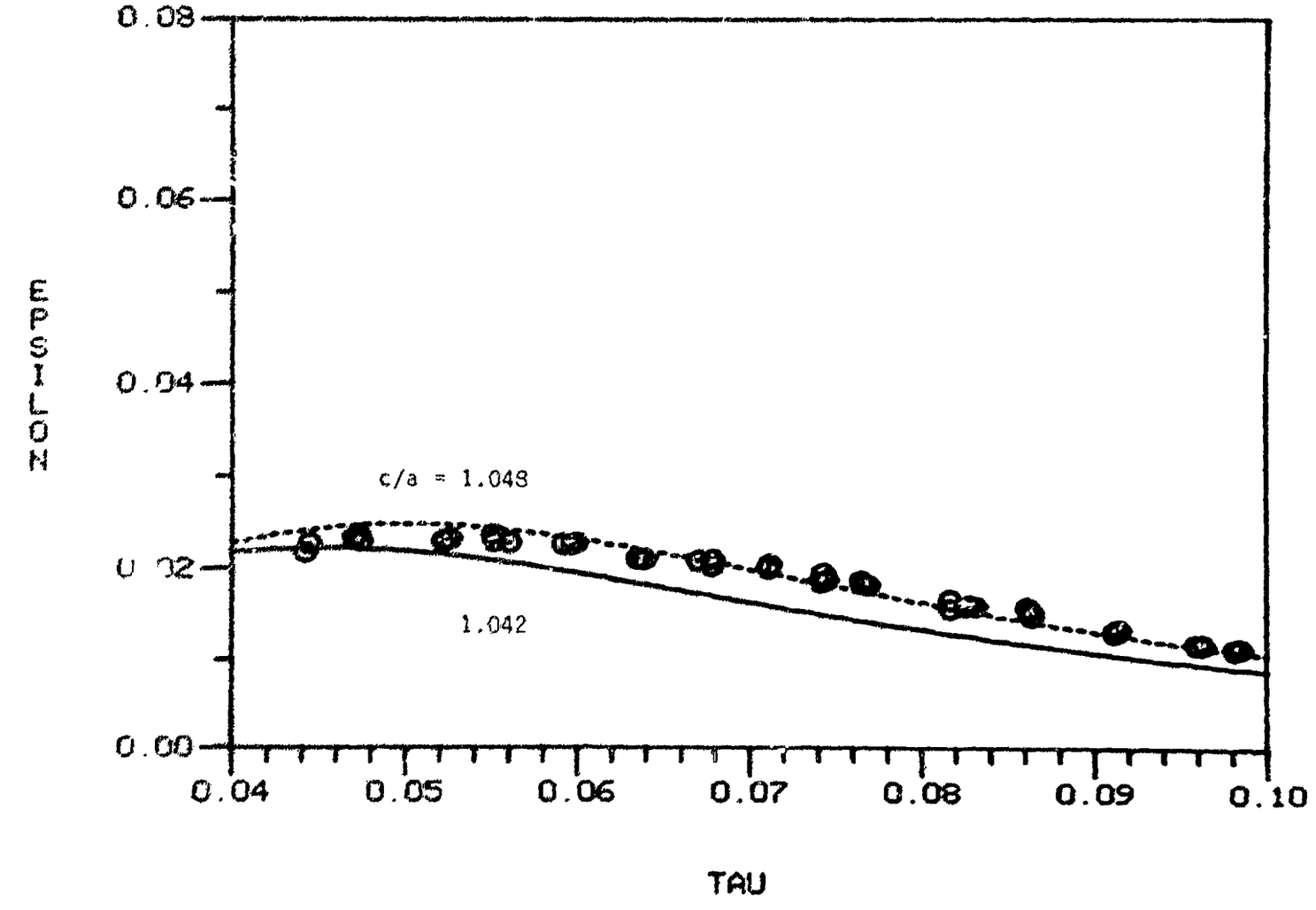

Figure 18b. ϵ vs τ for a Fully-Filled Cavity, Predicted Curve and D'Amico Data (see Ref 23, Fig 6), Re = 2400, c/a = 1.042 (Nominal) and 1.048 (Fitted), $m_L a^2/I_x$ = .0632

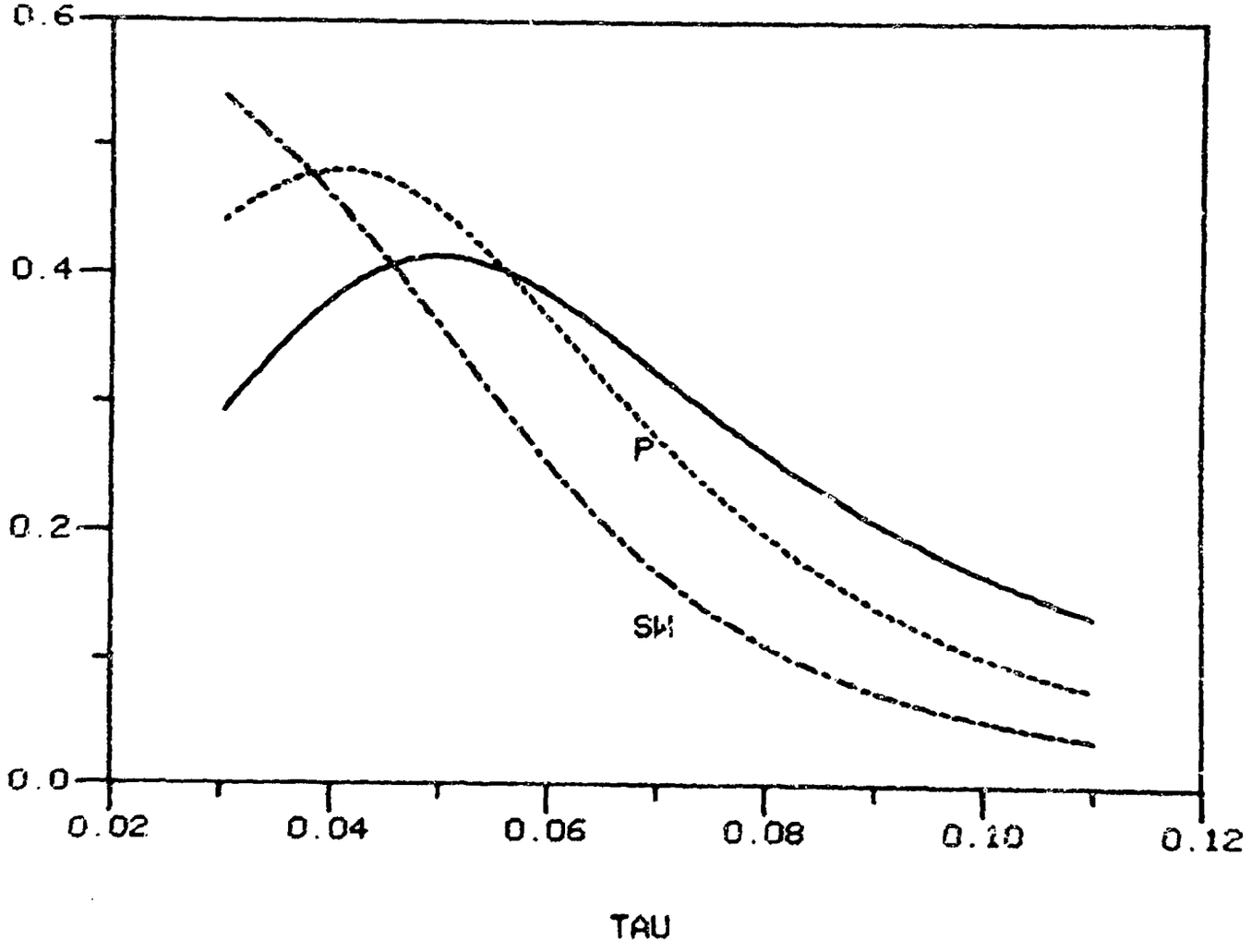

Figure 19. The Total, the Pressure Component and the Stewartson-Wedemeyer Values of C_{LSM} vs τ for Re = 2400, c/a = 1.048, f = 1, ε = 0

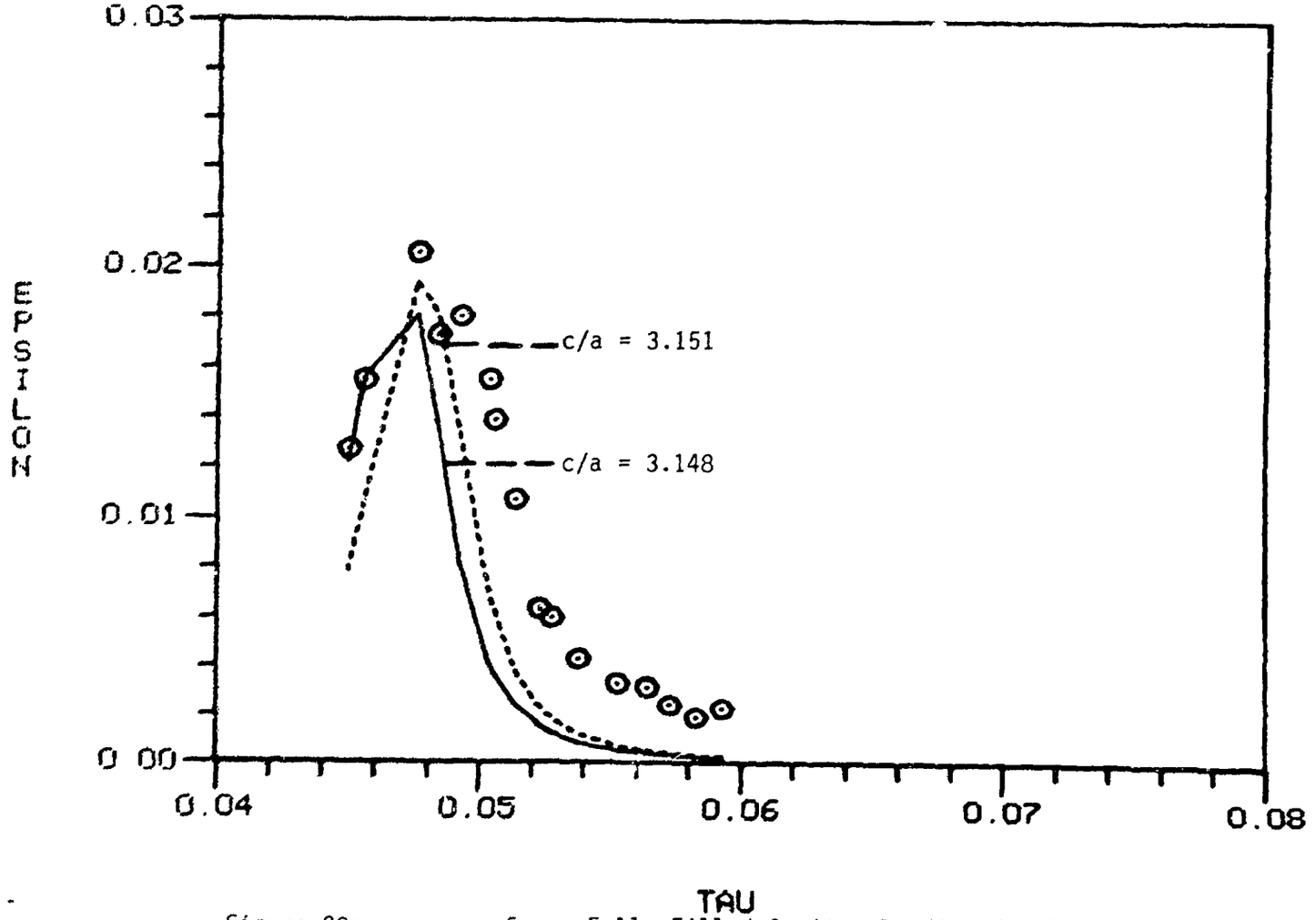

Figure 20a. ε vs τ for a Fully-Filled Cavity, Predicted Values and D'Amico-Kitchens Data (Circles) (see Ref 6, Fig 8a), Re = 520,000, c/a = 3.148 (Nominal) and 3.151 (Fitted), $m_L a^2/I_x$ Variable

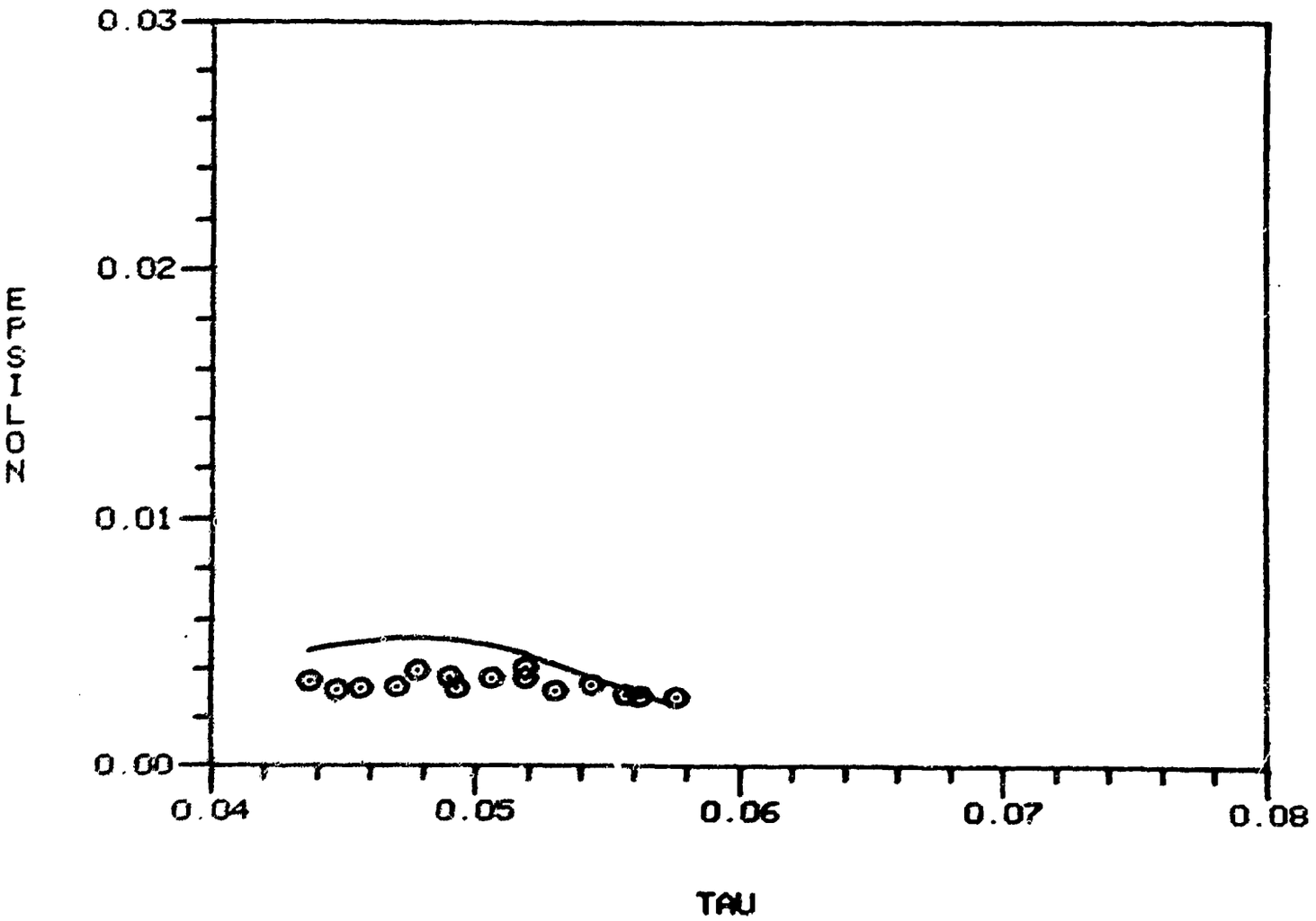

Figure 20b. ε vs τ for a Fully-Filled Cavity, Predicted Values and D'Amico-Kitchens Data (Circles) (see Ref 6, Fig 8b), Re = 9000, c/a = 3.148, $m_L a^2/I_x$ Variable

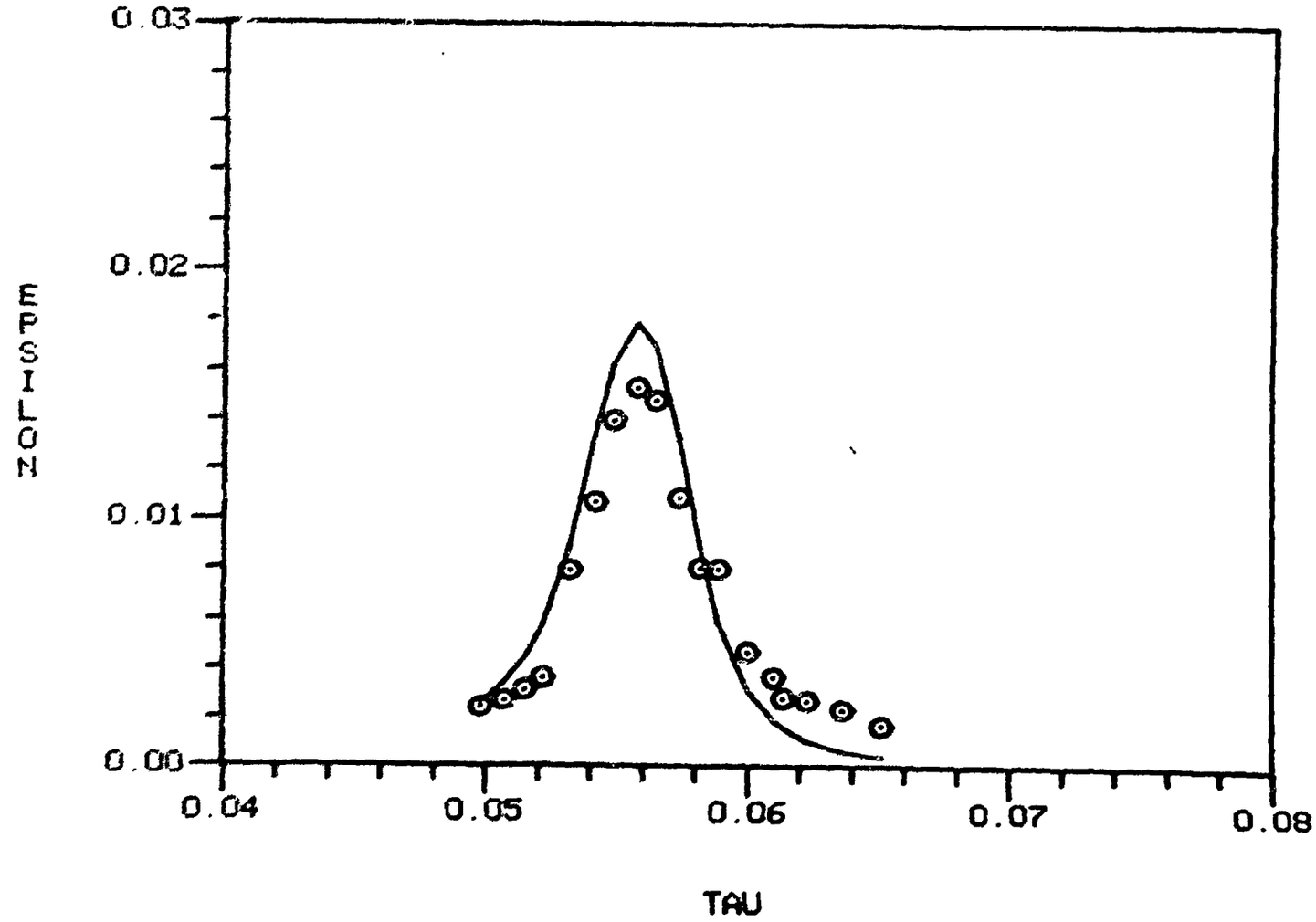

Figure 21a. ε vs τ for a Partially-Filled Cavity (f = .790), Predicted Values and D'Amico Data (Circles) (see Ref 6, Fig 6a), Re = 520,000, c/a = 3.013, $m_L a^2/I_x$ Variable

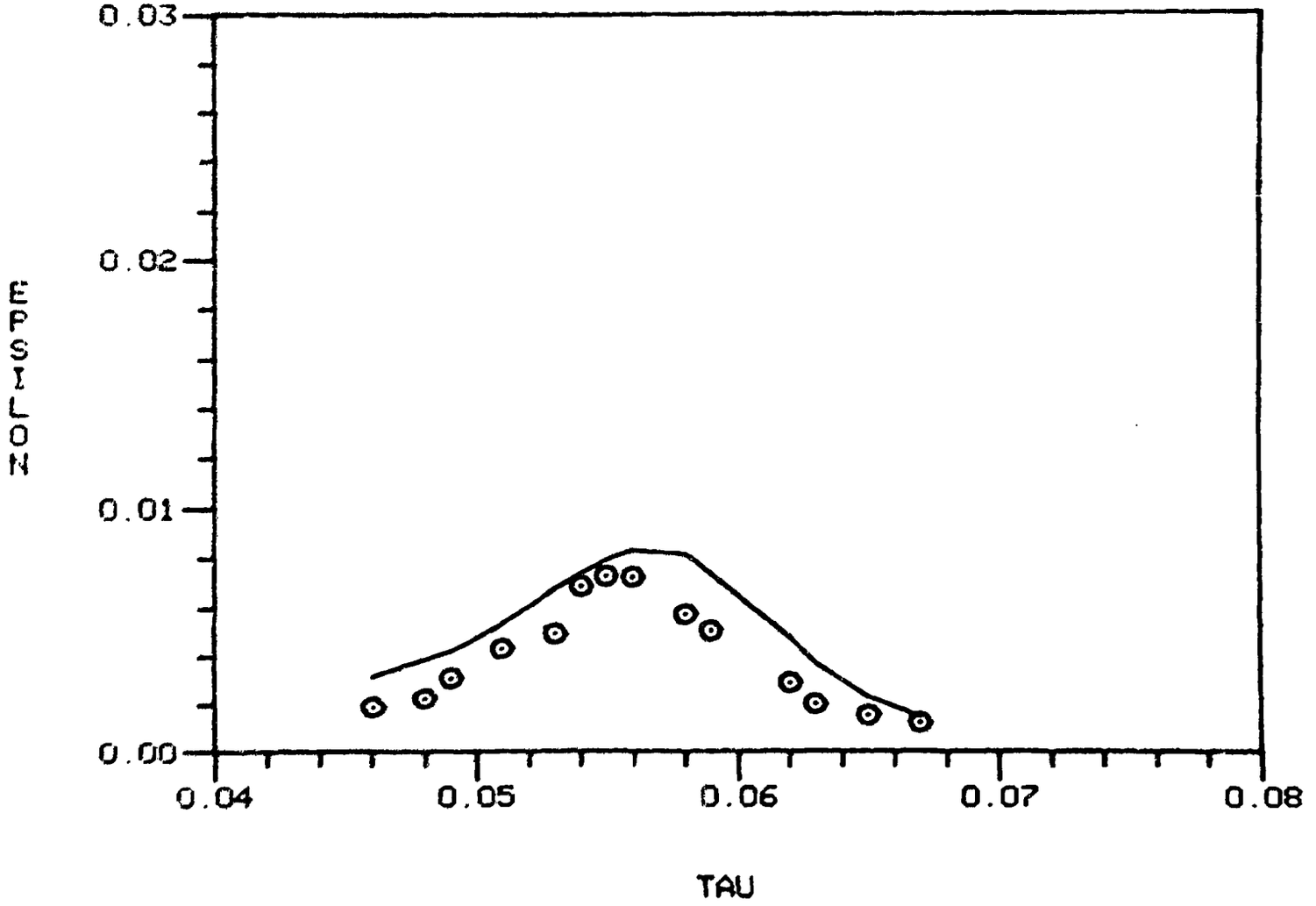

Figure 21b. ε vs τ for a Partially-Filled Cavity (f = .790), Predicted Values and D'Amico Data (Circles) (see Ref 6, Fig 6b), Re = 40,000, c/a = 3.013, $m_L a^2/I_x$ Variable

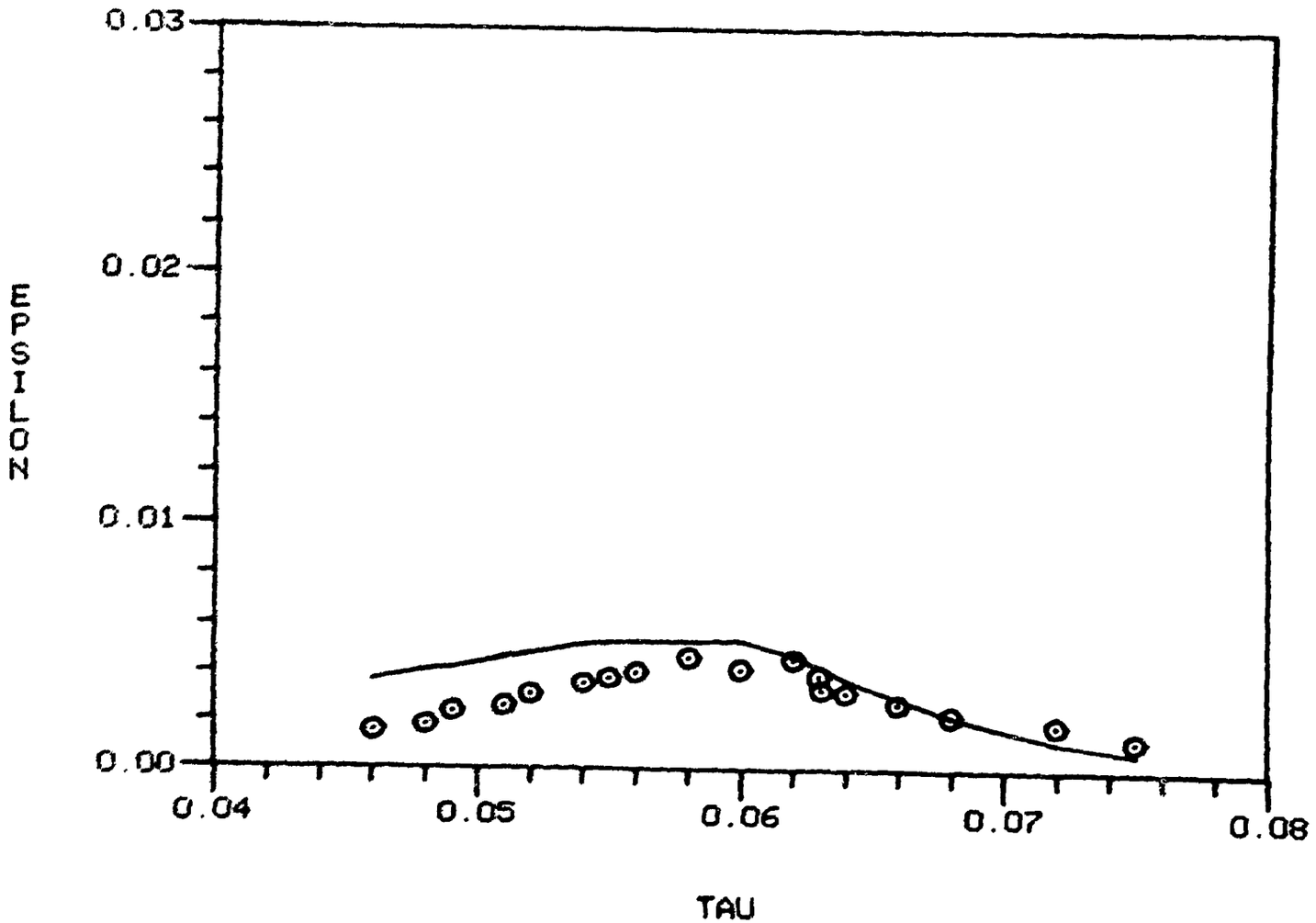

Figure 21c. ϵ vs τ for a Partially-Filled Cavity (f = .790), Predicted Values and D'Amico Data (Circles) (see Ref 6, Fig 7a), Re = 11,000, c/a = 3.013, $m_L a^2/I_x$ Variable

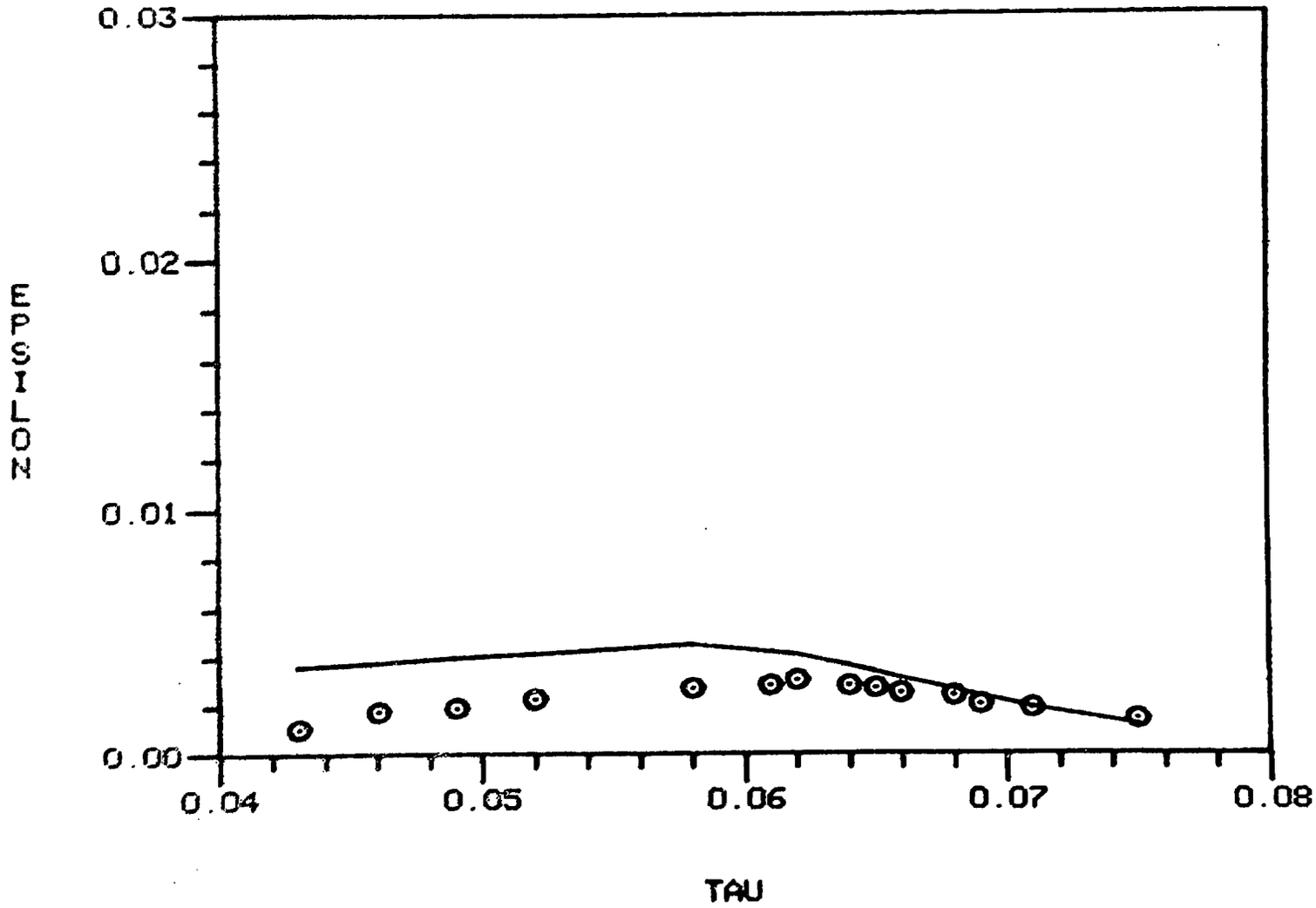

Figure 21d. ϵ vs τ for a Partially-Filled Cavity (f = .790), Predicted Values and D'Amico Data (Circles) (see Ref 6, Fig 7b), Re = 5200, c/a = 3.013, $m_L a^2/I_x$ Variable

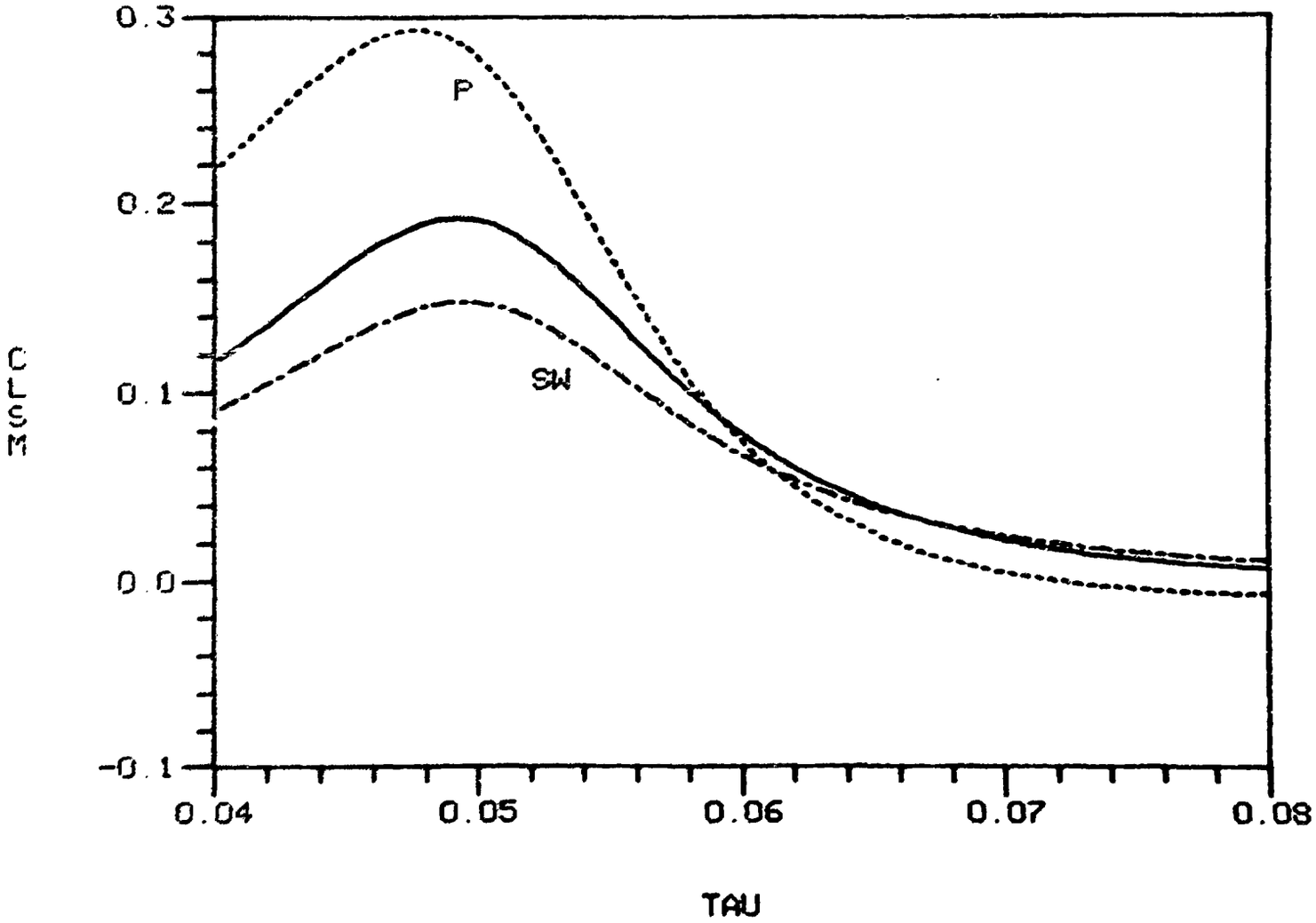

Figure 22. The Total, the Pressure Component and the Stewartson-Wedemeyer Values of C_{LSM} vs τ for Re = 9000, c/a = 3.148, f = 1. ε = 0

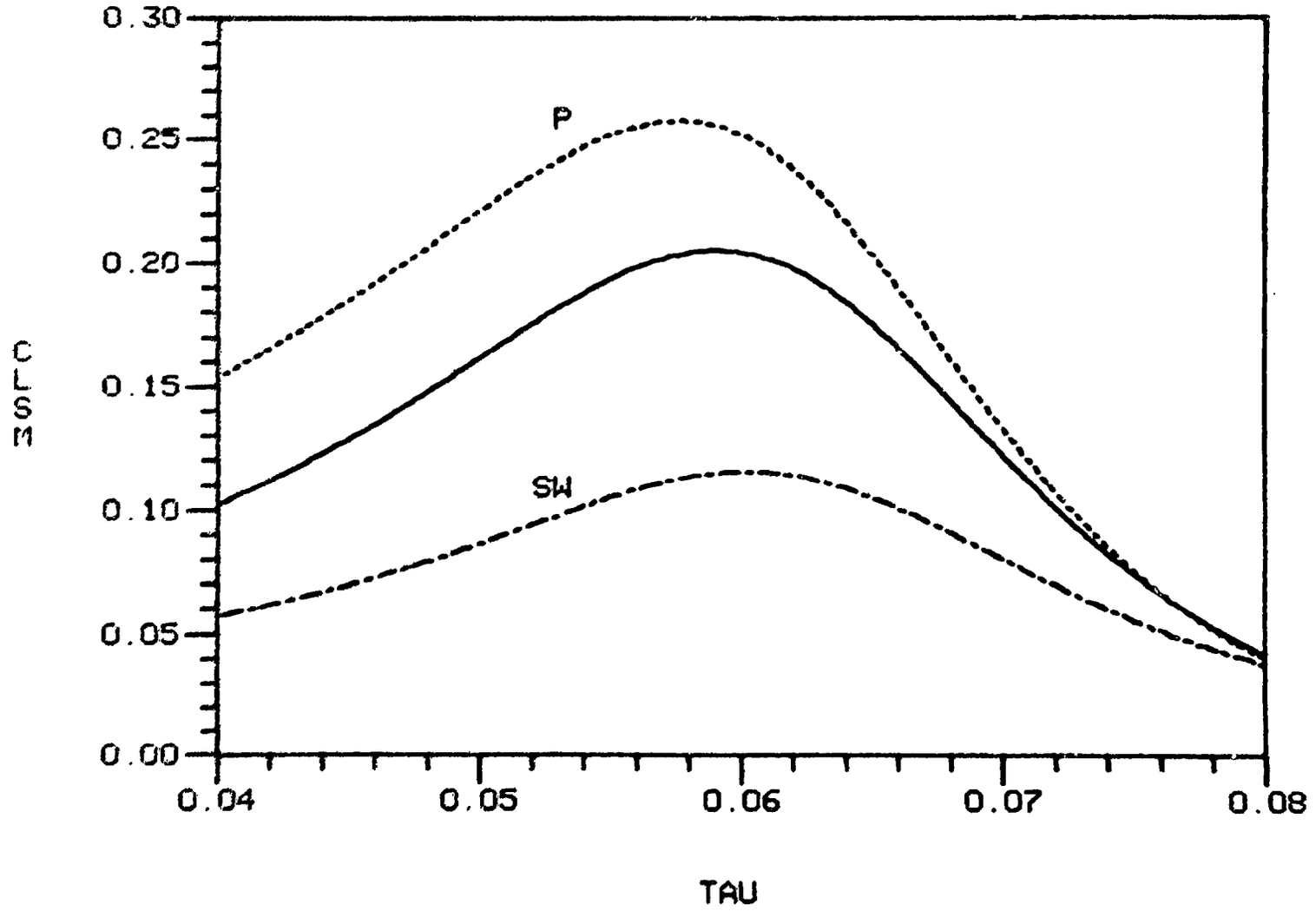

Figure 23. The Total, the Pressure Component and the Stewartson-Wedemeyer Values of C_{LSM} vs τ for a Partially-Filled Cavity (f = .790), Re = 5200, c/a = 3.013, ε = 0

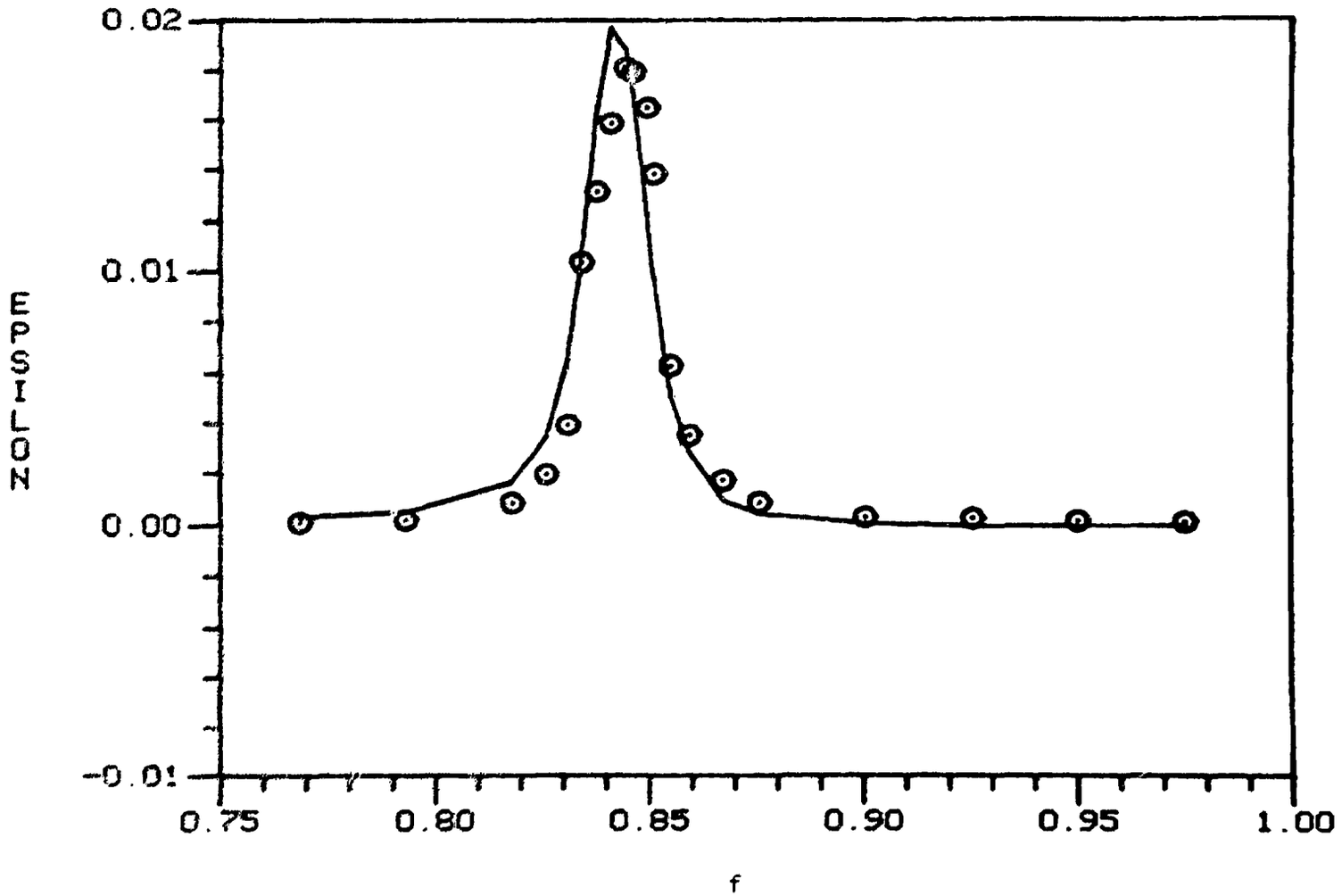

Figure 24a. ε vs Fill Ratio f, Predicted Values and Karpov Data (Circles) (see Ref 6, Fig 3), Re = 520,000, c/a = 3.077

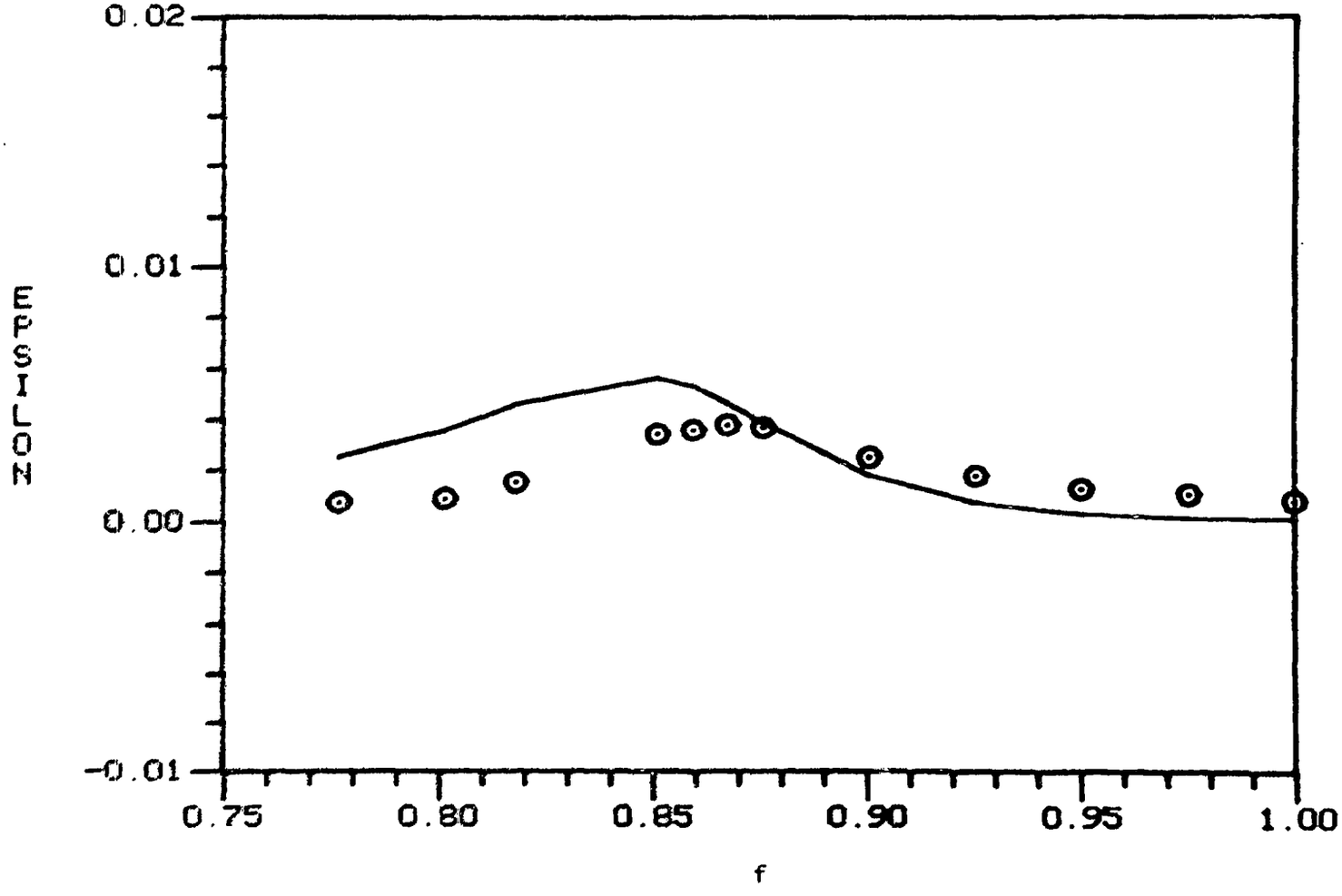

Figure 24b. ε vs Fill Ratio f, Predicted Values and Karpov Data (Circles) (see Ref 6, Fig 4), Re = 5200, c/a = 3.077

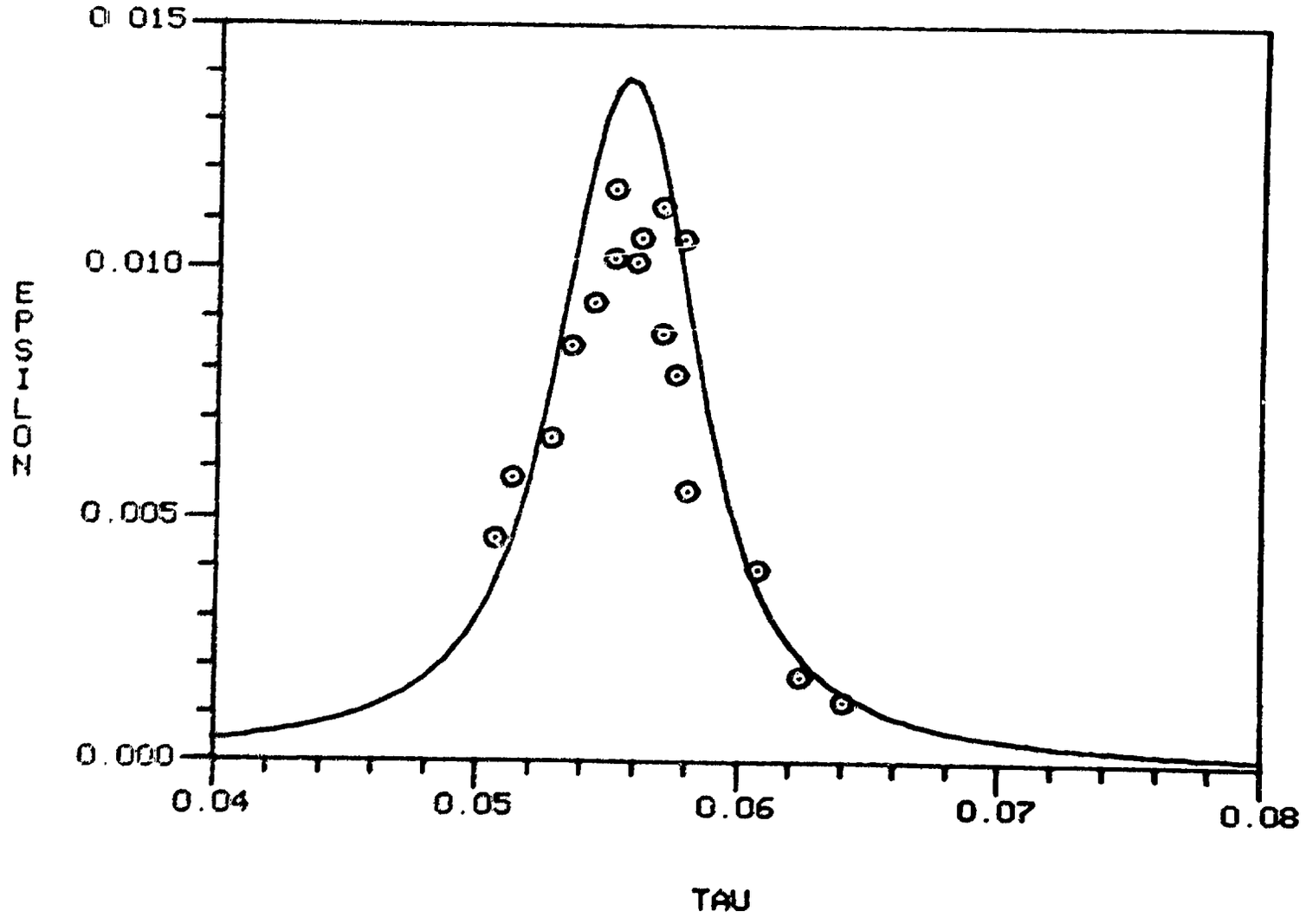

Figure 25a. ε vs τ for a Cavity With Rod (f_1 = .977), Predicted Curve and Frasier Data (see Ref 6, Fig 9a), Re = 520,000, c/a = 2.866, $m_L a^2/I_x$ = .0240

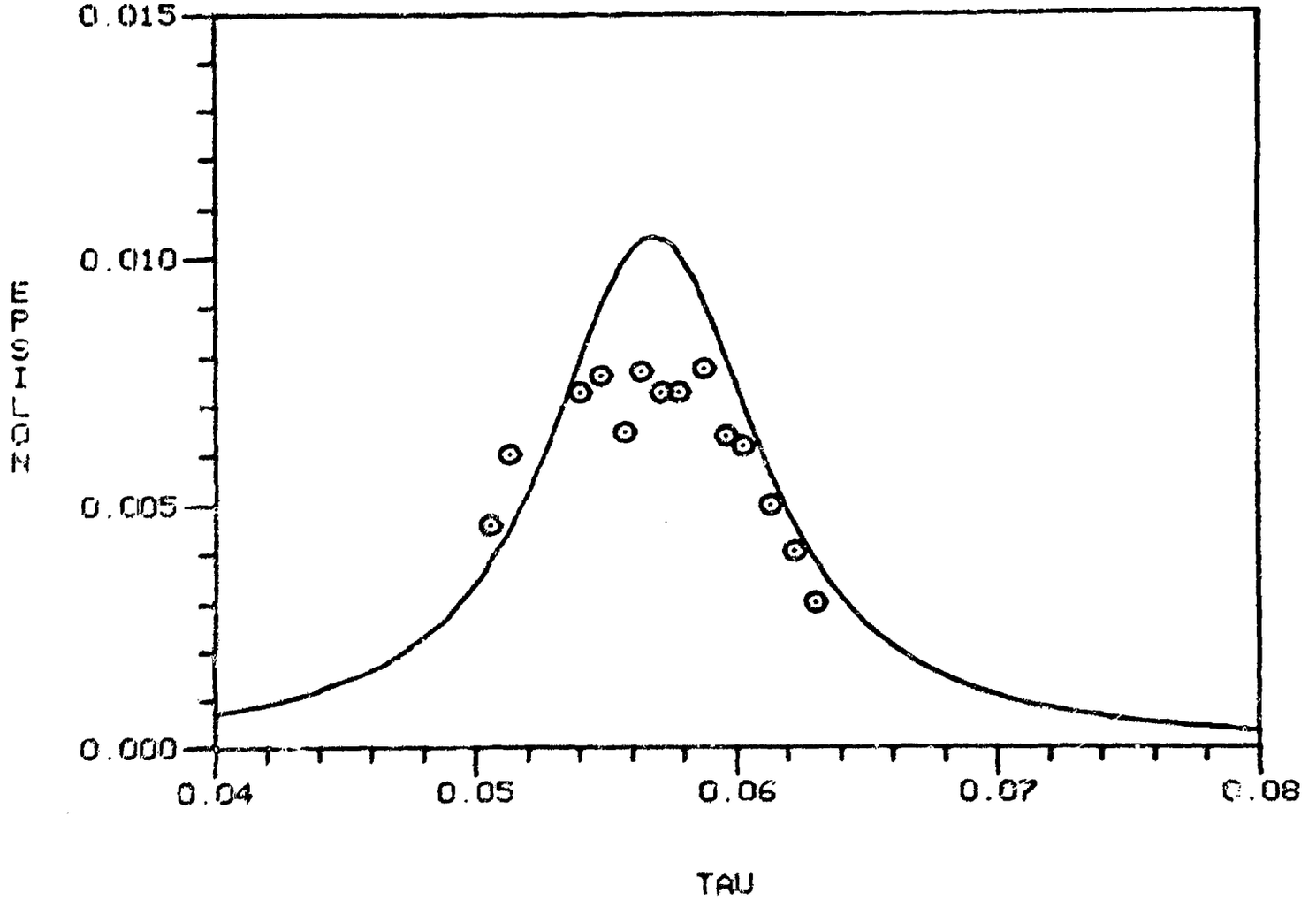

Figure 25b. ε vs τ for a Cavity With Rod (f_d = .977), Predicted Curve and Frazier Data (see Ref 6, Fig 9b), Re = 173,000, c/a = 2.856, m_{Le}/I_x = .0265

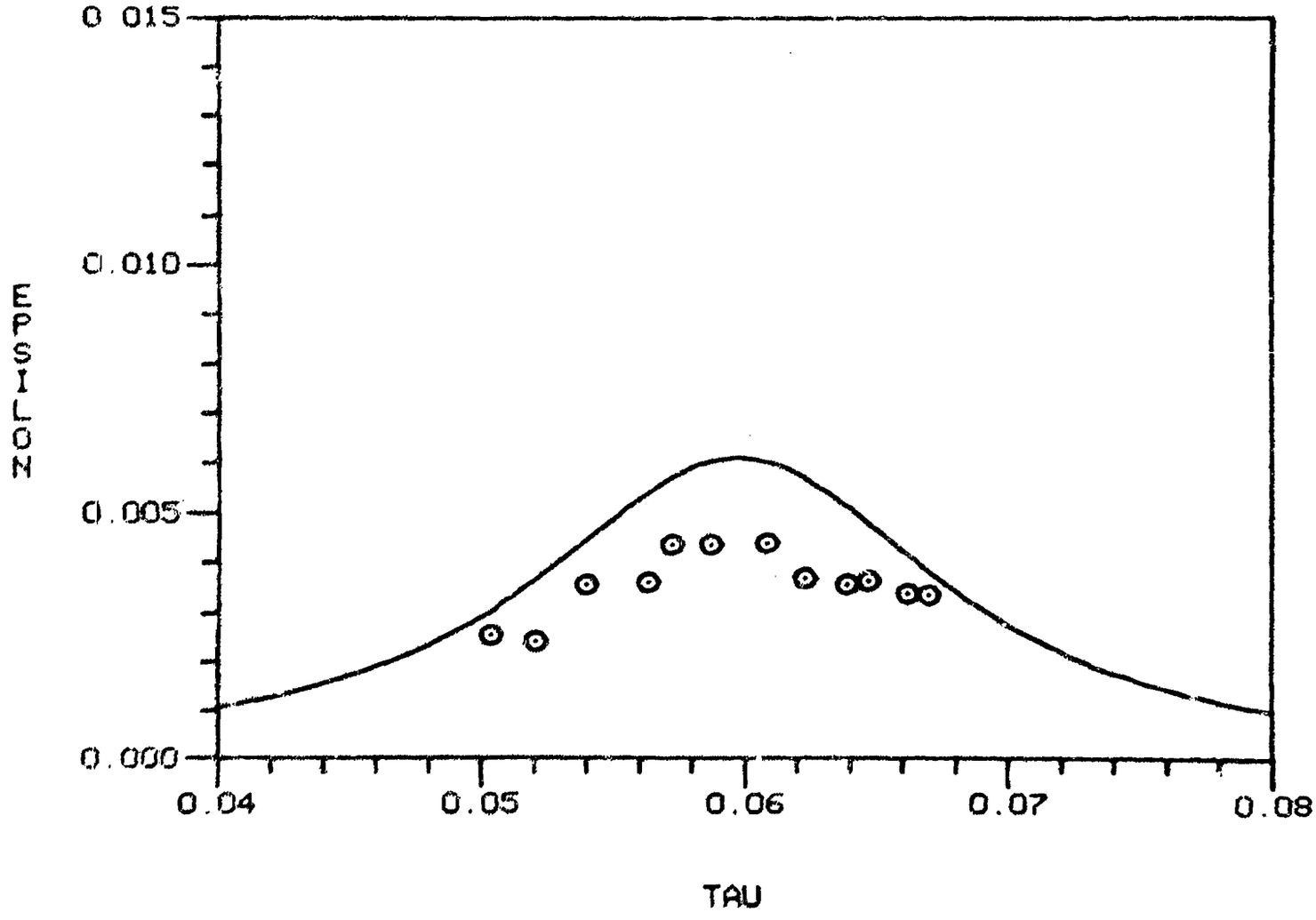

Figure 25c. ε vs τ for a Cavity With Rod (f_d = .977), Predicted Curve and Frasier Data (see Ref 6, Fig 10), Ke = 40,000, c/a = 2.866, $m_L a^2/I_x$ = .0276

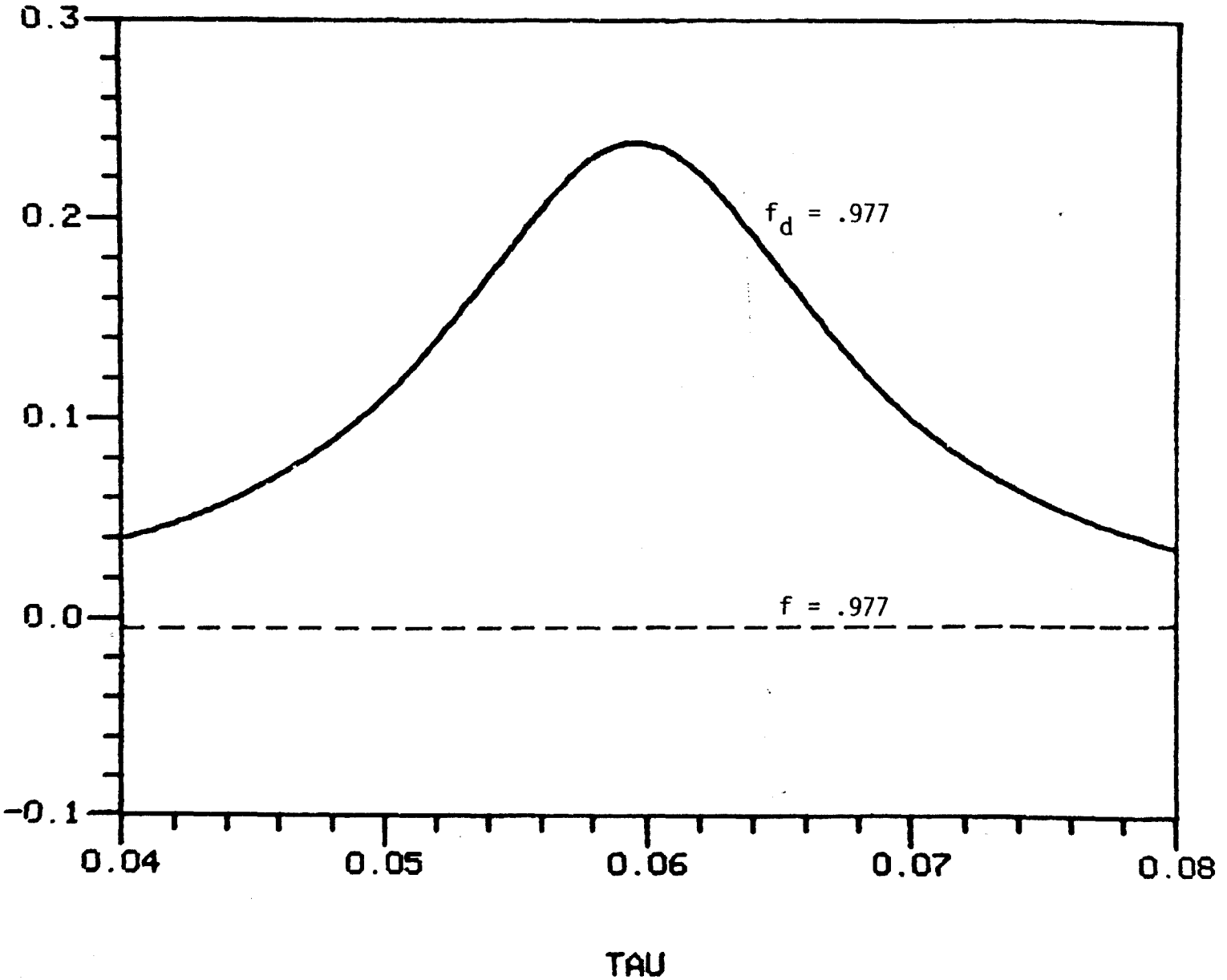

Figure 26. C_{LSM} vs τ for a Rodded (f_d = .977) and for a Partially-Filled (f = .977) Cavity, Re = 40,000, c/a = 2.866, ε = 0

REFERENCES

1. B. G. Karpov, "Experimental Observations of the Dynamic Behavior of Liquid Filled Shell," BRL Report 1171, August 1961. AD 287142.

2. A. Mark and W. H. Mermagen, "Measurement of Spin Decay and Instability of Liquid-Filled Projectiles via Telemetry," BRL Memorandum Report 2333, October 1973. AD 771919.

3. K. Stewartson, "On the Stability of a Spinning Top Containing Liquid," Journal of Fluid Mechanics, Vol. 5, Part 4, September 1959, pp. 577-592.

4. B. G. Karpov, "Dynamics of Liquid-Filled Shell: Resonance and Effect of Viscosity," BRL Report 1279, May 1965. AD 468054.

5. E. H. Wedemeyer, "Viscous Corrections to Stewartson's Stability Criterion," BRL Report 1325, June 1966. AD 489687.

6. R. D. Whiting and N. Gerber, "Dynamics of a Liquid-Filled Gyroscope: Update of Theory and Experiment," BRL Technical Report ARBRL-TR-02221, March 1980. AD A083886.

7. J. T. Frasier and W. E. Scott, "Dynamics of a Liquid-Filled Shell: Cylindrical Cavity with a Central Rod," BRL Report 1391, February 1968. AD 667365.

8. J. T. Frasier, "Dynamics of a Liquid Filled Shell: Viscous Effects in a Cylindrical Cavity with a Central Rod," BRL Memorandum Report 1959, January 1969. AD 684344.

9. J. T. Frasier and W. P. D'Amico, "Stabilization of a Liquid-Filled Shell by Inserting a Cylindrical Partition in the Liquid Cavity," BRL Report 1492, August 1970. AD 874739.

10. C. H. Murphy, "Free Flight Motion of Symmetric Missiles," BRL Report 1216, July 1963. AD 442757.

11. C. H. Murphy, "Influence of Moving Internal Parts on Angular Motion of Spinning Projectiles," Journal of Guidance and Control, Vol. 1, March-April 1978, pp. 117-122. (See also BRL Memorandum Report 2731 dated February 1977. AD A037338.)

12. Y. M. Lynn, "Free Oscillations of a Liquid During Spin-Up," BRL Report 1663, August 1973. AD 769710.

13. C. W. Kitchens, Jr., N. Gerber, and R. Sedney, "Oscillations of a Liquid in a Rotating Cylinder: Part I. Solid-Body Rotation," BRL Technical Report ARBRL-TR-02081, June 1978. AD A057759.

14. W. P. D'Amico, W. G. Beims, and T. H. Rogers, "Pressure Measurements of a Rotating Liquid for Impulsive Coning Motion," BRL Memorandum Report in publication. (See also AIAA Paper No. 82-0249 dated January 1982.)

15. N. W. McLachlan, Bessel Functions for Engineers, Oxford University Press, London, 1955.

16. B. G. Karpov, "Dynamics of Liquid-Filled Shell: Aids for Designers: (a) Milne's Graph; (b) Stewartson's Tables," BRL Memorandum Report 1477, May 1963. AD 410484.

17. J. T. Frasier, "Dynamics of Liquid-Filled Shell. Aids for Designers," BRL Memorandum Report 1892, December 1967. AD 665356.

18. J. W. Bradley, "Calculations of Liquid Payload Moment," BRL Memorandum Report in preparation.

19. W. P. D'Amico and M. C. Miller, "Flight Instability Produced by a Rapidly Spinning, Highly Viscous Liquid," Journal of Spacecraft and Rockets, Vol. 16, January-February 1979, pp. 62-64.

20. M. C. Miller, "Flight Instabilities of Spinning Projectiles Having Nonrigid Payloads," Journal of Guidance, Control, and Dynamics, Vol. 5, pp. 151-157, March-April 1982.

21. R. D. Whiting, "An Experimental Study of Forced Asymmetric Oscillations in a Rotating Liquid-Filled Cylinder," BRL Technical Report ARBRL-TR-02376, October 1981. AD A107948.

22. N. Gerber, R. Sedney, and J. M. Bartos, "Pressure Moment on a Liquid-Filled Projectile: Solid Body Rotation," BRL Technical Report in press.

23. W. P. D'Amico and T. H. Rogers, "Yaw Instabilities Produced by Rapidly Rotating, Highly Viscous Liquids," AIAA Paper No. 81-0224, January 1981.

24. W. P. D'Amico, "Dynamics of Liquid Filled Shell: Liquid-Central Burster Interference," BRL Memorandum Report 1985, June 1969. AD 855134.

25. W. E. Scott, "The Inertial Wave Frequency Spectrum in a Cylindrically Confined, Inviscid, Incompressible, Two Component Liquid," BRL Report 1609, September 1972. AD 752439.

26. W. E. Scott, "The Dynamical Effect of Inertial Waves on the Free Flight Motion of a Body Containing Several Eccentrically Located, Liquid-Filled Cylinders," BRL Report 1551, September 1971. AD 733365.

27. E. H. Wedemeyer, "Dynamics of Liquid Filled Shell: Non-Cylindrical Cavity," BRL Report 1326, August 1966. AD 489899.

28. B. G. Karpov, "Dynamics of Liquid-Filled Shell: Resonance in Modified Cylindrical Cavities," BRL Report 1332, August 1966. AD 804825.

29. W. E. Scott and W. P. D'Amico, "Amplitude-Dependent Behavior of a Liquid-Filled Gyroscope," Journal of Fluid Mechanics, Vol. 60, Part 4, 1973, pp. 751-758.

30. W. E. Scott, "The Large Amplitude Motion of a Liquid-Filled Gyroscope and the Non-Interaction of Inertial and Rossby Waves," Journal of Fluid Mechanics, Vol. 72, Part 4, 1975, pp. 649-660.

31. E. H. Wedemeyer, "The Unsteady Flow Within a Spinning Cylinder," Journal of Fluid Mechanics, Vol. 20, Part 3, 1964, pp. 383-399. (See also BRL Report 1225, October 1963, AD 431846.)

32. C. W. Kitchens, Jr., "Ekman Compatibility Conditions in Wedemeyer Spin-Up Model," Physics of Fluids, Vol. 23, Part 5, May 1980, pp. 1062-1064.

33. C. W. Kitchens, Jr., N. Gerber, and R. Sedney, "Spin Decay of Liquid-Filled Projectiles," Journal of Spacecraft and Rockets, Vol. 15, November-December 1978, pp. 348-354. (See also BRL Report 1996, July 1977, AD A043275 and BRL Report 2026, October 1977, AD A050311.)

34. B. G. Karpov, "Dynamics of Liquid-Filled Shell: Instability During Spin-Up," BRL Memorandum Report 1629, January 1965. AD 463926.

35. K. D. Aldridge, "Experimental Verification of the Inertial Oscillations of a Fluid in a Cylinder During Spin-Up," BRL Contract Report 273 dated November 1975. AD A018797.

36. K. D. Aldridge, "Axisymmetric Inertial Oscillations of a Fluid in a Cylindrical Cavity During Spin Up from Rest," Geophys. Astrophys. Fluid Dynamics, Vol. 8, 1977, pp. 279-301.

BIBLIOGRAPHY

A. Yawsonde Data Reports

1. W. P. D'Amico, V. Oskay, and W. H. Clay, "Flight Tests of the 155mm XM687 Binary Projectile and Associated Design Modifications Prior to the Nicolet Winter Test 1974-1975," BRL Memorandum Report 2748, May 1977. AD B019969L.

2. V. Oskay and J. H. Whiteside, "Flight Behavior of 155mm (XM687 Mod I and XM687 Mod II) and 8-Inch (XM736 Mod I) Binary Shell at Nicolet, Canada, During the Winter of 1974-1975," BRL Memorandum Report 2608, March 1976. AD B010566L.

3. W. H. Mermagen, W. H. Clay, and V. Oskay, "Yawsonde Data from Firings in the Nicolet Winter Program 1974-1975," BRL Memorandum Report 2612, April 1976. AD B011225L.

4. W. P. D'Amico, "Early Flight Experiments with the XM761," BRL Memorandum Report 2791, September 1977. AD B024975L.

5. W. P. D'Amico, "Field Tests of the XM761: First Diagnostic Test," BRL Memorandum Report 2792, September 1977. AD B024976L.

6. A. Mark, "Measurements of Angular Momentum Transfer in Liquid-Filled Projectiles," BRL Technical Report ARBRL-TR-02029, November 1977. AD A051056.

7. W. P. D'Amico, "Field Tests of the XM761: Second Diagnostic Test," BRL Memorandum Report ARBRL-MR-02806, January 1978. AD B025305L.

8. W. P. D'Amico and W. H. Clay, "Flight Tests for Prototype Felt Wedge/White Phosphorous Improved Smoke Concept," BRL Memorandum Report ARBRL-MR-02824, April 1978. AD A054643.

9. W. P. D'Amico and A. Mark, "The Application of a Highly Permeable Medium to Reduce Spin-Up Time and to Stabilize a Liquid-Filled Shell," BRL Memorandum Report ARBRL-MR-02851, July 1978. AD A058595.

10. W. P. D'Amico and M. C. Miller, "Flight Instability Produced by a Rapidly Spinning, Highly Viscous Liquid," Journal of Spacecraft and Rockets, Vol. 16, January-February 1979, pp. 62-64.

11. W. P. D'Amico, "Aeroballistic Testing of the XM825 Projectile: Phase I," BRL Memorandum Report ARBRL-MR-02911, March 1979. AD B037680L.

12. W. P. D'Amico and V. Oskay, "Aeroballistic Testing of the XM825 Projectile: Phase II," BRL Memorandum Report ARBRL-MR-03072, January 1981. AD A098036.

13. W. P. D'Amico, W. H. Clay, and A. Mark, "Diagnostic Tests for Wick-Type Payloads and High Viscosity Liquids," BRL Memorandum Report ARBRL-MR-02913, April 1979. AD A072812.

14. W. P. D'Amico, W. H. Clay, and A. Mark, "Yawsonde Data for M687-Type Projectiles with Application to Rapid Spin Decay and Stewartson-Type Spin-Up Instabilities," BRL Memorandum Report ARBRL-MR-03027, June 1980. AD A089646.

15. W. P. D'Amico and W. H. Clay, "High Viscosity Liquid Payload Yawsonde Data for Small Launch Yaws," BRL Memorandum Report ARBRL-MR-03029, June 1980. AD A088411.

B. Gyroscope Data Reports

1. B. G. Karpov, "Dynamics of Liquid-Filled Shell: Resonance and Effect of Viscosity," BRL Report 1279, May 1965. AD 468054.

2. B. G. Karpov, "Liquid Filled Gyroscope: The Effect of Reynolds Number on Resonance," BRL Report 1302, October 1965. AD 479430.

3. B. G. Karpov, "Dynamics of Liquid-Filled Shell: Resonance in Modified Cylindrical Cavities," BRL Report 1332, August 1966. AD 804825.

4. W. P. D'Amico, "Dynamics of Liquid Filled Shell: Liquid-Central Burster Interference," BRL Memorandum Report 1985, June 1969. AD 855134.

5. W. P. D'Amico, "Dynamics of Liquid Filled Shell: Treatment of Cavities with Partial Bursters," BRL Technical Note 1744, February 1971. AD 882230.

6. J. T. Frasier and W. E. Scott, "Stability of a Liquid-Filled Gyroscope: Inviscid Analysis, Viscous Corrections, and Experiments," Journal of Spacecraft and Rockets, Vol. 8, May 1971, pp. 523-526.

7. B. G. Karpov, J. T. Frasier, and W. P. D'Amico, "Experimental Studies with a Liquid-Filled Gyroscope," Journal of Spacecraft and Rockets, Vol. 9, March 1972, pp. 220-222.

8. W. E. Scott and W. P. D'Amico, "Amplitude-Dependent Behavior of a Liquid Filled Gyroscope," Journal of Fluid Mechanics, Vol. 60, Part 4, 1973, pp. 751-758.

9. R. D. Whiting and Nathan Gerber, "Dynamics of a Liquid-Filled Gyroscope: Update of Theory and Experiment," BRL Report ARBRL-TR-02221, March 1980. AD A083886.

10. W. P. D'Amico and M. D. Fuller, "Experimental Study of a Liquid Filled Cylinder with Unequal Internal Diameters," BRL Memorandum Report ARBRL-MR-03070, January 1981. AD A096800.

11. W. P. D'Amico and T. H. Rogers, "Yaw Instabilities Produced by Rapidly Rotating, Highly Viscous Liquids," AIAA Paper 81-0224, January 1981.

12. R. D. Whiting, "An Experimental Study of Forced Asymmetric Oscillations in a Rotating Liquid Filled Cylinder," BRL Technical Report ARBRL-TR-02376, October 1981.

13. W. P. D'Amico, W. G. Beims, and T. H. Rogers, "Pressure Measurements of a Rotating Liquid for Impulsive Coning Motion," BRL Memorandum Report in publication. (See also AIAA Paper No. 82-0249 dated January 1982.)

APPENDIX A

DERIVATIONS OF EQUATIONS (3.7-3.9)

For single mode coning motion, the earth-fixed components of unit vectors along the non-rotating aeroballistic axes have the following simple form accurate to the first order in K_j.

$$\vec{e}_{\hat{x}} = (1, -K_j \cos \phi_j, -K_j \sin \phi_j) \tag{A1}$$

$$\vec{e}_{\hat{y}} = (K_j \cos \phi_j, 1, 0) \tag{A2}$$

$$\vec{e}_{\hat{z}} = (K_j \sin \phi_j, 0, 1) \tag{A3}$$

The vector from the projectile's center of mass to any point on the projectile can be given by aeroballistic cylindrical coordinates $(\hat{x}, \hat{r}, \hat{\theta})$ and can then be related to earth-fixed coordinates (x_e, y_e, z_e) by the following equation:

$$(x_e, y_e, z_e) = \hat{x}\, \vec{e}_{\hat{x}} + \hat{r} \left(\cos \hat{\theta}\, \vec{e}_{\hat{y}} + \sin \hat{\theta}\, \vec{e}_{\hat{z}} \right) \tag{A4}$$

If we now introduce earth-fixed cylindrical coordinates (x_e, r_e, θ_e), the three component equations of vector Equation (A4) are:

$$x_e = \hat{x} + \hat{r} K_j \cos (\phi_j - \hat{\theta}) \tag{A5}$$

$$r_e \cos \theta_e = \hat{r} \cos \hat{\theta} - \hat{x} K_j \cos \phi_j \tag{A6}$$

$$r_e \sin \theta_e = \hat{r} \sin \hat{\theta} - \hat{x} K_j \sin \phi_j \tag{A7}$$

Since the earth-fixed cylindrical coordinates will be used throughout this report, and missile-fixed cylindrical coordinates are never used, we can omit the subscript "e" without any ambiguity problem and will do so as a convenience. Equation (A6) can be multiplied by sin θ, Equation (A7) by cos θ, and the results subtracted to yield:

$$\sin (\theta - \hat{\theta}) = -(\hat{x} K_j / \hat{r}) \sin (\phi_j - \theta) \tag{A8}$$

or

$$\theta \doteq \tilde{\theta} + R \left\{ i(x/r) \hat{K} e^{s\phi} - i\theta \right\} \tag{A9}$$

Next we square Equations (A6 - A7) and add the results.

$$r^2 = \tilde{r}^2 - 2 \tilde{x} \tilde{r} K_j \cos(\phi_j - \theta) + K_j^2 \tilde{x}^2 \tag{A10}$$

or

$$r \doteq \tilde{r} - R \left\{ x \hat{K} e^{s\phi} - i\theta \right\} \tag{A11}$$

Finally, Equation (A9) can be used to obtain a revised version of Equation (A5).

$$x = \tilde{x} + R \left\{ r \hat{K} e^{s\phi} - i\theta \right\} \tag{A12}$$

For any fixed point on the projectile, $\dot{\tilde{x}} = \dot{\tilde{r}} = 0$, $\dot{\tilde{\theta}} = \dot{\phi}$. Its velocity in earth-fixed cylindrical coordinates can be computed by differentiating Equations (A9, A11, A12).

$$V_x = \dot{x} = R \left\{ \dot{\phi} (s - i) r \hat{K} e^{s\phi} - i\theta \right\} \tag{A13}$$

$$V_r = \dot{r} = -R \left\{ \dot{\phi} (s - i) x \hat{K} e^{s\phi} - i\theta \right\} \tag{A14}$$

$$V_\theta = r\dot{\theta} = r\dot{\phi} + R \left\{ i\dot{\phi} (s - i) x \hat{K} e^{s\phi} - i\theta \right\} \tag{A15}$$

APPENDIX B

SOLUTION OF BOUNDARY LAYER EQUATIONS

For an incompressible fluid with constant viscosity, the Navier-Stokes and continuity equations in cylindrical coordinates are:

$$\frac{\partial V_r}{\partial t} + V_r \frac{\partial V_r}{\partial r} + \frac{V_\theta}{r} \frac{\partial V_r}{\partial \theta} - \frac{V_\theta^2}{r} + V_x \frac{\partial V_r}{\partial x}$$

$$= - \frac{1}{\rho_L} \frac{\partial p}{\partial r} + \nu \left[\nabla_c^2 V_r - \frac{V_r}{r^2} - \frac{2}{r^2} \frac{\partial V_\theta}{\partial \theta} \right] \tag{B1}$$

$$\frac{\partial V_\theta}{\partial t} + V_r \frac{\partial V_\theta}{\partial r} + \frac{V_\theta}{r} \frac{\partial V_\theta}{\partial \theta} + \frac{V_r V_\theta}{r} + V_x \frac{\partial V_\theta}{\partial x}$$

$$= - \frac{1}{\rho_L r} \frac{\partial p}{\partial \theta} + \nu \left[\nabla_c^2 V_\theta - \frac{V_\theta}{r^2} + \frac{2}{r^2} \frac{\partial V_r}{\partial \theta} \right] \tag{B2}$$

$$\frac{\partial V_x}{\partial t} + V_r \frac{\partial V_x}{\partial r} + \frac{V_\theta}{r} \frac{\partial V_x}{\partial \theta} + V_x \frac{\partial V_x}{\partial x} = - \frac{1}{\rho_L} \frac{\partial p}{\partial x} + \nu \nabla_c^2 V_x \tag{B3}$$

$$\frac{\partial V_r}{\partial r} + \frac{V_r}{r} + \frac{1}{r} \frac{\partial V_\theta}{\partial \theta} + \frac{\partial V_x}{\partial x} = 0 \tag{B4}$$

where

$$\nabla_c^2 = \frac{\partial^2}{\partial r^2} + \frac{1}{r} \frac{\partial}{\partial r} + \frac{\partial^2}{\partial x^2} + \frac{1}{r^2} \frac{\partial^2}{\partial \theta^2}$$

Equations (3.10 - 3.13) can be substituted in Equations (B1 - B4), and products of u_s, v_s, w_s neglected to yield

$$(s - i)v_s - 2w_s + a \frac{\partial p_s}{\partial r} = \gamma Re^{-1} \left[\nabla_\theta^2 v_s - \frac{a^2 v_s}{r^2} + \frac{2a^2 i w_s}{r^2} \right] \tag{B5}$$

$$(s - i)w_s + 2v_s - \frac{iap_s}{r} = \gamma Re^{-1}\left[\nabla_\theta^2 w_s - \frac{a^2 w_s}{r^2} - \frac{2a^2 i v_s}{r^2}\right] \tag{B6}$$

$$(s - i)u_s + a\frac{\partial p_s}{\partial x} = \gamma Re^{-1}\nabla_\theta^2 u_s \tag{B7}$$

$$\frac{\partial(rv_s)}{\partial r} - iw_s + r\frac{\partial u_s}{\partial x} = 0 \tag{B8}$$

where

$$\nabla_\theta^2 = a^2\left[\frac{\partial^2}{\partial r^2} + \frac{\partial}{r\partial r} + \frac{\partial^2}{\partial x^2} - \frac{1}{r^2}\right]$$

Next we assume that the velocity components and pressure can be written as the sum of inviscid and viscous terms. The inviscid terms satisfy Equations (B5 - B8) for $Re^{-1} = 0$ and the viscous terms satisfy Equations (B5 - B8) but are zero except for small regions near the walls extending a distance δ from the walls. We will make the usual boundary layer assumptions that $\delta \sim Re^{-1/2}$ and derivatives normal to the wall vary as δ^{-1} while deviations along the wall are of order unity. Positive spin will be assumed ($\gamma=1$) since the effect of negative spin follows from Eq. (2.8).

$$\therefore\ u_s = u_{si} + u_{sv} \tag{B9}$$

$$v_s = v_{si} + v_{sv} \tag{B10}$$

$$w_s = w_{si} + w_{sv} \tag{B11}$$

$$p_s = p_{si} + p_{sv} \tag{B12}$$

where $u_{sv} = v_{sv} = w_{sv} = p_{sv} = 0$ far from wall.

u_s, v_s, w_s must satisfy Eqs. (3.7 - 3.9) at the wall.

$$\therefore\ u_{sv} = (s - i)(r/a)\dot{K} - u_{si} \tag{B13}$$

$$v_{sv} = -(s - i)(x/a)\dot{K} - v_{si} \tag{B14}$$

$$w_{sv} = i(s - i)(x/a)\dot{K} - w_{si} \tag{B15}$$

Near the cylindrical lateral wall, r = a, Eqs. (B5 - B7) become

$$a \frac{\partial p_{sv}}{\partial r} = 2w_{sv} - (s - i)v_{sv} + a^2 Re^{-1} \frac{\partial^2 v_{sv}}{\partial r^2} \tag{B16}$$

$$(s - i)w_{sv} = a^2 Re^{-1} \frac{\partial^2 w_{sv}}{\partial r^2} - 2v_{sv} + \frac{iap_{sv}}{r} \tag{B17}$$

$$(s - i)u_{sv} = a^2 Re^{-1} \frac{\partial^2 u_{sv}}{\partial r^2} - a \frac{\partial p_{sv}}{\partial x} \tag{B18}$$

The continuity Equation (B8) shows that $\partial v_{sv}/\partial r$ is of order w_{sv} and, therefore, v_{sv} is of order δw_{sv} and can be neglected in Equations (B16) and (B17). (B16) now shows that p_{sv} is of order δw_{sv} and can be neglected in Eq. (B18).

$$\therefore \quad a \frac{\partial p_{sv}}{\partial r} = 2w_{sv} \tag{B19}$$

$$(s - i)w_{sv} = a^2 Re^{-1} \frac{\partial^2 w_{sv}}{\partial r^2} \tag{B20}$$

$$(s - i)u_{sv} = a^2 Re^{-1} \frac{\partial^2 u_{sv}}{\partial r^2} \tag{B21}$$

The solutions to Eqs. (B20 - B21) that satisfy Eqs. (B13, B15) are:

$$w_{sv} = \left[(1 + is)(x/a)\dot{K} - w_{si} \right] e^{(r-a)/a\delta_a} \tag{B22}$$

$$u_{sv} = -\left[(i - s)\dot{K} - u_{si} \right] e^{(r-a)/a\delta_a} \tag{B23}$$

where $$\delta_a = \left[\frac{1 + i}{\sqrt{2(1+is)}} \right] Re^{-1/2}$$

Substituting Eqs. (B22 - B23) in Eq. (B8) and integrating, we can obtain v_{sv} near the lateral wall r = a.

$$v_{sv} = \delta_a \left[(i - s)(x/a)\dot{K} - v_{si} - a \frac{\partial v_{si}}{\partial r} \right] e^{(r-a)/a\delta_a} \tag{B24}$$

Eq. (B24) can then be inserted in boundary condition (B14) to give a boundary condition on the inviscid radial velocity at r = a.

$$v_{si} - a\delta_a \frac{\partial v_{si}}{\partial r} = (i - s)\,(x/a)\,\hat{K} \tag{B25}$$

Turning now to the endwalls, $\hat{x} \equiv (x-h)/c = \pm 1$, similar boundary layer size arguments give the following equations:

$$(s - i)v_{sv} - 2w_{sv} = a^2 Re^{-1} \frac{\partial^2 v_{sv}}{\partial x^2} \tag{B26}$$

$$(s - i)w_{sv} + 2v_{sv} = a^2 Re^{-1} \frac{\partial^2 w_{sv}}{\partial x^2} \tag{B27}$$

$$\frac{\partial p_{sv}}{\partial x} = 0 \tag{B28}$$

Next Eq. (B26) is multiplied by i and both added and subtracted from Eq. (B27) to give two simpler differential equations.

$$(s - 3i)\,A = a^2 Re^{-1} \frac{\partial^2 A}{\partial x^2} \tag{B29}$$

$$(s + i)\,B = a^2 Re^{-1} \frac{\partial^2 B}{\partial x^2} \tag{B30}$$

where

$$A = w_{sv} + i v_{sv}$$

$$B = w_{sv} - i v_{sv}$$

The solution to Eqs. (B29 - B30) which satisfies Eqs. (B14 - B15) is

$$w_{sv} + i\, v_{sv} = -\,(w_{si} + i\, v_{si})\, e^{-(1\mp\hat{x})\alpha} \tag{B31}$$

$$w_{sv} - i\, v_{sv} = -\left[w_{si} - i\, v_{si} - 2(1-is)\left(\frac{h\pm c}{a}\right)\bar{K}\right] e^{-(1\mp\hat{x})\bar{\alpha}} \tag{B32}$$

where

$$\alpha = (c/a)\,\delta_a^{-1}\,\sqrt{(3+is)/(1+is)}$$

$$\beta = i(c/a)\ \delta_a^{-1}\ \sqrt{(1-is)/(1+is)}$$

Substituting Eqs. (B31 - B32) in Eq. (B8) and integrating, we can obtain u_{sv} near the end walls $\hat{x} = \pm 1$.

$$u_{sv} = \pm (a/2c)\ \delta_a\ (1+is)^{-1/2} \left\{ \frac{(1-is)}{\sqrt{3+is}}\ e^{-(i\mp\hat{x})\alpha} \right. \tag{B33}$$

$$\left. + \frac{i(3+is)}{\sqrt{1-is}}\ e^{-(1\mp\hat{x})\beta} \right\} \frac{\partial u_{si}}{\partial \hat{x}}$$

(B33) can now be inserted in boundary condition (B13) to give boundary conditions on the inviscid axial velocity at $\hat{x} = \pm 1$.

$$u_{si} \mp \delta_c \frac{\partial u_{si}}{\partial \hat{x}} = -(i-s)(r/a)\ \hat{K} \tag{B34}$$

where

$$\delta_c = \frac{-(a/c)\delta_a}{2\sqrt{1+is}} \left\{ \frac{1-is}{\sqrt{3+is}} + i\left(\frac{3+is}{\sqrt{1-is}}\right) \right\}$$

APPENDIX C

SOLUTION OF INVISCID EQUATIONS

If the assumed solution for p_{si} as given by Eq. (5.11) is placed in the partial differential equation for p_{si} (Eq. (5.1)), a pair of ordinary differential equations involving a parameter λ_k can be obtained.

$$X_k'' (\hat{x}) + \lambda_k^2 X_k (\hat{x}) = 0 \tag{C1}$$

$$r^2 R_k'' (r) + r R_k' (r) - \left[1 - (r/c)^2 \hat{\lambda}_k^2 \right] R_k (r) = 0 \tag{C2}$$

where $\hat{\lambda}_k^2 = -(s^2 - 2is + 3)(s \cdot i)^{-2} \lambda_k^2$

If the assumed p_{si} solution is used in the endwall boundary conditions, Eq. (5.5), two conditions that determine the eigenvalue λ_k can be written.

$$X_k' (1) - \delta_c X_k'' (1) = 0 \tag{C3}$$

$$X_k' (-1) + \delta_c X_k'' (-1) = 0 \tag{C4}$$

The general solution of Equation (C1) is:

$$\left.\begin{aligned} X_k &= A_k \cos (\lambda_k \hat{x}) + B_k \sin (\lambda_k \hat{x}) \qquad \lambda_k \neq 0 \\ X_0 &= A_0 + B_0 \hat{x} \qquad\qquad\qquad\quad \lambda_k = 0 \end{aligned}\right\} \tag{C5}$$

Equations (C3 - C4) can now be used to obtain two sets of solutions from Eq. (C5) for $\lambda_k \neq 0$ and to simplify the X_0 function to $X_0 = 1$.

$$A_k = 1, \quad B_k = 0, \quad \sin \lambda_k - \lambda_k \delta_c \cos \lambda_k = 0 \tag{C6}$$

$$A_k = 0, \quad B_k = 1, \quad \cos \lambda_k + \lambda_k \delta_c \sin \lambda_k = 0 \tag{C7}$$

For $\delta_c = 0$, the solutions to Eq. (C6 - C7) are $\lambda_k = \pi k/2$, where the k's are even integers for Eq. (C6) and odd integers for Eq. (C7). For small δ_c it can be easily shown that the solutions are

$$\lambda_k = k\pi \tag{C8}$$

where $\lambda \doteq (\pi/2)\ [1 + \delta_c]$ (C9)

Finally, direct substitution shows that the solutions to Equation (C2) are

$$R_0 = (h/c)\ [E_0\ r/a + F_0\ a/r] \tag{C10}$$

$$R_k = a_k\ [E_k\ J_1\ (k\hat{\lambda}\ r/c) + F_k\ Y_1\ (k\hat{\lambda}\ r/c)] \tag{C11}$$

$$(k \neq 0)$$

where $\hat{\lambda}^2 = -(s^2 - 2is + 3)\ (s - i)^{-2}\ \lambda^2$

APPENDIX D

LEAST SQUARES COEFFICIENTS OF SERIES (5.15)

In solving the inviscid equations it is necessary to expand x as a series in the X_k's.

$$x/c = \hat{x} + h/c = \sum_{k=0}^{N} a_k X_k(\hat{x}) \tag{D1}$$

By observation, $a_0 = h/c$. The remaining a_k's can be determined by requiring the series to be a least squares fit. That is, $\hat{R}^2$ should be a minimum where

$$\hat{R}^2 = \int_{-1}^{1} \left(\hat{x} - \sum_{k=1}^{N} a_k X_k\right)\left(\hat{x} - \sum_{k=1}^{N} \bar{a}_k \bar{X}_k\right) d\hat{x} \tag{D2}$$

If $a_m = a_{Rm} + a_{Im}$, then $\hat{R}^2$ is a minumum when

$$\frac{\partial \hat{R}^2}{\partial a_{Rm}} = \frac{\partial \hat{R}^2}{\partial a_{Im}} = 0 \tag{D3}$$

Both of these conditions are satisfied when

$$\sum_{k=1}^{N} b_{mk} a_k = b_m \tag{D4}$$

where

$$b_m = \int_{-1}^{1} \hat{x}\, \bar{X}_m\, d\hat{x}$$

$$= \begin{cases} 0 & m \text{ even} \\ 2\int_0^1 \hat{x}\, \bar{X}_m\, dx & m \text{ odd} \end{cases}$$

$$b_{mk} = \int_{-1}^{1} \bar{X}_m X_k\, d\hat{x}$$

If the eigenfunctions, X_k, are orthogonal,

$$b_{mk} = 0 \qquad m \neq k \tag{D5}$$

$$a_k = b_k / b_{kk} \tag{D6}$$

For $\delta_c \neq 0$, the functions are not orthogonal and the a_k's must be computed by inverting an N × N order matrix (b_{mk}). This computation can be simplified in a relation that comes from Equation (C1).

$$\begin{aligned} b_{mk} &= \int_{-1}^{1} \bar{X}_m \, X_k \, d\hat{x} \\ &= -\lambda_k^{-2} \int_{-1}^{1} \bar{X}_m \, X_k'' \, d\hat{x} \\ &= -\lambda_k^{-2} \left[X_k' \, \bar{X}_m - X_k \, \bar{X}_m' \right]_{-1}^{1} + \left(\frac{\bar{\lambda}_m}{\lambda_k} \right)^2 b_{mk} \end{aligned} \tag{D7}$$

Eqs. (C3 -C4) reduce Eq. (D7) to

$$\left[1 - \left(\frac{\bar{\lambda}_m}{\lambda_k} \right)^2 \right] b_{mk} = \left[\delta_c - \left(\frac{\bar{\lambda}_m}{\lambda_k} \right)^2 \bar{\delta}_c \right] \left[\bar{X}_m (1) \, X_k (1) + \bar{X}_m (-1) \, X_k (-1) \right] \tag{D8}$$

$$\left.\begin{aligned} &= 0 \quad \text{if } m + k \text{ odd} \\ &= 2 \left[\delta_c - \left(\frac{\bar{\lambda}_m}{\lambda_k} \right)^2 \bar{\delta}_c \right] \bar{X}_m (1) \, X_k (1) \\ &\qquad \text{if } m + k \text{ even} \end{aligned}\right\} \tag{D9}$$

According to Eq. (D9), the odd and even subscripts separate in the matrix (b_{mk}) so that the odd a_k depend only on the matrix with both m and k odd. Thus, the matrix to be inverted is a square matrix with $(N + 1)/2$ rows and $(N + 1)/2$ columns.

LIST OF SYMBOLS

A	$w_{sv} + i\, v_{sv}$
A_k, B_k	general coefficients in Eq. (C5)
a	radius of a right-circular cylindrical cavity containing liquid
a_k	solution of the system $\sum_k b_{mk}\, a_k = b_m$
a_{Rk}, a_{IK}	real and imaginary parts of a_k
B	$w_{sv} - i\, v_{sv}$
b	radius of the cylindrical air core within a partially-filled spinning cavity
b_k	$\int_{-1}^{1} \hat{x}\, \bar{X}_k\, (\hat{x})\, d\hat{x}$
b_{mk}	$\int_{-1}^{1} \bar{X}_m\, (\hat{x})\, X_k\, (\hat{x})\, d\hat{x}$
C_{LIM}	liquid in-plane moment coefficient for one-mode coning or spiral motion; the imaginary part of C_{LM}
C_{LIM_j}	fast (j=1) and slow (j=2) mode liquid in-plane moment coefficients; the imaginary part of C_{LM_j}
C_{LM}	$\left(M_{L\hat{Y}} + i\, M_{L\hat{Z}}\right) \Big/ \left(m_L a^2 \dot{\phi}^2\, \tau\, \hat{K}\, e^{S\phi}\right)$
C_{LN_j}	fast (j=1) and slow (j=2) mode liquid moment coefficients defined by Eq. (2.7)
C_{LMq}	$\sigma_L\, C_{LSM}$
C_{LMq_j}	$\sigma_L\, C_{LSM_j}$
C_{LSM}	liquid side moment coefficient for one-mode coning or spiral motion; the real part of C_{LM} is $\gamma\, C_{LSM}$
C_{LSM_j}	fast (j=1) and slow (j=2) mode liquid side moment coefficients; the real part of C_{LM_j} is $\gamma\, C_{LSM_j}$

$C_{M_{p\alpha}}$ $\quad \dfrac{\left|\text{Magnus moment}\right|}{(1/2\ \rho S \ell^2\ V\ \dot{\phi}\ \ \left|\hat{\xi}\right|}$

$C_{M_q} + C_{M_{\dot{\alpha}}}$ $\quad \dfrac{\left|\text{sum of the damping moments}\right|}{(1/2)\ \rho S \ell^2\ V\ \left|\text{cross spin}\right|}$

C_{M_α} $\quad \dfrac{\left|\text{static moment}\right|}{(1/2\ )\ \rho S \ell^2\ V\ \left|\hat{\xi}\right|}$

C_{N_α} $\quad \dfrac{-\ (F_{\hat{y}} + i\ F_{\hat{z}})}{(1/2\ \rho S V^2\ \hat{\xi}}$

C_p $\quad (\Delta p)\ \max\ /\ (K_j\ \rho L\ a^2\ \dot{\phi}^2)$; a nondimensional, real pressure coefficient

$C_{pk}(r)$ $\quad R_k\ (r) + (s - 2i)\ s\ (r/a)\ a_k$, $k = 0, \ldots N$

c one-half the length of the cylindrical cavity containing liquid

d radius of a central rod within a fully-filled cylindrical cavity

E_k, F_k parameters in the expressions (5.18-5.19) for R_k; determined in the inviscid case by boundary conditions (6.6-6.7)

$\hat{E}_k\ (\tau_{kn})$ $\quad \left[\dfrac{G_k\ (\tau)}{dG_k\ (\tau)/d\tau}\right]_{\tau_{kn}} \cdot\ E_k$

$\hat{e}_{\hat{x}}$, $\hat{e}_{\hat{y}}$, $\hat{e}_{\hat{z}}$ unit vectors along the aeroballistic axes $\hat{X}\ \hat{Y}\ \hat{Z}$

$\hat{F}_k\ (\tau_{km})$ $\quad \left[\dfrac{G_k\ (\tau)}{dG_k\ (\tau)/d\tau}\right]_{\tau_{kn}} \cdot\ F_k$

$F_{\hat{X}}$, $F_{\hat{Y}}$ $\hat{Y}$, $\hat{Z}$ components of the normal force

f $1 - (b/a)^2$; the fill ratio: the fraction of the cavity occupied by liquid.

f_d $1 - (d/a)^2$; the rodded fill ratio

f_j — $1 + (m_L a^2/I_x) C_{LIM_j}$

f^* — c/ka, the reduced fineness ratio

$G_k(\tau)$ — the determinant of the boundary value system determining E_k and F_k. Thus for system (6.6-6.7),

$$G_k = C_{11} C_{22} - C_{12} C_{21}$$

$\hat{H}$ — $(\rho S\ell/2m)(V/\ell)\left[C_{N_\alpha} - k_y^{-2}\left(C_{M_q} + C_{M_{\dot{\alpha}}}\right)\right]$

$\hat{H}_{L_j}$ — $-(\rho S\ell^3/2I_y)(V/\ell) C_{LMq_j}$

h — distance from the projectile's center of mass to the center of the cylindrical cavity

I_{Lx}, I_{Ly} — axial and transverse moments of inertia of a "frozen liquid"

I_x, I_y — axial and transverse moments of inertia of the projectile

$J_n(\ )$ — Bessel function (of a complex argument) of the first kind, of order n

$\hat{K}$ — $K_{j0} \exp(i\phi_{j0})$, j = 1 or 2

K_j — magnitude of the j-th yaw arm (j = 1, 2)

K_{j0} — initial value of K_j

k — longitudinal wave number; when k=2j+1 for j=0, 1, 2..., subscript k refers to the number of nodes in the liquid's longitudinal wave pattern

k_x — $(I_x/m\ell^2)^{1/2}$, the projectile's axial radius of gyration

k_y — $(I_y/m\ell^2)^{1/2}$, the projectile's transverse radius of gyration

ℓ — reference length

$\hat{M}$ — $(\rho S\ell^3/2I_y)(V/\ell)^2 C_{M_\alpha}$

$M_{L\hat{Y}}$, $M_{L\hat{Z}}$ — $\hat{Y}$, $\hat{Z}$ components of the aerodynamic moment

m	projectile mass
m_L	$2\pi a^2 c\rho_L$, the liquid mass in a fully-filled cylindrical cavity with no rod
m_p	$m_{pe} + m_{p\ell}$
m_{pe}	that part of C_{LM} due to pressure on the two end walls of the cylindrical cavity
$m_{p\ell}$	that part of C_{LM} due to pressure on the lateral wall of the cylindrical cavity
$m_{p\ell h}$	(that part of $m_{p\ell}$ due to offset h) / $(h/c)^2$
m_{ve}	that part of C_{LM} due to shear on the two end walls of the cylindrical cavity; Eq. (7.4)
m_{veh}	(that part of m_{ve} due to offset h) / $(h/c)^2$
m_{vel}	that part of C_{LM} due to shear on the forward flat end wall of the cylindrical cavity
m^*_{vel}	function defined after Eq. (7.3)
$m_{v\ell}$	that part of C_{LM} due to shear on the lateral wall of the cylindrical cavity; Eq. (7.1)
$m_{v\ell h}$	(that part of $m_{v\ell}$ due to offset h) / $(h/c)^2$
$m^*_{v\ell}$	function defined after Eq. (7.1)
N	maximum considered value of k
n	radial wave number; subscript n refers to the number of nodes in the liquid's radial wave pattern
n_{XE}, n_{YE}, n_{ZE}	earth-fixed components of a unit vector along the X-axis
p	liquid pressure
p_s	liquid pressure perturbation
p_{si}	inviscid part of p_s
p_{sv}	viscous part of p_s

R	the residue associated with each eigenfrequency τ_{nk}; in the Stewartson model, C_{LM} near an eigenfrequency τ_{nk} is proportional to $R^2 / (s - i\,\tau_{nk})$
$\hat{R}$	the square root of the error function to be minimized in determining a_k, Eq. (D2)
$R\{\ \}$	real part of $\{\ \}$
$R_k(r)$	function in the assumed expression (5.11) for p_{si}; the form of this function is given in (5.18-5.19)
Re	$a^2\|\dot{\phi}\|/\nu$, Reynolds number
r	radial coordinate in an earth-fixed cylindrical system
$\hat{r}$	radial coordinate in an aeroballistic non-rolling system
S	reference area
s	$(\gamma\varepsilon + i)\,\tau$
s_g	$\sigma^{2,2}\dot{\phi}/4\hat{M}$, the gyroscope stability factor
s_{kn}	eigenvalue of s for the liquid's (k, n)-th wave mode
$\hat{T}$	$(\rho S\ell/2m)\,(V/\ell)\left[C_{N_\alpha} + k_x^{-2}\,C_{M_{p\alpha}}\right]$
t	time
u_s, v_s, w_s	components of the liquid velocity perturbation in the earth-fixed cylindrical system x, r, θ
u_{si}, v_{si}, w_{si}	inviscid part of u_s, v_s, w_s
u_{sv}, v_{sv}, w_{sv}	viscous part of u_s, v_s, w_s
V	magnitude of the projectile's velocity vector
V_x, V_r, V_θ	velocity components of any point on the projectile in the earth-fixed cylindrical system (3.7-3.9); assumed to be the liquid's velocity components as well (3.10-3.12)
X	coordinate axis along the projectile's axis of symmetry, positive forward
$X_k(\hat{x})$	function in the assumed expression (5.11) for p_{si}; the form of this function is approximately that of (5.12-5.13)

XYZ	missile-fixed axes, origin at the projectile's center of mass
$\tilde{\tilde{XYZ}}$	aeroballistic non-rolling axes, origin at the projectile's center of mass, Z-axis initially downward
$X_e\ Y_e\ Z_e$	earth-fixed axes, X_e initially along the velocity vector, Z_e downward
$x,\ x_e$	X_e-axis coordinate in the earth-fixed Cartesian system
$\hat{x}$	X-axis coordinate in the aeroballistic Cartesian system
$\hat{x}$	$(x - h)/c$
$Y_n(\ )$	Bessel function (of a complex argument) of the second kind, of order n
$y,\ y_e$	Y_e-axis coordinate in the earth-fixed Cartesian system
$z,\ z_e$	Z_e-axis coordinate in the earth-fixed Cartesian system
α	$(c/a)\left[(3 + is) / (1 + is)\right]^{1/2}\ \delta_a^{-1}$
$\hat{\alpha}$	angle of attack: the angle in the $\hat{XZ}$-plane from the X-axis to the velocity vector
β	$i\ (c/a)\left[(1 - is)\ (1 + is)\right]^{1/2}\ \delta_a^{-1}$
$\hat{\beta}$	angle of side-slip: the angle in the $\hat{XY}$-plane from the X-axis to the velocity vector
γ	[illegible]
Δp	the fluctuating part of p
δ	boundary layer thickness
δ_a	$(1 + i)\left[2(1 + is)\ Re\right]^{-1/2}$
δ_c	$\frac{-(a/c)\ \delta_a}{2\sqrt{1 + is}}\left[\frac{1 - is}{\sqrt{3 + is}} + i\left(\frac{3 + is}{\sqrt{1 - is}}\right)\right]$

ϵ	ϵ_j for one-mode yawing motion
ϵ_j	non-dimensionalized growth rate of the j-th yaw mode ($j = 1, 2$)
ϵ_{kn}	eigenvalue of ϵ for the liquid's (k, n)-th wave mode
θ	aximuthal coordinate in an earth-fixed cylindrical system
$\hat{\theta}$	aximuthal coordinate in an aeroballistic cylindrical system
λ	$(\pi/2)\ (1 + \delta_c)$
$\hat{\lambda}$	$\left[\frac{s^2 - 2is + 3}{-(s - i)^2}\right]^{1/2} \lambda$
λ_k	solution of the equation $\cos \lambda_k + \lambda_k \delta_c \sin \lambda_k = 0$, k odd or of the equation $\sin \lambda_k - \lambda_k \delta_c \cos \lambda_k = 0$, k even
$\hat{\lambda}_k$	$\left[\frac{s^2 - 2is + 3}{-(s - i)^2}\right]^{1/2} \lambda_k$
ν	kinematic viscosity
$\tilde{\xi}$	$\tilde{\beta} + i\tilde{\alpha}$
ρ	air density
ρ_L	liquid density
σ	I_x/I_y
q_L	$2\pi_L a^2 \lvert\dot{\phi}\rvert/(\rho S L^2 V)$
τ	τ_j for one-mode yawing motion
τ_j	$\dot{\phi}_j/\dot{\phi}$, the non-dimensionalized frequency of the j-th yaw mode ($j = 1, 2$)
τ_{kn}	the eigenfrequency of the liquid's (k, n)-th wave mode; root of the equation $G_k(\tau) = 0$
τ_{kn0}	inviscid value of τ_{kn}

ϕ	$\dot{\phi}\, t$
ϕ_p	orientation angle associated with C_p
ϕ_j	$\phi_{j0} + \tau_j \dot{\phi}\, t \quad (j = 1, 2)$
ϕ_{j0}	initial orientation angle of the j-th yaw arm (j = 1, 2)
$\dot{\phi}$	spin rate

Superscripts:

$(\bar{\ })$	complex conjugate
$(\dot{\ })$	time derivative
$(\ )'$	derivative with respect to the independent variable involved

DISTRIBUTION LIST

No. of Copies	Organization
12	Administrator Defense Technical Info Center ATTN: DTIC-DDA Cameron Station Alexandria, VA 22314
1	Commander US Army Engineer Waterways Experiment Station ATTN: R.H. Malter Vicksburg, MS 39181
1	Commander US Army Materiel Development and Readiness Command ATTN: DRCDMD-ST 5001 Eisenhower Avenue Alexandria, VA 22333
1	Commander US Army Armament Research and Development Command ATTN: DRDAR-TDC (Dr. D. Gyorog) Dover, NJ 07801
3	Commander US Army Armament Research and Development Command ATTN: DRDAR-TSS (2 cys) DRDAR-LC, Dr. J. Frasier Dover, NJ 07801
6	Commander US Army Armament Research and Development Command ATTN: DRDAR-LCA-F Mr. D. Mertz Mr. E. Falkowski Mr. A. Loeb Mr. R. Kline Mr. S. Kahn Mr. S. Wasserman Dover, NJ 07801
1	Commander US Army Armament Materiel Readiness Command ATTN: DRSAR-LEP-L, Tech Lib Rock Island, IL 61299
1	Director US Army Armament Research and Development Command Benet Weapons Laboratory ATTN: DRDAR-LCB-TL Watervliet, NY 12189
1	Commander US Army Aviation Research and Development Command ATTN: DRDAV-E 4300 Goodfellow Blvd St. Louis, MO 63120
1	Director US Army Air Mobility Research and Development Laboratory ATTN: SAVDL-D, W.J. McCroskey Ames Research Center Moffett Field, CA 94035
1	Commander US Army Communications Research and Development Command ATTN: DRDCO-PPA-SA Fort Monmouth, NJ 07703
1	Commander US Army Electronics Research and Development Command Technical Support Activity ATTN: DELSD-L Fort Monmouth, NJ 07703
1	Commander US Army Missile Command ATTN: DRSMI-R Redstone Arsenal, AL 35898

DISTRIBUTION LIST

No. of Copies	Organization
1	Commander US Army Missile Command ATTN: DRSMI-YDL Redstone Arsenal, AL 35898
1	Commander US Army Missile Command ATTN: DRSMI-RDK Mr. R. Deep Redstone Arsenal, AL 35898
1	Commander US Army Tank Automotive Research and Development Command ATTN: DRDTA-UL Warren, MI 48090
1	Commander US Army Jefferson Proving Ground ATTN: STEJP-TD-D Madison, IN 47251
2	Commander US Army Research Office ATTN: Dr. R.E. Singleton Dr. Jagdish Chandra P.O. Box 12211 Research Triangle Park NC 27709
1	AGARD-NATO ATTN: R.H. Korkegi APO New York 09777
1	Director US Army TRADOC Systems Analysis Activity ATTN: ATAA-SL, Tech Lib White Sands Missile Range NM 88002
3	Commander Naval Air Systems Command ATTN: AIR-604 Washington, DC 20360
2	Commander David W. Taylor Naval Ship Research & Development Center ATTN: H.J. Lugt, Code 1802 S. de los Santos, Head, High Speed Aero Div. Bethesda, MD 20084
1	Commander Naval Surface Weapons Center ATTN: DX-21, Lib Br Dahlgren, VA 22448
5	Commander Naval Surface Weapons Center Applied Aerodynamics Division ATTN: K.R. Enkenhus M. Ciment S.M. Hastings A.E. Winklemann W.C. Ragsdale Silver Spring, MD 20910
1	AFATL (DLDL, Dr. D.C.Daniel) Eglin AFB, FL 32542
2	AFFDL (W.L. Hankey; J.S.Shang) Wright-Patterson AFB, OH 45433
4	Director National Aeronautics and Space Administration Ames Research Center ATTN: D.R. Chapman P. Kutler J. Rakich B. Wick Moffett Field, CA 94035
1	Director National Aeronautics and Space Administration Lewis Research Center ATTN: MS 60-3, Tech Lib 21000 Brookpark Road Cleveland, OH 44135

DISTRIBUTION LIST

No. of Copies	Organization
4	Director National Aeronautics and Space Administration Langley Research Center ATTN: E. Price J. South J.R. Sterrett Tech Library Langley Station Hampton, VA 23365
2	Director National Aeronautics and Space Administration Marshall Space Flight Center ATTN: A.R. Felix, Chief SaE-AERO-AE Dr. W.W. Fowlis Huntsville, AL 35812
2	Director Jet Propulsion Laboratory ATTN: L.M. Mach Tech Library 4800 Oak Grove Drive Pasadena, CA 91103
3	Arnold Research Organization, Inc. ATTN: J D. Whitfield R.K. Matthews J.C. Adams Arnold AFB, TN 37389
1	Aerospace Corporation Aero-Engineering Subdivision ATTN: Walter F. Reddall El Segundo, CA 90245
3	Aerospace Corporation ATTN: H. Mirels R.L. Varwig Aerophysics Lab P.O. Box 92957 Los Angeles, CA 90009
1	AVCO Systems Division ATTN: B. Reeves 201 Lowell Street Wilmington, MA 01887
3	Boeing Commerical Airplane Company ATTN: G.M. Bowes M.S. 1W-82, Org B-8120 P.E. Rubbert, MS 3N-19 J.D. McLean, MS 3N-19 Seattle, WA 98124
3	Calspan Corporation ATTN: A. Ritter G. Homicz W. Rae P.O. Box 400 Buffalo, NY 14225
1	General Dynamics ATTN: Research Lib 2246 P.O. Box 748 Fort Worth, TX 76101
1	General Electric Company, 3198 Chestnut Street Philadelphia, PA 19101
2	Grumman Aerospace Corporation ATTN: R.E. Melnik L.G. Kaufman Bethpage, NY 11714
2	Lockheed-Georgia Company ATTN: B.H. Little, Jr. G.A. Pounds Dept 72074, Zone 403 86 South Cobb Drive Marietta, GA 30062
1	Lockheed Missiles and Space Company ATTN: Tech Info Center 3251 Hanover Street Palo Alto, CA 94304

DISTRIBUTION LIST

No. of Copies	Organization
3	Martin-Marietta Laboratories ATTN: S.H. Maslen S.C. Traugott H. Obremski 1450 S. Rolling Road Baltimore, MD 21227
2	McDonnell-Douglas Corporation Douglas Aircraft Company ATTN: J. Xerikos H. Tang 5301 Bolsa Avenue Huntington Beach, CA 92647
2	McDonnell-Douglas Corporation Douglas Aircraft Company ATTN: T. Cebeci K. Stewartson 3855 Lakewood Boulevard Long Beach, CA 90801
3	Sandia Laboratories ATTN: F.G. Blottner W.L. Oberkampf Tech Library Albuquerque, NM 87115
2	United Aircraft Corporation Research Laboratories ATTN: M.J. Werle Library East Hartford, CT 06108
1	LTV Aerospace Corporation Vought Systems Division ATTN: J.M. Cooksey, Chief Gas Dynamics Lab. 2-53700 P.O. Box 5907 Dallas, TX 75222
1	Arizona State University Department of Mechanical and Energy Systems Engineering ATTN: G.P. Neitzel Tempe, AZ 85281
3	California Institute of Technology ATTN: Tech Library H.B. Keller, Mathematics Dept. D. Coles, Aeronautics Dept. Pasadena, CA 91109
1	Cornell University Graduate School of Aero Engr ATTN: Library Ithaca, NY 14850
2	Illinois Institute of Technology ATTN: M.V. Morkovin H.M. Nagib 3300 South Federal Chicago, IL 60616
4	The Johns Hopkins University Applied Physics Laboratory ATTN: Dr. R.D. Whiting Dr. D.A. Hurdif Dr. R.S. Hirsh Mr. E.R. Bohn Johns Hopkins Road Laurel, MD 20707
1	The Johns Hopkins University Department of Mechanics and Materials Science ATTN: S. Corrsin Baltimore, MD 21218
1	Louisiana State University Department of Physics and Astronomy ATTN: Dr. R.G. Hussey Baton Rouge, LA 70803
3	Massachusetts Institute of Technology ATTN: E. Covert H. Greenspan Tech Library 77 Massachusetts Avenue Cambridge, MA 02139

DISTRIBUTION LIST

No. of Copies	Organization
2	North Carolina State University Mechanical and Aerospace Engineering Department ATTN: F.F. DeJarnette J.C. Williams Raleigh, NC 27607
1	Northwestern University Department of Engineering Science and Applied Mathematics ATTN: Dr. S.H. Davis Evanston, IL 60201
1	Notre Dame University Department of Aero Engr ATTN: T.J. Mueller South Bend, IN 46556
2	Ohio State University Department of Aeronautical and Astronautical Engineering ATTN: S.L. Petrie O.R. Burggraf Columbus, OH 43210
2	Polytechnic Institute of New York ATTN: G. Moretti S.G. Rubin Route 110 Farmingdale, NY 11735
3	Princeton University James Forrestal Research Center Gas Dynamics Laboratory ATTN: S.M. Bogdonoff S.I. Cheng Tech Library Princeton, NJ 08540
1	Purdue University Thermal Science and Prop Center ATTN: Tech Library W. Lafayette, IN 47907
1	Rensselaer Polytechnic Institute Department of Math Sciences ATTN: R.C. DiPrima Troy, NY 12181
1	Rutgers University Department of Mechanical, Industrial, and Aerospace Engineering ATTN: R.H. Page New Brunswick, NJ 08903
1	San Diego State University Department of Aerospace Engineering and Engineering Mechanics College of Engineering ATTN: K.C. Wang San Diego, CA 92182
1	Southern Methodist University Department of Civil and Mechanical Engineering ATTN: R.L. Simpson Dallas, TX 75272
1	Southwest Research Institute Applied Mechanics Reviews 8500 Culebra Road San Antonio, TX 78228
1	Texas A&M University College of Engineering ATTN: R.H. Page College Station, TX 77843
1	University of California-Berkeley Department of Aerospace Engineering ATTN: M. Holt Berkeley, CA 94720
1	University of California-Davis ATTN: H.A. Dwyer Davis, CA 95616

DISTRIBUTION LIST

No. of Copies	Organization
2	University of California-San Diego Department of Aerospace Engineering and Mechanical Engineering Sciences ATTN: P. Libby Tech Library La Jolla, CA 92037
1	University of Cincinnati Department of Aerospace Engineering ATTN: R. T. Davis Cincinnati, OH 45221
2	University of Colorado Department of Astro-Geophysics ATTN: E. R. Benton G. R. Inger Boulder, CO 80302
1	University of Hawaii Department of Ocean Engineering ATTN: G. Venezian Honolulu, HI 96822
2	University of Maryland ATTN: W. Melnik J. D. Anderson College Park, MD 20742
2	University of Michigan Department of Aeronautical Engineering ATTN: W. W. Wilmarth Tech Library East Engineering Building Ann Arbor, MI 48104
1	University of Rochester Department of Mechanical and Aerospace Sciences ATTN: R. Gans Rochester, NY 14627
1	University of Santa Clara Department of Physics ATTN: R. Greeley Santa Clara, CA 95053
3	University of Southern California Department of Aerospace Engineering ATTN: T. Maxworthy P. Weidman L. G. Redekopp Los Angeles, CA 90007
1	University of Tennessee Department of Physics ATTN: Prof. W. E. Scott Knoxville, TN 37916
1	University of Texas Department of Aerospace Engineering ATTN: J. C. Westkaemper Austin, TX 78712
1	University of Virginia Department of Aerospace Engineering and Engineering Physics ATTN: I. D. Jacobson Charlottesville, VA 22904
1	University of Washington Department of Mechanical Engineering ATTN: Tech Library Seattle, WA 98105
1	University of Wyoming ATTN: D. L. Boyer University Station Laramie, WY 82071

DISTRIBUTION LIST

No. of Copies	Organization
2	Virginia Polytechnic Institute and State University Department of Aerospace Engineering ATTN: Tech Library Dr. W. Saric Blacksburg, VA 24061
1	Woods Hole Oceanographic Institute ATTN: J. A. Whitehead Woods Hole, MA 02543

Aberdeen Proving Ground

Director, USAMSAA
ATTN: DRXSY-D
DRXSY-MP, H. Cohen

Commander, USATECOM
ATTN: DRSTE-TO-F

Commander/Director, USACSL, EA
ATTN: Munitions Div, Bldg. E3330
E. A. Jeffers
W. C. Dee
W. J. Pribyl
J. McKivrigan
C. Hughes

Director, USACSL, Bldg. E3516, EA
ATTN: DRDAR-CLB-PA
M. Miller

USER EVALUATION OF REPORT

Please take a few minutes to answer the questions below; tear out this sheet, fold as indicated, staple or tape closed, and place in the mail. Your comments will provide us with information for improving future reports.

1. BRL Report Number _____

2. Does this report satisfy a need? (Comment on purpose, related project, or other area of interest for which report will be used.)

_____

_____

_____

3. How, specifically, is the report being used? (Information source, design data or procedure, management procedure, source of ideas, etc.) _____

_____

_____

4. Has the information in this report led to any quantitative savings as far as man-hours/contract dollars saved, operating costs avoided, efficiencies achieved, etc.? If so, please elaborate.

_____

_____

5. General Comments (Indicate what you think should be changed to make this report and future reports of this type more responsive to your needs, more usable, improve readability, etc.) _____

_____

_____

_____

6. If you would like to be contacted by the personnel who prepared this report to raise specific questions or discuss the topic, please fill in the following information.

Name: _____

Telephone Number: _____

Organization Address: _____

_____

_____